University of Illinois at Urbana-Champaign

ACRC

Air Conditioning and Refrigeration Center A National Science Foundation/University Cooperative Research Center

An Investigation of Electrochemical Methods for Refrigeration

D. W. Gerlach and T. A. Newell

ACRC TR-234 October 2004

For additional information:

Air Conditioning and Refrigeration Center
University of Illinois
Mechanical & Industrial Engineering Dept.
1206 West Green Street
Urbana, IL 61801

(217) 333-3115

Prepared as part of ACRC Project #125
Investigation of Electrochemical Processes for Refrigeration
T. A. Newell, Principal Investigator

The Air Conditioning and Refrigeration Center was founded in 1988 with a grant from the estate of Richard W. Kritzer, the founder of Peerless of America Inc. A State of Illinois Technology Challenge Grant helped build the laboratory facilities. The ACRC receives continuing support from the Richard W. Kritzer Endowment and the National Science Foundation. The following organizations have also become sponsors of the Center.

Alcan Aluminum Corporation
Arçelik A. S.
Behr GmbH and Co.
Carrier Corporation
Cerro Flow Products, Inc.
Copeland Corporation
Daikin Industries, Ltd.
Danfoss A/S
Delphi Thermal and Interior
Embraco S. A.
Ford Motor Company
Fujitsu General Limited
General Motors Corporation
Hill PHOENIX
Hydro Aluminum Adrian, Inc.
Ingersoll-Rand/Climate Control
Lennox International, Inc.
Manitowoc Ice, Inc.
LG Electronics, Inc.
Modine Manufacturing Co.
Parker Hannifin Corporation
Peerless of America, Inc.
Samsung Electronics Co., Ltd.
Sanden Corporation
Sanyo Electric Co., Ltd.
Tecumseh Products Company
Trane
Visteon Automotive Systems
Wieland-Werke, AG
Wolverine Tube, Inc.

For additional information:

Air Conditioning & Refrigeration Center
Mechanical & Industrial Engineering Dept.
University of Illinois
1206 West Green Street
Urbana, IL 61801

217 333 3115

Abstract

Electrochemical processes can be combined into thermodynamic cycles that can produce refrigeration effects. The technical feasibility and design parameters of electrochemical refrigeration systems were studied. Modeling of thermodynamic, kinetic, and transport processes have been undertaken.

The systems under investigation are divided into two groups: direct methods and indirect methods. Direct methods utilize the heat absorption and rejection associated with the entropy change of reaction that occurs as part of an electrically-driven chemical reaction. Indirect methods use some other aspect of an electrochemical reaction such as pressure production to drive a cooling system.

Thermodynamic equilibrium analyses of direct methods have been performed including development of a proof of Carnot limitations. A variety of potential chemical reaction systems have been investigated with respect to feasibility for laboratory prototype systems and future applications. The properties of an ideal reaction system are discussed and several possible reaction types are suggested for investigation.

The continuous flow direct method consists of two electrochemical cells operating in reverse of each other with reactants pumped between them via a regenerative heat exchanger. More detailed analyses including irreversibilities have shown technical feasibility. These analyses included ohmic resistance, limitations due to the reaction rate kinetics, mass transport losses, and losses due to the internal regenerative heat exchange process. This model identifies some of the tradeoffs in design and places upper and lower bounds on design parameters such as surface heat flux and COP. The model calculation is based on published measurements of reaction data. The system is very sensitive to losses in the cells because the electricity cycled internally is much larger than the heat transferred externally.

Small scale laboratory tests have demonstrated cooling using a D-sized NiCd battery and a cell generating gaseous chlorine and hydrogen from hydrochloric acid.

A number of indirect methods for refrigeration are reviewed.

Table of Contents

List of Figures

Page

List of Tables

Page

Chapter 1. Introduction and Overview

1.1 Introduction

Electrochemical processes are primarily utilized for chemical production (e.g., chlorine, aluminum, copper) and for electrical power generation (e.g., batteries and fuel cells). In addition, electrochemical systems have the potential of producing cooling effects in various ways, due to the strong coupling of electrochemical processes to pressure generation and thermal processes.

Electrochemistry has been defined as:

> The science dealing with chemical changes accompanying the passage of an electrical current, or the reverse process in which a chemical reaction is used as the source of energy to produce an electrical current, as in a battery. (Parker, 1982)

The major objectives of this research project are to investigate the use of existing electrochemical theory for cooling and refrigeration processes. This includes the conceptual development of possible techniques and initial modeling to assess their technical feasibility and performance. Some simple systems were constructed and tested as proofs of concept. The research presented here focuses on cooling near room temperature, such as heat rejection from electronics, air conditioning for space cooling or refrigeration for food preservation. Cryogenic cooling is not discussed and high temperature cooling is addressed only in the context of literature reviews.

1.2 Reasons for Investigation

Electrochemical cooling systems could potentially be used in any area that utilizes cooling and refrigeration. Electrochemical reactions are a novel route to controlling the thermodynamic state of the working substance and could have several advantages over other cooling systems in current use or development, including vapor compression, absorption, thermoelectric, thermoacoustics, magnetic, or thermionic emission. One unique feature of electrochemical systems is the ability to operate with very few or no moving parts, a distinct advantage in electronics cooling. Electrochemical systems also have a different set of design constraints and therefore allow new physical configurations. For instance, the bulky compressor and evaporator compartments in refrigerators could be eliminated and replaced with thin reactors lining the walls or shelving. In addition, electrochemical systems might operate more efficiently and use less environmentally hazardous materials than conventional systems.

Electrochemistry is an established field with well developed theory and voluminous literature. This wealth of knowledge can be reapplied to cooling systems. Recent advances in other electrochemical fields such as fuel cells and chlor-alkali production have opened new possibilities. A variety of electrode and separator materials have been developed that could be reapplied to cooling systems.

1.3 Definition of Direct and Indirect Methods

The systems under investigation are divided into two groups: direct methods and indirect methods. Direct electrochemical refrigeration cycles (DERC) utilize the heat absorption and rejection that occur as an intrinsic part of an electrically-driven chemical reaction. Indirect electrochemical refrigeration methods (IERM) use some other aspect of an electrochemical process such as pressure production to drive a cooling system. For the IERMs, the term "electrochemical" was defined fairly loosely and includes systems that may not directly cause a chemical change in the substances' makeup, such as electrokinetic systems or membrane separations driven by an electrical field. As the direct methods are theoretically simpler, they have been the primary focus of this project.

1.4 Direct Electrochemical Cooling Theory

The use of electrochemical effects to directly produce a cooling effect has been proposed (Newell, 2000; Gerlach, 2003). The electrical energy consumed or produced by an electrochemical reaction is equal to the Gibbs free energy change of the reaction (ΔG):

$$\Delta G = -nFE_0 \qquad 1.4.1$$

where n is the number of electrons involved in the reaction, and E_0 is the equilibrium voltage of the system. F is the Faraday constant (96485 Coulomb/mole) and is the ratio of the number of particles in a mole to the number of electrons in a Coulomb or the charge per mole of electrons. The minus sign is due to the electrochemical convention with respect to the definition of E_0. ΔG consists of the enthalpy of reaction (ΔH) and the reversible heat effect ($T\Delta S$):

$$\Delta G = \Delta H - T\Delta S \qquad 1.4.2$$

where T is the temperature and ΔS is the entropy change of the reaction. At a constant temperature and pressure, the reversible heat effect is a heat exchange with the environment. A reversible electrochemical cell that absorbs heat when voltage is applied will release the same amount of heat when the voltage is reversed.

The value and sign of the reversible heat effect depend on the reaction involved. Table 1.4.1 shows the reversible heat effect of several different rechargeable battery systems (lead acid, nickel cadmium, nickel metal hydride, and the fuel cell-water electrolyser system):

Table 1.4.1 Thermodynamic characteristics of some example electrochemical systems.

System	Lead-acid	Ni/Cd	Ni/hyd	Water
$T\Delta S$ (kJ/mol)	13.2	-27	-40	-48.6
ΔG (kJ/mol)	-372.6	-255	-259	-237.2

From Berndt (1993)

For instance, a lead acid battery when discharged slowly will absorb heat and will release the same heat when charged. Theoretically, a water electrolyser will absorb heat and a hydrogen-oxygen fuel cell will release heat (Berndt, 1993; Newell, 2000).

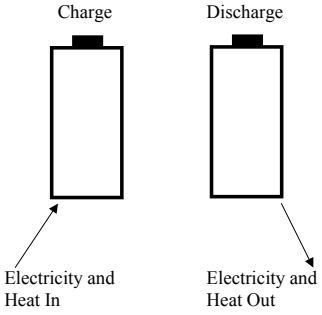

Figure 1.4.1 A battery with a negative reversible heat effect absorbs heat on charging and rejects heat on discharging.

A fuel cell connected in a cycle with an electrolyser at a different temperature can act as an electrochemical refrigeration cycle (ERC). Because of the second law of thermodynamics, electricity must be put in to the system in order to account for the difference in temperature. Coefficients of performance (COP) of 20-30 have been calculated for temperature regimes of practical interest (Newell, 2000). However, these calculations assume ideal reversible components. In practice, fuel cells and electrolysers have large losses due to ohmic losses in the electrolyte and electrodes and energy needed to overcome the chemical activation barriers. The difference between the reversible

voltage and the actual voltage is termed overpotential. These losses increase with higher current densities. Much fuel cell and electrolyser research has been done with the goal of increasing current density in order to decrease the cost and weight of the unit.

1.5 Difference between Batch and Continuous Flow Processes

The electrochemical processes may be performed either as a batch process or a continuous flow process. In the batch process a set amount of reactants are placed in the reactor and connected to an electrical circuit. The reaction proceeds to a set point, when the applied field is reversed or the process stopped. This is similar to battery charging and will be discussed in Chapter 2. In the continuous flow process, reactants are pumped through the system, reacted in the cell, pumped to another cell where the process is reversed, and then returned to the first cell. This is discussed in greater detail in Chapters 3 through 6.

1.6 Literature Review

A review of literature pertinent to this project has been performed. The use of electrochemical cycles as heat engines at high temperatures has been researched by a number of investigators. Several papers have been published on the use of these cycles as heat pumps. The logic of using them for heat pumps appears to be that a heat pump is at worst 100% efficient and anything the electrochemical systems does to move heat is better than nothing. Little thought has been given to the complexity or cost of the system. Since direct electrochemical processes have not been extensively researched for cooling cycles near room temperature, there are very few published papers directly on this topic. Chapter 6 contains a literature review of indirect methods.

However, the literature related to electrochemical systems for electricity production (e.g. batteries and fuel cells) and industrial processes (e.g. chlorine production) is voluminous and has been consulted with a focus on applying existing knowledge toward a new goal. The pertinent publications will be cited as needed throughout this work

1.6.1 Thermally Regenerative Electrochemical Systems

Thermally regenerative electrochemical systems (TRES) have been researched for use in power generation systems (Chum 1980 and 1981). There are a wide variety of proposed designs and cycles. All of these systems produce power from an electrochemical cell and take in heat from the environment as an energy source. They are the reversed analogues of the electrochemical cooling systems present in this work in the direct and indirect cycles.

Most of the work on TRES has been for high temperature heat sources such as solar and nuclear power. Most are in the range of several hundred degrees C to 1200ºC. Therefore the electrochemical couples are not directly transferable to the room temperature and below systems needed for cooling applications.

Chum and Osteryoung break the TRES into two broad categories by whether the systems are regenerated by heat addition or by addition of heat and electricity. The second type is more pertinent to the present work.

The systems that Chum and Osteryoung term as “type 4” are identical in concept to the direct system analyzed here. They state that no systems of this type have yet been demonstrated as feasible and that very few low temperature systems have been explored. Although, they give no references to the few that have been studied, they recommend further exploration of low temperature systems. An interesting system is mentioned using the following reactions:

$$Sn^{2+} + 2e^- \leftrightarrow Sn$$

$$Cr^{3+} + e^- \leftrightarrow Cr^{2+} \qquad 1.6.1.1$$

The low side temperature is given as 20ºC and the high side 80ºC. Because this involves an electroplating reaction, the system must be run in a batch mode. However, no reference is cited for the research on this cell (Chum 1980).

The coupled fuel cell-electrolyser system suggested by Newell (2000) for use in cooling has been studied as a TRES. Liebhafsky (1959) and deBethune (1960) analyzed the thermodynamics of the system as will be discussed in greater detail in Chapter 3. Morehouse (1990) performed a parametric study of a present technology system operating at 1300K and a projected technology system at 1800K. The present technology system was determined to be "large, heavy and costly." Its performance was also very sensitive to the electrical current efficiency and side reactions. The projected technology system would need extensive development but could compete with solar thermal power sources for space applications.

Hammond (1980) studied electrochemical cells for use in solar thermal power generation and heat recovery applications. The design was for a high temperature reservoir at 90ºC and the low temperature reservoir at 30ºC. A heat engine system directly analogous to the continuous flow system described in chapter 3 was studied. The entropy changes for several transition metal coordination compound reactions were measured. The following reaction set was selected for prototype testing:

$$Cu(NH_3)_4^{+2} + e^- \leftrightarrow Cu(NH_3)_2^{+} + 2NH_3$$

$$Fe(CN)_6^{-3} + e^- \leftrightarrow Fe(CN)_6^{-4} \qquad 1.6.1.2$$

The prototype cell used an unusual membrane consisting of $BaSO_4$ precipitated on a cellophane support. The cell produced 6.4W per m2 of membrane. The authors state that this is too low for practical applications. However, they conclude that a useful system could be produced by reducing the resistance, increasing the entropy change of reaction, and possibly increasing the temperature difference between the cells,

1.6.2 Aqueous Electrochemical Heat Pump

Kreysa (1990) and Dittmar (1995) modeled and tested systems similar to the batch process cycles investigated in Chapter 2. The heat pumps consist of two identical cells operating in opposite directions of each other at different temperatures. At some point the voltage is reversed and the process run backwards. The papers refer to changing the cell temperatures by "differential heat exchange." This is apparently some form of regenerative heat transfer between the cells. Losses in this heat transfer and the mismatch between cell specific heats are not addressed.

The modeling in Kreysa (1990) focuses heavily on the effect of changes in concentration on the equilibrium voltage. The thermodynamic analysis appears to claim that if a reaction with a lower entropy change at the higher temperature is chosen, the cycle will have a COP greater than the Carnot COP. The authors do not go into this claim in detail. However, one term had been dropped from the equation as negligible and this may have caused the unusual result. In addition, neglecting the specific heat mismatch during heat exchange could have caused this.

The batch process was simulated with a constant current applied to the cells and stepping through time. The final state of one cell is the initial state of the other cell. Several variables in the equations calculating the irreversibilities are undefined. However, it appears that the voltage losses (overpotentials) are viewed as mass transfer dominated for oxidation-reduction reactions. For the metal dissolution reaction the losses are due to chemical kinetics and are a linear function of current. The reactions modeled are the following fast transition metal reactions:

$$Fe^{3+} + e^- \leftrightarrow Fe^{2+}$$

$$Ag^{+} + e^- \leftrightarrow Ag$$

$$Cu^{2+} + 2e^- \leftrightarrow Cu \qquad 1.6.2.1$$

The first reaction is one used in the modeling in Chapter 6 and experiments in Appendix D. The three possible combinations of these were modeled and the silver-iron system has a slightly higher heat pump COP than the others.

The systems with copper in them take twice as long to charge at constant current due to the two electron reaction. The authors conclude that the systems are worthy of future study as heat pumps and for energy recovery.

Dittmar (1995) discusses the charging and discharging of NiCd and lead acid batteries in calorimeters. In addition, experiments were run with the fast reactions mentioned above. These tests are discussed in Chapter 2.

1.6.3 High Temperature Water Gas Shift Reaction Electrochemical Heat Pump

Ishihara et al. (1998, 1999, and 2001) describe an electrochemical heat pump operating near 1000K. This heat pump is designed to accept waste heat from an industrial process such as a coke oven and upgrade it to a higher temperature by the application of electricity.

The proposed design uses an electrochemical reactor at the lower temperature to drive an endothermic process and absorb heat. The reactants are then moved to the higher temperature and reacted exothermically. No electricity is recovered at the higher temperature. As the Gibbs free energy of reaction at the higher level is abandoned to heat and not recovered electrically, it is advantageous for efficiency reasons to use a reaction with a Gibbs free energy change as close to zero as possible and smaller than that at the lower temperature level. Several reactions are proposed that have a zero ΔG in the temperature range considered. However, the water gas shift reaction:

$$CO+H_2O \leftrightarrow CO_2+H_2 \qquad 1.6.3.1$$

was chosen as its kinetics are well known.

If the reactors are operated near the equilibrium concentrations of reactants, the COP increases. At the limit of the same equilibrium concentrations of the reactants at the two temperature levels, the Carnot COP is achieved. The COP is of course dependent on the temperature lift in the usual manner. The temperature lifts are on the order of 50K to 100K with high side temperatures from 800K to 1200K. The COP at constant temperature lift increases with increasing high side temperature.

The utility and necessity of upgrading heat in this temperature range is questionable. The heat is already of fairly high quality and the temperature lift is small compared to the overall absolute temperature.

1.7 COP Convention

All COPs (Coefficient Of Performance) given in this work are refrigeration COPs, not heat pump COPs except where noted. The COP is defined as:

$$COP= Q_{cold}/W \qquad 1.7.1$$

where Q_{cold} is the heat absorbed on the cold side and W is the total work into the system.

Chapter 2. Battery Tests and Batch Processes

2.1 Introduction

Qualitative tests have been conducted by discharging and charging commercially available rechargeable batteries and measuring the heat absorption and rejection. These tests demonstrated a small cooling effect when a commercially available D-sized NiCd battery was slowly charged in an insulated container. In addition, published data from lithium ion battery tests were used to estimate the COP of using commercial batteries for cooling.

Rechargeable batteries were chosen as an initial model system because they are inherently electrochemically reversible. In addition, they are inexpensive and easy to handle. The expected cooling effect and consequent temperature change in the battery are small. Therefore the battery must be well insulated in order to measure the temperature drop. Several different designs for calorimeters that were tried are described below.

2.2 Lithium-ion Battery COP

Hong et al. (1998) have published data on the heating and cooling rates of lithium ion batteries during charge and discharge. The entropy change for this reaction causes cooling during the charging cycle. The batteries were charged and discharged several times to break them in and eliminate the initial decrease in capacity due to the first few charging cycles. Each test was run starting at a set initial temperature. During the test the batteries were discharged, allowed to relax to the initial temperature, and recharged, all in a carefully monitored calorimeter. The tests were run at starting temperatures of 35, 45, and 55ºC.

The cells were charged at rates expressed as a fraction of the overall cell capacity in amp-hours (C). A charging rate of C/2 means total charging time was 2 hours. The rates used were C/1, C/2, and C/3.

The time versus temperature profiles are very similar to the one presented for NiCd batteries in section 2.4. An initial temperature drop during charging is followed by a temperature increase as reactants are depleted and irreversibilities increase. The temperature decrease was at most 1 or 2ºC and the increase during charging was somewhat smaller. The temperature increase on discharge was as high as 17ºC.

The time versus heating rate data can be used to calculate the COP of a hypothetical refrigeration cycle based on Li-ion cells. As the cell charges it absorbs heat from the low temperature reservoir. When the cell starts to heat up during charging this heat is rejected to the high temperature reservoir. The heat rejected during discharge is also rejected to the high temperature reservoir. All of the electricity produced in the system is recycled.

The data was taken from the published graphs. Photocopies of the graphs were scanned into a computer file and then overlaid with a grid. The data was then read off and inputted into a spreadsheet file. The total heat put out by the cell during discharge was determined by integrating the heating rate with the trapezoidal rule. A similar procedure was used separately for the cooling and heating parts of the charging.

Some error was certainly introduced due to distortion in the photocopying and scanning and approximation in the reading of the chart. For the lower values the error could be as much as 25% and for the larger values less than 10%. The paper does not explicitly state the uncertainty in the heat dissipation rates. However other uncertainties in the paper range of 2-10%. The integration of the data probably smoothed out some of the error. Consequently, the values computed have a relatively large error possibly approaching 50%. However, the calculations are only to get a rough idea of the COP of lithium ion batteries as cooling devices.

The refrigeration COP of the system was calculated as follows:

$$COP = -Q_{endocharge} / (Q_{discharge} + Q_{exocharge} + Q_{endocharge}) \qquad 2.2.1$$

where $Q_{discharge}$ is the heat rejected during discharge and relaxation, $Q_{exocharge}$ is the heat rejected in charging, and $Q_{endocharge}$ is the heat absorbed during charging. By the First Law of Thermodynamics, the work input to the cycle is the difference between the heat out and the heat in.

The COPs are quite low (see Figure 2.2.1). This is unsurprising as the batteries are designed as power storage devices rather than cooling systems. A car engine running in reverse would make a poor refrigerator too. However, the COPs are positive and demonstrate the possibility of using actual electrochemical systems for cooling. The data point for C/2 charging rate at an initial temperature of 45ºC appears anomalous. As only the first part of the charging period is endothermic, it may be advantageous to only partially charge and discharge the battery.

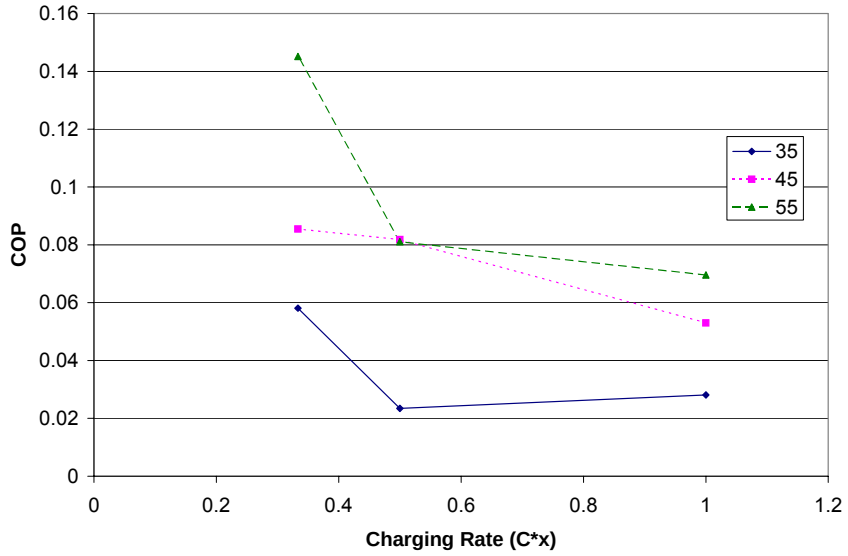

Figure 2.2.1 COP of Li-ion cells used as a refrigeration device as a function of charging rate and initial temperature.

Further information could be extracted from this data using a few assumptions. Hong et al. (1998) published the cell voltage versus the fraction of the total charge at various charging rates. This information could be correlated with the time series versus heating rate data. In addition, the thermodynamic data for the Li-ion reaction could be used to estimate the equilibrium voltage at various charge states using the assumption of a Nernstian reaction (see Chapter 6 for more discussion of the Nernst equation). From these data sets an optimal voltage versus charge curve could be developed as discussed in greater detail in Section 2.5.

Li-ion batteries have problems with thermal run away and overheating during discharge. The reversible heat effect and losses heat the battery, causing the reaction rate to increase and feeding back into the heating processes. Because this can cause the battery to catch fire or explode, commercial Li-ion battery packs contain circuitry to prevent thermal runaway. For safety reasons battery testing for this project was not conducted with Li-ion cells.

2.3 Battery Colonnade and Calorimeter Design

The first calorimeter design was made from expanded polystyrene foam board (see Figure 2.3.1). The foam was layered in such a way that the lid was in the form of an inverted stepped pyramid. This was intended to prevent air from entering the chamber. Soft foam strips were also used around the lid opening to stop air leakage. The corners of each foam layer were sealed with aluminized tape and the layers were glued together with silicone caulk. Several flexible heater strips with a total resistance of 1985 Ohms were placed on the bottom of the chamber and a

0.32 cm aluminum plate placed on top of them to spread the heat. Four thermocouples were taped to the inside of the chamber so that they extend approximately 2.5 cm into the chamber airspace. Four thermocouples were taped to the floor of the chamber and four to the chamber roof. They were located near the center of the four quadrants of the top and bottom.

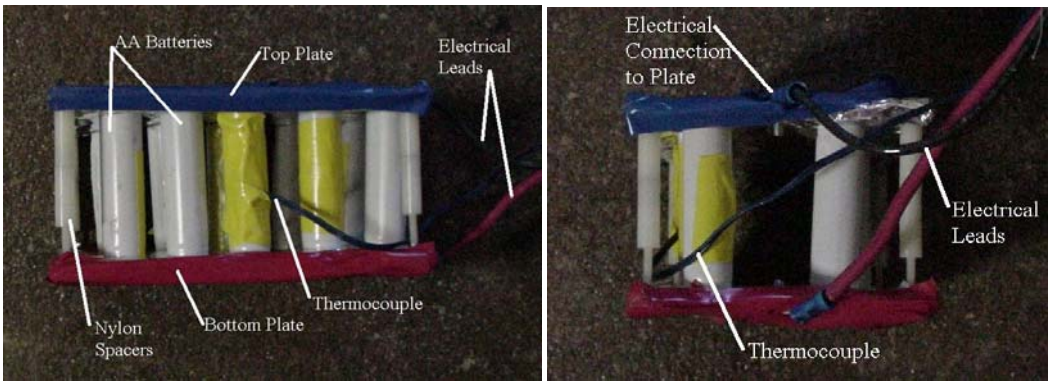

Figure 2.3.1 Photos of batteries sandwiched between plates to form colonnade

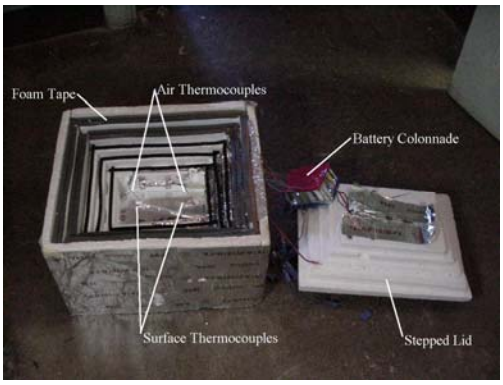

Figure 2.3.2 Calorimeter for demonstrating electrochemical cooling with battery colonnade

Eight NiCd AA batteries were arranged in two rows and clamped between two aluminum plates to form a sort of colonnade. The plates were covered in electrically conductive foam and aluminum foil to ensure a connection with the battery terminals. The plates were connected with nylon spacers. The colonnade design was built with the goal of blowing air through it as a heat exchanger. However, the cooling effect would have been much too small for this to be effective.

The heater strip was used to add an artificial load to the calorimeter and the temperature was plotted with respect to time. The thermal capacity of the calorimeter and its heat transfer coefficient were estimated by fitting to the temperature time curve. However, the curves were inconsistent, most likely due to air infiltration through the calorimeter seals and the corners between the foam panels.

The battery assembly was placed in this calorimeter and the batteries were charged. Over a series of several tests the temperature of the chamber did not change significantly during charging. The air temperature did not decrease due to the reversible heat effect or increase due to ohmic resistance or other irreversibilities. This may have been due to air leakage. Also, the thermal mass of the battery assembly in the chamber may have been too large with respect to the cooling power of the batteries.

2.4 Foamed In-Place Calorimeter

A different calorimeter was built to overcome the problems of the calorimeter discussed in the previous section (see Figure 2.4.1). A D-cell battery was used instead of the AA cells to maximize the ratio of active chemicals to the container mass. The active chemicals are proportional to the cell volume and the container mass is approximately proportional to the cell exterior surface area. Maximizing this ratio maximizes the possible temperature change.

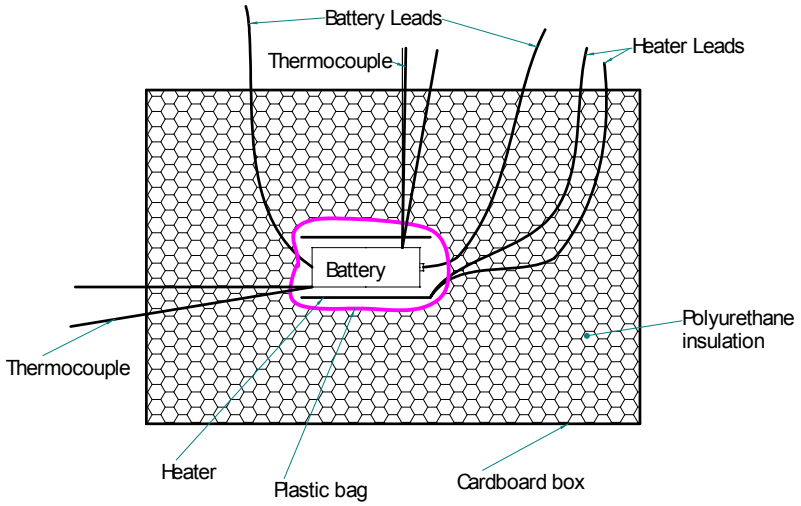

Figure 2.4.1 Diagram of insulated NiCd D-cell for use in charging tests

Leads were soldered to the battery terminals. Two thermocouples directly touched the battery, one near each end. A flexible strip heater battery was wrapped around the battery for measuring the insulation heat transfer coefficient and the battery's effective thermal mass. The assembly was wrapped in a polyethylene bag and suspended in a corrugated cardboard box (30 cm long by 23 cm wide by 28 cm tall). The box was then filled with expanding polyurethane foam to encase the battery. The foam hermetically sealed in the battery. The overall heat transfer coefficient (UA) of the calorimeter and the thermal mass including the battery were not measured.

The battery was charged and discharged several times at varying rates and the temperature recorded. In tests at higher charge rates the battery increased in temperature due to ohmic heating and other irreversibilities. At lower charge rates there was no significant temperature increase or decrease, because the chemical reaction was slower than the rate at which heat was conducted into or out of the calorimeter. In order for cooling to be measurable, the reaction rate must proceed faster than heat diffuses into the calorimeter, but slow enough that the irreversibilities do not swamp the reversible heat effect.

The battery was charged at a constant current of 0.17 Amps for the test shown in Figure 2.4.2. The battery temperature decreases even though the ambient temperature is increasing. This demonstrates the reversible heat effect cooling. As charging progresses, the irreversibilities increase, causing the battery temperature to rise. For example, one irreversibility could be due to depletion of the reactants at the electrode surfaces causing mass transport losses. When the reactants are depleted a different chemical reaction becomes active. This is almost certainly the electrolysis of water. This reaction is much less reversible and the heating rate increases. This is shown by the change in slope of the temperature-time curve at approximately 450 minutes.

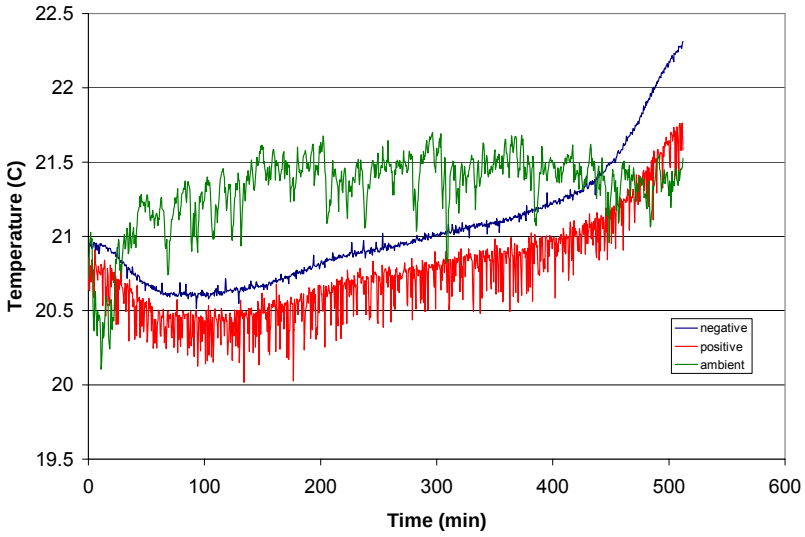

Figure 2.4.2 NiCd battery temperature drops during charging

Dittmar (1995) charged and discharged NiCd D-cells in a differential calorimeter to measure their performance as a heat pump at a temperature lift of 25ºC to 60ºC. The heat pump COP was measured as 5 at the start of charging and dropping to around 2 for most of the charging time.

A few similar tests were performed with a 12 V lead acid camcorder battery embedded in a box filled with polyurethane foam (31 cm long by 39 cm wide by 21 cm tall). The sign of the reversible heat effect of a lead acid battery is the opposite of that of a NiCd (Berndt, 1993). Therefore it would be expected to cool during discharge. During discharge the temperature of the lead acid battery increased due to irreversibilities. As the NiCd tests demonstrated a cooling effect it was not necessary to perform additional tests to find the optimal charging rate for a lead acid battery. Dittmar (1995) tested D-sized lead acid batteries in a calorimeter and stated that they were not usable for heat pumps due to irreversibilities and the complexity of the reaction system. Dittmar makes no mention of the opposite sign of the reversible heat effect.

2.5 Metal Ion Redox Systems

Batch tests of three transition metal ion reactions were tested. These are detailed in Appendix D. The goal of theses tests was to develop a simple laboratory cell that could be used to check which cell reactions produced a cooling effect under simple conditions and then to form the basis for a continuous flow cycle. The reactions tested were:

$$Fe^{3+} + e^- \leftrightarrow Fe^{2+}$$

$$Cu^{2+} + e^- \leftrightarrow Cu^{+}$$

$$Sn^{4+} + 2e^- \leftrightarrow Sn^{2+} \qquad 2.5.1$$

All experiments were performed with chlorides. However, all of the tests showed poor current-voltage curves and did not demonstrate any cooling effects.

These reactions are similar to the reactions modeled in Kreysa (1990) and tested by Dittmar (1995). Dittmar et al. achieved a heat pump COP in the range of 4 for a temperature lift from 25ºC to 60ºC using the system $Cu/CuSO_4$, $NaSO_4$//membrane//$Na_3[Fe(CN)_6]$,$Na_4[Fe(CN)_6]$, $NaSO_4$/Pt. This value does not include any losses due

to the heat exchange needed for moving the cells to the other temperature levels. The article states that a complete heat pump system was under construction. Kreysa (1993) also discusses this work.

2.6 Limitations of Batteries and Batch Electrochemical Processes for Cooling

Batteries such as NiCd, lead acid, or lithium ion cells are optimized for energy density and safety in the packaged form. Other electrochemical reactions should show a larger reversible heat effect and prove to be superior for refrigeration use. Also, batteries must be charged and discharged in a batch process instead of a continuous flow process. The maximum temperature drop achievable with a batch process is determined by the reversible heat effect with respect to the specific heat of the components:

$$C_p \Delta T = T \Delta S \qquad 2.6.1$$

where C_p is the specific heat of the reactants, solvent, and container, ΔT is the temperature change, T is the average temperature of the process, and ΔS is the entropy change of reaction at T. This equation is not rigorous since the left hand side includes a temperature change and the right hand side assumes a constant temperature. The equation is accurate if the temperature range considered is small and the thermodynamic properties do not change significantly. The total cooling effect available per mole is the reversible heat effect. The temperature change possible with this cooling effect is set by the molar specific heat. As both scale with quantity of the substance, increasing mass does not affect the temperature change.

The temperature change achievable in batch mode can be calculated from equation 2.6.1. The entropy change is assumed on the high end at 200 J/mol*K and the temperature is 298K. The electrolyte is dissolved at 1M concentration and the specific heat is assumed that of water at 298K (4183 J/kg*K) and the reactant does not affect the specific heat. With these values the achievable temperature change is 14.3K. If the concentration were doubled the temperature lift would double. The additional reactant would also increase the thermal mass per liter of solvent and the effect would be less pronounced. However, it is a general principle that increasing the concentration of the active substance with respect to the solvent, container, etc. will increase the temperature lift. In most systems the entropy change is lower and the specific heat of all components with respect to concentration would be higher. Therefore the possible temperature lift for a batch process is under 10K.

A continuous flow process could achieve a lower temperature by using two electrochemical cells at different temperatures and exchanging heat between the working substance as it is pumped between the cells. This is discussed in further detail in Chapter 3.

2.7 Conclusions

Published data from tests on lithium ion batteries show a cooling COP of under 0.2. Published data from tests on NiCd batteries claim a heat pump COP of 2-5. An insulated NiCd battery demonstrated cooling while charging. However, batteries such as NiCd, lead acid, or lithium ion cells are optimized for energy density and safety in the packaged form. Other electrochemical reactions should show a larger reversible heat effect and prove to be superior for refrigeration use. Also, batteries must be charged and discharged in a batch process instead of a continuous flow process. The maximum temperature drop achievable with a batch process is determined by the reversible heat effect with respect to the specific heat of the components and is limited to about 10K maximum. A continuous flow process could achieve a lower temperature by using two electrochemical cells at different temperatures and exchanging heat between the working substance as it is pumped between the cells.

Chapter 3. Continuous Flow System Description and General Characteristics

3.1 Introduction

The general performance characteristics and design parameters of an electrochemical refrigeration system can be calculated using simple models. These models show that the maximum COP is the Carnot COP. Calculating the orders of magnitude of various cell parameters reveals insights into the operation of direct electrochemical cooling systems.

3.2 General Characteristics

In vapor compression systems, the working fluid is expanded or compressed as a whole. The thermodynamic state of the entire volume changes at once. The heat transfer into or out of the fluid occurs at the surface of the heat exchanger. In contrast, electrochemical reactions occur on the surface of the electrodes and not in the volume of the electrolyte. Therefore, the total size of the system is determined by how much surface area can be packed in the smallest volume. Large surface areas are needed for high COP at reasonable cooling powers. Because the need for a large surface area is a characteristic of all electrochemical systems, large surface area electrodes have been developed for batteries and fuel cells. Frequently, the electrodes are porous. They may also be thin and rolled up or stacked.

Inherently, the electrolyte must be a reactive and electrically conductive medium. The reactivity will lead to corrosion and material compatibility issues that must be handled carefully. If a liquid solution leaks it can short circuit electronic equipment. This will limit the use of electrochemical methods for electronics cooling. A solid state reaction system would eliminate the leakage risk, but would have the limitations mentioned in section 2.6 on batch processes.

The total temperature lift achievable is limited by the freezing and boiling points of the solvent. Nonaqueous solvents could be used to extend the range beyond that possible with water.

3.3 Continuous Flow Process Description

A continuous flow process could achieve a larger temperature lift than a batch process by using two electrochemical cells at different temperatures and exchanging heat between the working substance as it is pumped between the cells.

Figure 3.3.1 shows a schematic of a system based on the reaction $Fe^{2+} + Mn^{3+} \Leftrightarrow Fe^{3+} + Mn^{2+}$. One cell accepts heat and acts analogous to an evaporator in a vapor compression system. The other cell rejects heat and acts analogous to a condenser. A separator may be necessary inside the cell to conduct ions and prevent the reactants from spontaneously mixing and reacting without exchanging electrons through the external circuitry. This reaction was picked simply because the thermodynamic data for it was easily available. There is no reason to believe that this reaction is optimal.

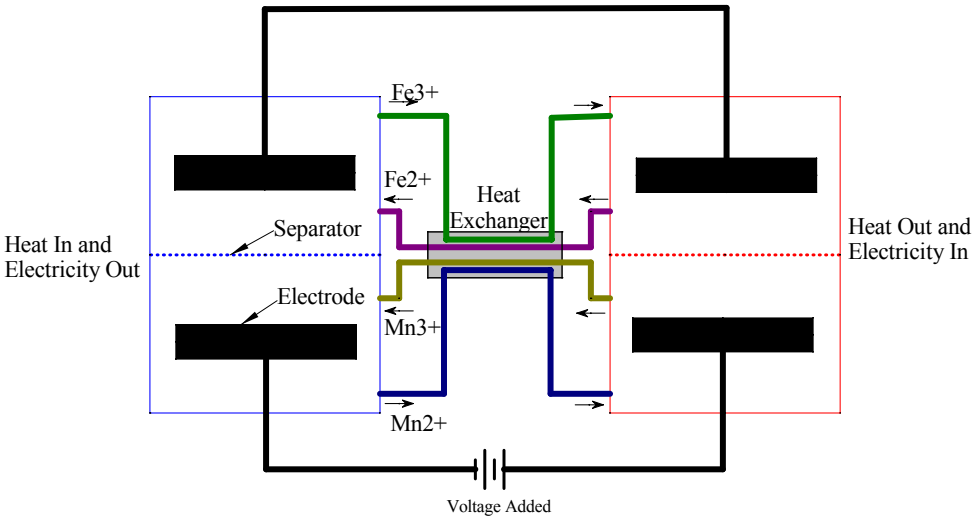

Figure 3.3.1. Schematic of continuous flow electrochemical cooling system

Figure 3.3.2 shows a T-s diagram and a voltage-concentration diagram for the cycle. The voltage-concentration diagram is somewhat analogous to the P-v diagram for a conventional refrigeration system. The thermodynamic potential that drives the system (pressure or voltage) is on the vertical axis and the density of the working substance (specific volume or concentration) is on the horizontal axis. The concentration is either the concentration of the reduced or the oxidized form of one of the electrochemical couples involved. Therefore the concentration changes as it passes through the cells.

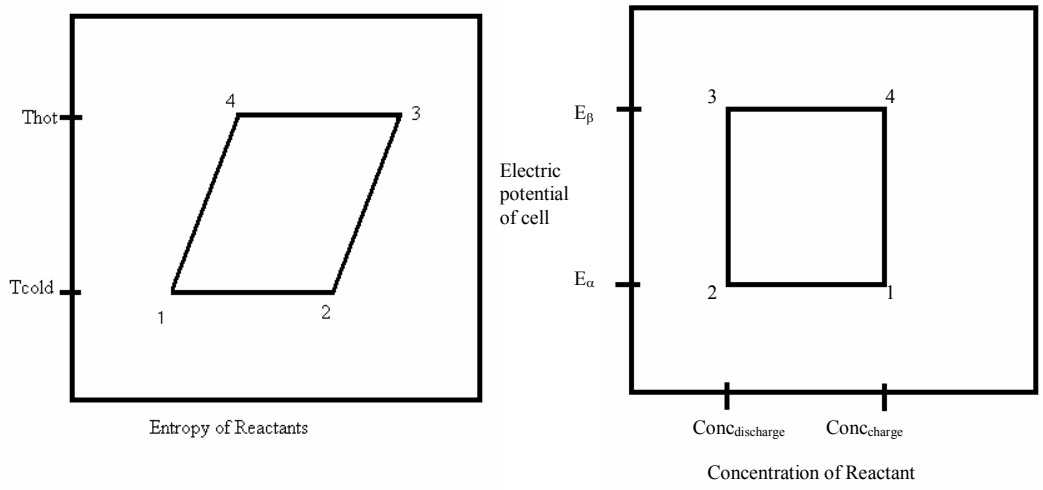

Figure 3.3.2 T-s and voltage-concentration diagrams for continuous flow electrochemical cooling system

On the cold side (1-2) of the cell the reaction proceeds as written above. Electricity is produced by the cell and heat is absorbed. On the hot side (3-4) the heat absorbed is rejected and the electricity generated on the cold side is consumed. The voltage from the cold side must be raised in order to drive the reaction in reverse at the higher temperature. The power input to the system is the current times the voltage difference. Heat is transferred between the four streams in one or two heat exchangers. This is depicted by processes 2-3 and 4-1. Since the heat capacities of the fluids are not equal, the slopes of 2-3 and 4-1 would not be equal as shown on the T-s diagram.

However, heat transfer between streams of different specific heats is a source of irreversibility and is discussed in section 3.4.1. Because one stream will not heat up or cool down sufficiently to reach the temperature of the reactor it is entering, a section of the reactor will be changing the temperature of the fluid instead of exclusively exchanging heat with the ambient.

Figure 3.3.3 depicts the Gibbs free energy versus temperature. This is the combined Gibbs free energy of the reduced and oxidized forms of the reactant in solution.

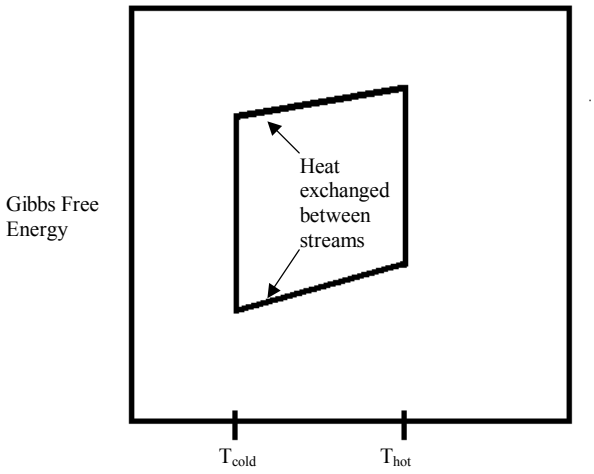

Figure 3.3.3 Temperature-Gibbs Free Energy diagram for continuous flow electrochemical cooling system

Another advantage of the continuous flow process over the batch process is that the reactors could be separately optimized for the temperature and reactions occurring. Different catalyst combinations, surface areas, etc. could be used for each electrode depending on operating temperature and whether reduction or oxidation occurs. The design of gas producing and a gas absorbing cells will certainly differ in the mass transport methods to and from the electrodes. In the batch process some type of less optimized design must be used so that it will perform adequately in forward and reverse modes.

3.4 Carnot COP Calculations

The theoretical equilibrium coefficient of performance (COP) of the continuous flow direct system can be calculated by several methods. The first method is adapted from an analysis of the performance of an electrochemical heat engine by Hammond (1980). The second method is original and uses the concept of solution activities.

3.4.1 Proof of Carnot Limitation after Hammond

The work put into the cycle per mole of reaction is equal to the difference between the electricity put in to the cold side and that returned from the hot side:

$$w=nF(E_h-E_c)=nF\Delta E \qquad 3.4.1.1$$

where E_h is the hot side cell electrical potential, E_c is the cold side voltage, ΔE is the difference between the two cell voltages, n is the number of electrons exchanged in the fundamental reaction, and F is the Faraday constant. Note that w is a negative quantity with the convention that positive work is work by the system. This analysis is for a system with cooling and electricity addition simultaneously. The analysis would also work with appropriate sign changes for a system that cools as it puts out electricity.

The work is also equal to the difference between the Gibbs free energy change of reaction on the hot side (ΔG_h) and the Gibbs free energy change of reaction on the cold side (ΔG_c).

$$w= \Delta G_h-\Delta G_c \qquad 3.4.1.2$$

This equation can be decomposed into the entropy changes of reaction (ΔS) and enthalpy change terms (ΔH) and regrouped as follows:

$$w= \Delta H_h-T_h\Delta S_h-(\Delta H_c-T_c\Delta S_c) \qquad 3.4.1.3a$$

$$w= \Delta H_h-T_h\Delta S_h+T_h\Delta S_c-T_h\Delta S_c-\Delta H_c+T_c\Delta S_c \qquad 3.4.1.3b$$

$$w= (T_c-T_h)\Delta S_c+T_h(\Delta S_c-\Delta S_h)+(\Delta H_h-\Delta H_c) \qquad 3.4.1.3c$$

$$w=-\Delta T\Delta S_c+T_h(\Delta S_c-\Delta S_h)+(\Delta H_h-\Delta H_c) \qquad 3.4.1.4d$$

The last two quantities may be substituted as follows:

$$\Delta H_h - \Delta H_c = \int_{T_c}^{T_h} (\Delta C_p) \, dT \qquad 3.4.1.5a$$

$$T_h \cdot (\Delta S_c - \Delta S_h) = -\int_{T_h}^{T_c} \left[\frac{\Delta C_p}{T}\right] dT \qquad 3.4.1.5b$$

These quantities are of opposite sign. Hammond assumes that they are of similar magnitude and cancel. He offers a calculation of these quantities for a specific case to justify this assumption. However, he does not offer a more general thermodynamic argument.

Both quantities could be assumed to equal zero by assuming that the entropy change of reaction and the enthalpy change of reaction do not significantly change with temperature over the range considered. This is equivalent to assuming that the temperature lift is small. Therefore, the reversible heat effect at the higher temperature is larger in absolute value because the temperature is higher. Consequently, the Gibbs free energy change of the reaction is lower at the higher temperature in reaction systems where the hot side produces electricity (or larger in magnitude where the cold side produces electricity). This argument is used by Kreysa (1990).

An alternative and more insightful view is that both quantities in 3.4.1.5 are zero if the change in specific heat during the reactions is zero. Therefore each flow has the same specific heat and the regenerative heat exchange process (2-3 and 4-1 in Figure 3.3.2) is ideal. A mismatch between the specific heats of these flows is the major source of irreversibility in the cycle. Liebhafsky (1959) discusses this in detail for a high temperature fuel cell-electrolyser system.

Therefore the reversible work is approximately equal to the difference between the heat absorbed on the low side and the heat rejected on the high side:

$$w=\Delta T\Delta S_c=Q_{3\text{-}4}-Q_{1\text{-}2} \qquad 3.4.1.6$$

The cooling COP is defined as the heat absorbed on the cold side over the work input:

$$COP= Q_{1\text{-}2}/w \qquad 3.4.1.7a$$

$$COP=Q_{1\text{-}2}/(Q_{3\text{-}4}-Q_{1\text{-}2})= T_c\Delta S_c/\Delta T\Delta S_c \qquad 3.4.1.7b$$

$$COP=T_c/(T_h-T_c) \qquad 3.4.1.7c$$

This COP is the same as that of the ideal Carnot refrigeration cycle and all other reversible cycles. By choosing a reaction with a small change in specific heat during reaction the Carnot efficiency can be approached.

3.4.2 Proof of Efficiency Limitation using Activities

The concept of thermodynamic activities can be used to derive the Carnot limitation for the electrochemical cycle. The activity adjusts property values to account for non-ideal behavior of a substance. For instance, the Gibbs free energy of a state can be calculated as:

$$G=G^0+RT\ln(a) \qquad 3.4.2.1$$

where G is the Gibbs free energy, G^0 is the Gibbs free energy at a standard state, R is the ideal gas constant, T is the temperature (the same as at G^0), and a is the activity. In a pure liquid or solid the activity equals 1, in an ideal gas the activity is the pressure divided by a reference pressure, and in an ideal solution it is the concentration divided by a reference concentration.

The overall energy use is again:

$$W_{in}=\Delta G_h+\Delta G_c \qquad 3.4.2.2$$

The cooling power is the reversible heat effect of the cold side reaction:

$$Q_{1\text{-}2}= T_c\Delta S_c \qquad 3.4.2.3$$

The overall cell reaction can be taken as:

$$\nu_\alpha A_\alpha+\nu_\beta A_\beta \leftrightarrow \nu_\gamma A_\gamma+\nu_\delta A_\delta \qquad 3.4.2.4$$

where the cold side reaction proceeds to the right and the hot side reaction proceeds to the left. The ν are the stoichiometric coefficients and α, β, γ, and δ designate the individual reactants and products. The half cell reactions are:

$$\nu_\delta A_\delta+\nu_\varepsilon e \leftrightarrow \nu_\beta A_\beta \qquad 3.4.2.5a$$

$$\nu_\alpha A_\alpha+\nu_\varepsilon e \leftrightarrow \nu_\gamma A_\gamma \qquad 3.4.2.5b$$

Using equation 3.4.2.1 the Gibbs free energy of the cold side reaction is calculated as:

$$\Delta G_c = \nu_\gamma G^0 + \nu_\delta G_\delta^0 - \nu_\beta G_\beta^0 - \nu_\alpha G_\alpha^0 + RT_c \ln\left(\frac{a_{\gamma c}^{\nu_\gamma} a_{\delta c}^{\nu_\delta}}{a_{\alpha c}^{\nu_\alpha} a_{\beta c}^{\nu_\beta}}\right) \qquad 3.4.2.6$$

using the cold side temperature as the reference temperature. However, this formula cannot be used for the hot side by simply exchanging reactants and products and changing the temperature. Another term must be added to account for the change in free energy due to the temperature change from the reference state.

The change in Gibbs free energy of reaction with temperature at constant pressure is equal to the entropy change of reaction:

$$\left(\frac{\delta G}{\delta T}\right)_P = \Delta S_c \qquad 3.4.2.7$$

If the entropy of reaction is taken as fairly constant over the temperature range in question, equation 3.4.2.6 can be integrated to obtain:

$$\Delta G_h-\Delta G_c=\Delta S_c(T_h-T_c)=\Delta S_c\Delta T \qquad 3.4.2.8$$

This term is added to the hot side equation to obtain the hot side Gibbs free energy of reaction:

$$\Delta G_h = \nu_\alpha G_\alpha^0 + \nu_\beta G_\beta^0 - \nu_\gamma G_\gamma^0 - \nu_\delta G_\delta^0 + RT_h \ln\left(\frac{a_{\alpha h}^{\nu_\alpha} a_{\beta h}^{\nu_\beta}}{a_{\gamma h}^{\nu_\gamma} a_{\delta h}^{\nu_\delta}}\right) + \Delta S_c(T_h - T_c) \qquad 3.4.2.9$$

When equation 3.4.2.6 and 3.4.2.9 are substituted into equation 3.4.2.2, the total electrical work input to the system is calculated:

$$W_{in} = RT_h \ln\left(\frac{a_{\alpha h}^{\nu_\alpha} a_{\beta h}^{\nu_\beta}}{a_{\gamma h}^{\nu_\gamma} a_{\delta h}^{\nu_\delta}}\right) - RT_c \ln\left(\frac{a_{\gamma c}^{\nu_\gamma} a_{\delta c}^{\nu_\delta}}{a_{\alpha c}^{\nu_\alpha} a_{\beta c}^{\nu_\beta}}\right) + \Delta S_c (T_h - T_c) \qquad 3.4.2.10$$

The cooling power (eq. 3.4.2.3) could be divided by the work input (eq. 3.4.2.10) to calculate the COP including the effect of activities. The stoichiometric coefficients ν_α and ν_γ are equal and ν_β equals ν_γ. The activities can be assumed to all be directly related to concentration in the same manner. For purposes of showing the Carnot limit, the concentrations of the reactants and products can be assumed equal. Therefore, the first two quantities in 3.4.2.9 equal zero and the electrical work input into the systems is the same as in the first derivation (eq. 3.4.1.6):

$$W_{in}=\Delta S_c(T_h-T_c) \qquad 3.4.2.11$$

The theoretical COP is the Carnot COP as derived before in equation 3.4.1.7.

3.5 Calculation of the Order of Magnitude of Various Design Parameters

The cooling power produced, assuming no losses, is directly proportional to the current. The current needed is large compared to the current in conventional refrigeration systems because the conversion between electrical and chemical units, the Faraday constant, is approximately 10^5. The order of magnitude of current needed to produce one watt of cooling is calculated by:

$$T \cdot \Delta S \cdot \frac{1}{F} \cdot i = 1 \cdot \text{Watt} \qquad 3.5.1$$

Assuming the temperature to be 300 K and the entropy change of reaction as 100 J/mol*K, the current needed per watt of cooling is 32 amps. For a lower entropy change, the required current increases e.g. 320 Amps/W for an entropy change of 10 J/mol*K. For the very high value of S of 250 J/mol*K, the current is still 13 Amps/Watt. These currents may seem high. However, the cells could be arranged in electrical series to gain a higher cooling power at lower total current. For example, if one cell each on high and low side requires a supplied current of 100 amp/watt cooling power at 0.1 volt, the same cooling power could be produced by1 amp at 100 volts for 100 cells in series. As power supplies are easier to build and have fewer losses at higher voltage and lower current, the cells in a real system will most likely have a series configuration.

The molar flow rate needed per watt of cooling is of the same order of magnitude as the molar flow in conventional refrigeration systems, because the entropy change of reaction is of the same order of magnitude as the entropy change due to refrigerant evaporation. The rate of reaction is the same as the mass flow rate of reactant needed to remain at steady state. The flow rate is simply:

$$\frac{1}{F} \cdot i = \text{ReactionRate} \qquad 3.5.2$$

Again assuming the temperature to be 300 K and the entropy change of reaction as 100 J/mol*K, the flow rate needed per watt of cooling is $3.3*10^{-5}$ mol/s. For a lower entropy change, the required flow rate increases, e.g. $3.3*10^{-4}$ mol/s for an entropy change of 10 J/mol*K. For the very high value of S of 250 J/mol*K, the reaction rate is only $1.3*10^{-5}$ mol/s. For comparison, the entropy change of vaporization for R134a at 25º C is 60.8 KJ/kmol*K.

Electrical power recycled between cells is 10-100 times that of the energy added to the system. The voltage of each cell is about one volt. However, the voltage difference between the cells is 10-100 times smaller. Therefore, the electrical energy added to the system is of a similar order of magnitude as the heat absorbed or rejected by the system for reasonable temperature lifts. This can be seen directly from the Carnot COP. For a system with large irreversibilities the energy added may be significantly larger than the heat transferred.

3.6 Conclusions

A continuous flow DERC is described. By choosing a reaction with a small change in specific heat during reaction the Carnot efficiency can be approached. A mismatch between the specific heats of the flows in the regenerative heat exchange is the major source of irreversibility in the cycle. The energy recycled within the DERC is much larger than the heat transferred or the electricity added to the system.

Chapter 4. Simplified Effects of Losses

4.1 Introduction

The electricity recycled in the DERC is much larger than the energy input to the system. The sensitivity of the system to small inefficiencies in the internal energy cycling is modeled. In addition, a DERC is modeled assuming that the electrochemical cells have a constant internal resistance

4.2 Estimation of the Effect of Cell Efficiency on Cycle COP

4.2.1 Introduction

The direct electrochemical refrigeration cycle can ideally reach Carnot COP. The electricity that is produced by one cell and consumed by the other cancels out and does not affect the ideal COP calculation. However, the flow of electrical energy is 10 to 100 times larger than the heat absorbed or rejected by the system and a similar number of orders of magnitude larger than the electrical input to the system. Therefore, a small inefficiency in the consumption or production of electricity greatly decreases the overall cycle efficiency.

4.2.2 Model Description

However, the sensitivity of the cycle to losses can be derived algebraically. The loss is assumed to be a fraction of the power sent through each cell:

$$loss = 2 \cdot V \cdot i_{tot} \cdot factor \qquad 4.2.2.1$$

where loss is the irreversibility per m^2 of electrode frontal surface area, V is the cell voltage, i_{tot} is the current density (amp/m^2), and factor is the fraction of the power flowing through the cell that is lost. Multiplying the equation by 2 accounts for both cells by assuming the loss is the same in each. The voltage of each cell is assumed to be 1 volt as a reasonable order of magnitude for electrochemical couples. The fact that the two cells should have different voltages due to the difference in temperatures does not significantly affect the model results or conclusions. The energy input to the cycle is handled without the explicit statement of cell voltages.

The non-ideal COP (COP_{actual}) is:

$$COP_{actual} = \frac{Coolpower}{W_{actual}} \qquad 4.2.2.2$$

where Coolpower is the heat absorbed on the cold side and W_{actual} is the non-ideal power consumed. These two quantities can be expanded into the ideal components ($heat_{flux}$ and W_{carnot}) and the loss contributions:

$$COP_{actual} = \frac{heat_{flux} - \frac{loss}{2}}{W_{carnot} + loss} \qquad 4.2.2.3$$

The total loss adds to the work put into the cycle. However, only the half of the loss expended on the cold side decreases the cooling power. The equation can be expanded further, as the ideal work input is related to the ideal heat flux and Carnot COP:

$$COP_{actual} = \frac{heat_{flux} - \frac{loss}{2}}{\frac{heat_{flux}}{COP_{carnot}} + loss} \qquad 4.2.2.4$$

All of the quantities can be expressed in terms of the current density and current density cancels out:

$$COP_{actual} = \frac{\frac{T \cdot \Delta S \cdot i_{tot}}{F} - V \cdot i_{tot} \cdot factor}{\frac{T \cdot \Delta S \cdot i_{tot}}{F \cdot COP_{carnot}} + 2 \cdot V \cdot i_{tot} \cdot factor} \qquad 4.2.2.5$$

$$COP_{actual} = \frac{\frac{T \cdot \Delta S}{F} - V \cdot factor}{\frac{T \cdot \Delta S}{F \cdot COP_{carnot}} + 2 \cdot V \cdot factor} \qquad 4.2.2.6$$

This final equation shows the influence of temperature, entropy change of reaction, loss fraction, and cell voltage.

Some additional calculations were made were made using a model based on the pumping and resistance loss tradeoff model described in Chapter 5. The major difference was that the loss was not calculated from transport properties. Instead, the loss was assumed to be a fraction of the power sent through each cell as in equation 4.2.2.1. The calculation of COP, work, and second law efficiency were the same as in the other model. The cooling rate and current were included in this model, although they drop out as shown above. The computed solution was virtually identical to that from the algebraic solution, equation 4.2.2.6. There was a slight offset in the solution most likely due to the numerical solution method and convergence criteria.

4.2.3 Results and Conclusions

The second law efficiency decreases with increasing loss fraction and decreasing magnitude of the entropy change of reaction (see Figure 4.2.3.1).

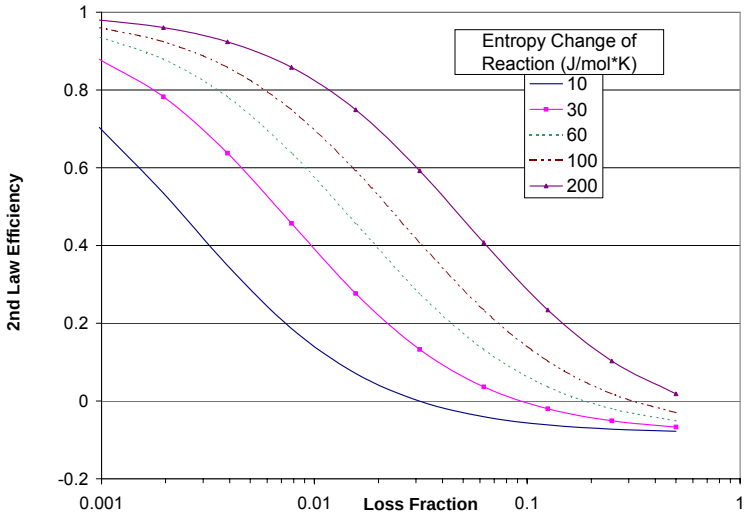

Figure 4.2.3.1 Second law efficiency versus loss fraction with varying entropy change of reaction.

This analysis also demonstrates that a higher entropy change of reaction with respect to the Gibbs free energy change leads to a higher COP at a constant loss fraction and temperature, because the reversible heat effect is larger in proportion to the energy cycled (see equation 3.6.2.6). In addition, the cycle will operate better at a higher temperature given a constant entropy change of reaction, for the same reason. In cases where the entropy change of reaction increases with temperature, the increase in COP is compounded. However, the need for a cooling cycle

decreases with temperature especially as the temperature of the cooled body exceeds the ambient temperature. In an unusual case where the entropy change decreases with temperature, the two effects partially cancel each other.

It may appear that a lower cell voltage is better due to the lower amount of energy cycled through the system. However, the losses are generally due to the absolute magnitude of deviations from the equilibrium voltage and not the magnitude of the cell voltage. This calculation could be reformulated by assuming that the voltage increases with increasing loss factor. However, the conclusions would be substantially the same.

4.3 Linear Resistance Model

Rough estimates of the performance of a real system can be made by assuming that the electrochemical cells (see Figure 4.3.1, cell 1 and cell 2) each have a constant internal resistance (R_{hot} and R_{cold} respectively). This model is similar to one proposed by Hammond (1980) for an electrochemical heat engine. This assumption is reasonable, because the cells will probably operate at low currents. Therefore, the kinetic and other non-linear losses can be lumped with the ohmic resistance. This assumption is also valid where the ohmic resistance dominates. As the cells are connected in series their resistances may be summed to obtain the total circuit resistance, R_{tot}. Resistances of the connecting wires can be ignored or viewed as included in these values.

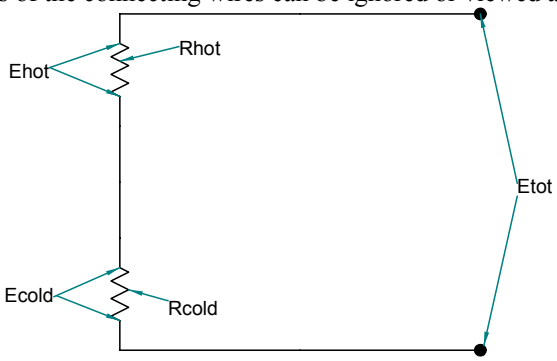

Figure 4.3.1 Simple cell model with constant resistance

When the voltage applied by the power supply equals the sum of thermodynamic equilibrium voltages of the two cells (E_{equib}), no net current flows and there are no resistance losses. The Carnot COP is achieved at an infinitesimal current flow subject to the assumptions in section 3.4. As the applied voltage increases, current begins to flow proportional to the total overvoltage (E_{over}), the difference between the actual potential and the equilibrium potential as determined by thermodynamics.

The increase in applied voltage causes the COP to drop. The reaction rate is assumed to be directly proportional to the current flow with 100% current efficiency. Therefore, the cooling power without losses ($Q_{coldequib}$) increases linearly with current:

$$Q_{coldequib} = I\frac{1}{nF}\Delta S_{cold} T_{cold} \qquad 4.3.1$$

However, the losses increase quadratically with current:

$$P_{coldloss} = I^2 R_{cold} \qquad 4.3.2$$

Eventually, the losses dominate and the total cooling power decreases. The total cooling power is:

$$Q_{coldequib} = I\frac{1}{nF}\Delta S_{cold} T_{cold} + I^2 R_{cold} \qquad 4.3.3a\ Q(current)$$

$$Q_{coldequib} = \frac{E_{over}}{R_{tot}} \frac{\Delta S_{cold} T_{cold}}{nF} + \left(\frac{E_{over}}{R_{tot}} \right)^2 R_{cold} \qquad \text{4.3.3b Q(voltage)}$$

The derivative of the cooling power with respect to overvoltage can be taken and set equal to zero in order to calculate the point of maximum cooling power:

$$\frac{dQ_{coldtot}}{dE_{over}} = \frac{\Delta S_{cold} T_{cold}}{nF} + \frac{E_{over}}{R_{tot}} R_{cold} \qquad \text{4.3.5}$$

The overvoltage at maximum cooling power is:

$$E_{over@Qmax} = \frac{-1}{2} \left(\frac{R_{tot}}{R_{cold}} \right) \frac{\Delta S_{cold} T_{cold}}{nF} \qquad \text{4.3.4}$$

The total electrical work input to the system is:

$$W_{in} = I_{tot} (\pm E_{coldequib} \mp E_{hotequib} + IR_{cold} + IR) \qquad \text{4.3.6a}$$

$$W_{in} = \frac{E_{over}}{R_{tot}} (E_{totequib} + IR_{tot}) \qquad \text{4.3.6b}$$

$$W_{in} = \frac{E_{over}}{R_{tot}} (E_{totequib} + E_{over}) \qquad \text{4.3.6c}$$

Therefore the refrigeration COP is:

$$COP_R = \frac{\frac{\Delta S_{cold} T_{cold}}{nF} + \frac{E_{over}}{R_{tot}} R_{cold}}{E_{totequib} + E_{over}} \qquad \text{4.3.7}$$

These calculations show the functional form of the system's performance. assuming that the resistance is constant. However, it says nothing about the size of the loss. The resistance value must be calculated from transport and kinetic properties. More complex models of this type are presented later and the results will be compared to the linear resistance model.

4.4 Conclusions

The heat exchanged with the environment and the electricity cycled within the system are closer in magnitude with a large entropy change of reaction. Therefore the cycle is less sensitive to losses with a larger entropy change of reaction. Assuming the resistance of the circuit as a constant, the total heat absorbed on the cold side is quadratically dependent on the current.

Chapter 5. Pumping and Resistance Loss Trade-Offs

5.1 Introduction

A simplified model was developed to estimate the spacing of electrode plates in a stacked plate design. Two of the main factors affecting the electrode spacing are the resistance loss, which increases with plate spacing and pumping losses that decrease with plate spacing. Both of these issues are addressed in rudimentary ways in the following model. EES (Engineering Equation Solver), a Newton-Raphson software package, was used to simultaneously solve the equation sets (Klein 2003). This particular model does not address mass transfer limitations and heat exchanger effects, which are treated in Chapter 6.

5.2 Pumping and Resistance Loss Model Description

The electrochemical cell is represented as two parallel infinite flat plates. The velocity profile is assumed to be fully developed Poiseuille flow. The electrolyte and electrodes are assumed isothermal. The overall performance of the system is assumed to be Carnot behavior minus resistance and pumping power losses.

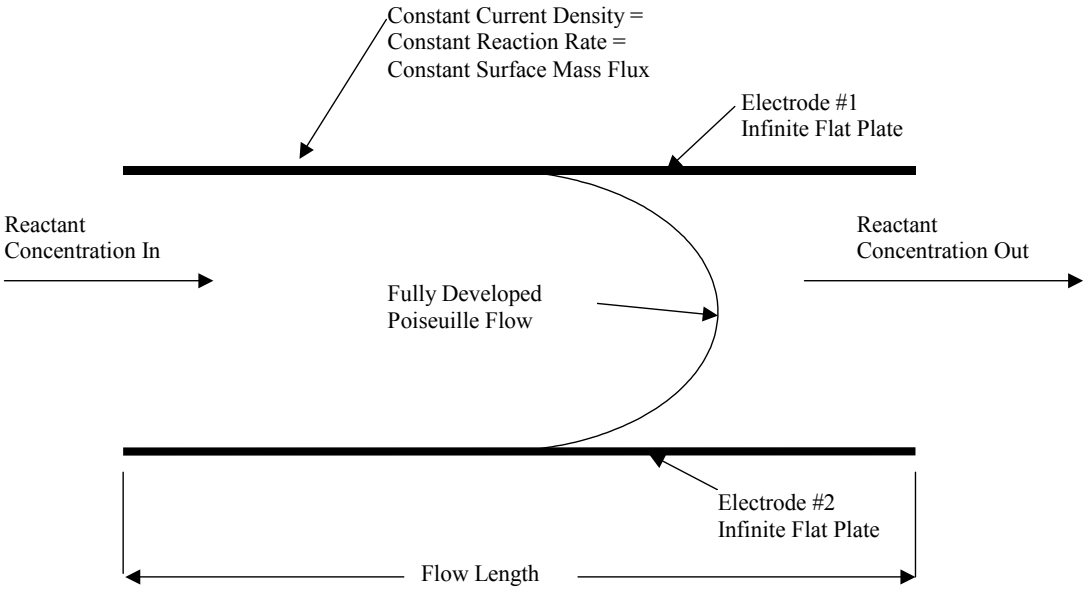

Figure 5.1.1 Schematic of simplified cooling system modeled as a flow between infinite parallel flat plate electrodes

The current density is assumed constant over the whole plate. Over a specified distance in the flow direction the concentration of the reactants drops by a set amount. In all the calculations presented here the concentration is arbitrarily assumed to drop 1 (mole/liter)/m. The reaction rate is related to the current density (i_{tot}):

$$i_{tot} = \frac{9.648670E7 \quad [Coulomb/kmole]}{1000} \cdot Reaction_{rate} \qquad 5.2.1$$

where the numerical quantity is the Faraday constant. The reversible heat effect is calculated as:

$$heat_{effect} = T_c \cdot \Delta S \qquad 5.2.2$$

where T_c is the cold side temperature. The ΔS is the entropy change of reaction and is assumed to be 100 J/(mole*K). The reaction rate, heat flux, and heat effect are related by:

$$\text{Reaction}_{rate} = \frac{\text{heat}_{flux}}{\text{heat}_{effect}} \qquad 5.2.3$$

The heat flux calculated in this equation is the cooling power due to the reversible heat effect. However, the actual cooling flux is reduced by any losses on the cold side.

The total loss is twice the individual losses on the hot and cold sides. The losses of each cell are assumed identical and not affected by temperature. The losses per unit electrode area equal the resistance heating plus the viscous dissipation:

$$\text{loss} = 2 \cdot \left[\text{Resistance} \cdot i_{tot}^{\,2} + \frac{\text{Viscous}_{dissipation}}{\text{unitmeter}} \right] \qquad 5.2.4$$

The unitmeter variable is to account for the depth of the electrode into the page (perpendicular to the flow and electrode height). This variable is needed for the program's internal unit checking.

The cell resistance is the electrolyte resistivity times the electrode spacing:

$$\text{Resistance} = ro_e \cdot \text{thickness} \qquad 5.2.5$$

Except where noted, the electrical resistivity of the electrolyte solution is arbitrarily assumed as 0.25 ohm*m approximately in the middle of the range of seawater.

The mass average velocity is calculated by:

$$0 = \text{Conc}_{in} \cdot \text{vel}_{avg} \cdot \text{thickness} - \text{Reaction}_{rate} \cdot \text{distance}_{conc} \qquad 5.2.6$$

The difference between the two quantities is zero because both are the rate at which reactant is removed from a volume of solution flowing through the electrode gap. The concentration drop in the section ($conc_{in}$) times the volumetric flow rate per unit depth (vel_{avg} times the thickness) equals the reaction rate per unit area times the distance ($distance_{conc}$) the solution travels before it is depleted by the concentration drop $conc_{in}$.

The viscous dissipation was calculated by two different methods. In both, the solution viscosity is assumed as that of water at the cold side temperature.

The first method uses the exact Pouiseulle flow solution for infinite flat plates. The pressure gradient is calculated by:

$$\text{GradP} = \frac{12 \cdot \text{vel}_{avg} \cdot \textbf{Visc}\left['\text{Water}', P = \frac{101.325\ [\text{kPa}]}{1000}, T = T_c\right]}{-\text{thickness}^{\,2}} \qquad 5.2.7$$

where the dynamic viscosity is obtained from the EES internal function Visc. The dissipation is then calculated as:

$$\text{Viscous}_{dissipation} = \text{thickness}^{\,3} \cdot \frac{\text{GradP}^{\,2}}{3 \cdot \textbf{Visc}\left['\text{Water}', P = \frac{101.325\ [\text{kPa}]}{1000}, T = T_c\right]} \qquad 5.2.8$$

The second method uses an EES library routine to calculate the friction factor from the Moody chart. The subroutine uses the laminar flow result of f=64/Re and the Colebrook formula for Reynolds numbers over 2100.

The hydraulic diameter (D), density(ρ_{fluid}), friction factor, and Reynolds number are calculated as follows:

$$f = \mathbf{MoodyChart}(Re, rough) \tag{5.2.9}$$

$$\rho_{fluid} = \rho\left['Water', P = \frac{101.325\ [kPa]}{1000}, T = T_c\right] \tag{5.2.10}$$

$$D = 2 \cdot thickness \tag{5.2.11}$$

$$Re = \rho_{fluid} \cdot vel_{avg} \cdot \frac{D}{\mathbf{Visc}\left['Water', P = \frac{101.325\ [kPa]}{1000}, T = T_c\right]} \tag{5.2.12}$$

The density is taken as that of water and no adjustment is made for the solute. However, the effect of density is only in the Reynolds number and otherwise cancels out of the other formulas. The Reynolds number never exceeds one even at unrealistically high flow rates. Therefore the assumption of water density does not affect the final solution and laminar flow is dominant. The pressure drop loss is calculated as:

$$Viscous_{dissipation} = \rho_{fluid} \cdot f \cdot \frac{vel_{avg}^2}{2 \cdot D} \cdot vel_{avg} \cdot thickness \cdot unitmeter \tag{5.2.13}$$

The Carnot COP is calculated by:

$$COP_{Carnot} = \frac{T_c}{T_h - T_c} \tag{5.2.14}$$

where T_h is the hot side temperature. The work needed to operate the system at the reversible limit is calculated from the Carnot COP:

$$W_{Carnot} = \frac{heat_{flux}}{COP_{Carnot}} \tag{5.2.15}$$

The actual work expended to drive the system is determined by the Carnot work plus the losses:

$$W_{actual} = W_{Carnot} + loss \tag{5.2.16}$$

The actual cooling power is the ideal heat flux calculated above minus the losses:

$$Coolpower = heat_{flux} - \frac{loss}{2} \tag{5.2.17}$$

Therefore the computed non-ideal COP is:

$$COP_{actual} = \frac{Coolpower}{W_{actual}} \tag{5.2.18}$$

and the second law efficiency is:

$$\eta_{2ndlaw} = \frac{COP_{actual}}{COP_{Carnot}} \tag{5.2.19}$$

The volumetric cooling power is calculated by:

$$Vol_{Coolpower} = \frac{Coolpower}{thickness} \tag{5.2.20}$$

5.3 Pumping and Resistance Loss Model Results

Assuming constant current density and laminar flow, the channel height for optimal COP is uniquely determined by the transport properties of the solution (viscosity and electrical conductivity) and the change in concentration per distance. The optimal plate spacing is independent of heat flux or current density, because losses due to resistance and viscous dissipation are both quadratic in volumetric flow or current and cancel out. Volumetric flow and current are proportional under the constraints given. Losses due to viscous dissipation are proportional to the negative second power of the thickness and ohmic losses are quadratically related to the thickness. This means that for a given length of channel the channel size can be optimized for all flow and cooling rates.

Figures 5.3.1 and 5.3.2 show the COP and cooling power as a function of thickness while holding the other variables constant. The maximum in cooling power and COP occur at the same thickness. For plate spacing less than the optimum, pressure losses dominant and above the optimum electrical resistance losses dominate. The cooling power and COP drop off dramatically with size reductions below the optimum using the given values for resistivity and viscosity. Therefore the system performance is more sensitive to reductions in size than to increases and it would be better to err in making the system slightly too thick than slightly too thin.

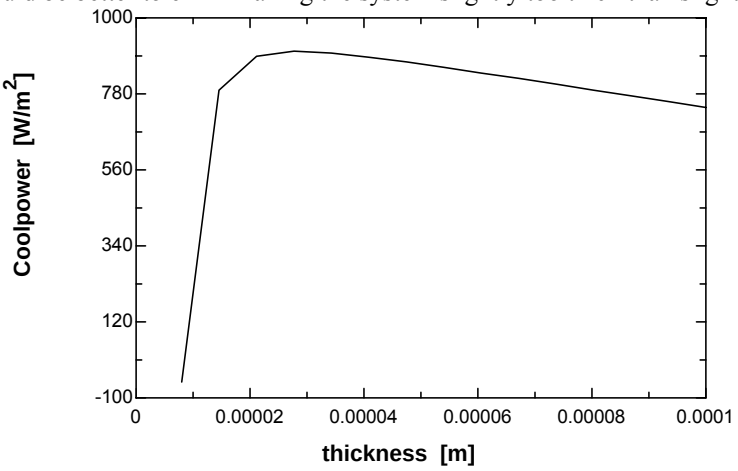

Figure 5.3.1 Computed cooling power versus thickness for a fixed electrolyte resistivity (0.25 Ohm*m), viscosity ($9.9x10^{-6}$ kg/m*s), and current density (3216 A/m^2).

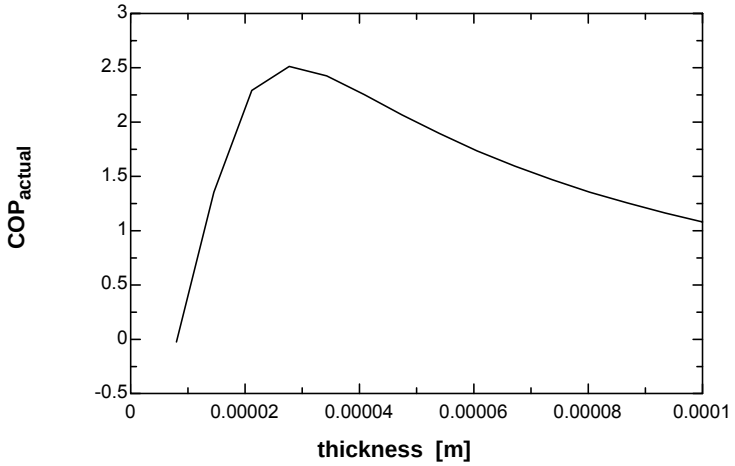

Figure 5.3.2 Computed COP versus thickness for a fixed electrolyte resistivity (0.25 Ohm*m), viscosity ($9.9x10^{-6}$ kg/m*s), and current density (3216 A/m^2).

Figure 5.3.3 shows the same quadratic dependence of cooling power on current density as presented in Chapter 4. The viscous dissipation simply adds a constant to quadratic term in the formula for the parabola, shifting it downward. This quadratic relationship is realistic and has been demonstrated in other electrochemical systems such as solid oxide fuel cells (e.g. Gorte,

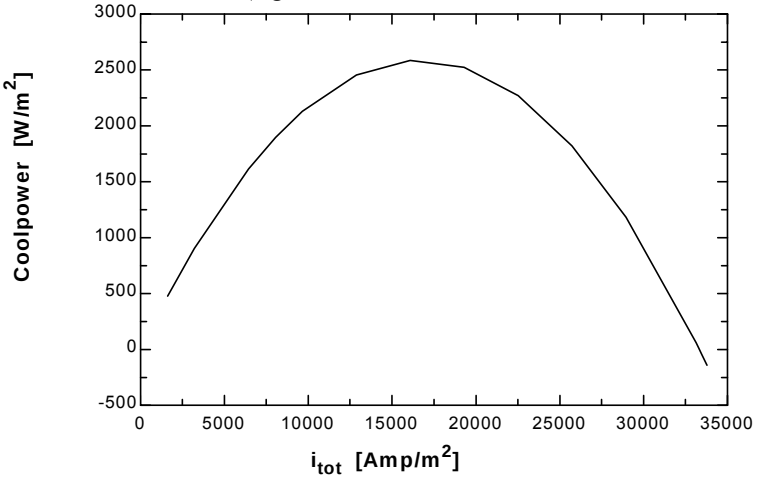

2002).

Figure 5.3.3 Computed cooling power produced versus current density for a fixed thickness ($28x10^{-6}$ m), electrolyte resistivity (0.25 Ohm*m), and viscosity ($9.9x10^{-6}$ kg/m*s)

The calculated COP drops off with increasing current as expected (see Figure 5.3.4). A general property of the models used in this study is that the maximum cooling capacity happens at a COP lower than those achievable by traditional systems. The system could be run at a high power and low COP for transient temperature pull down. It could then be run at a lower current density for holding the temperature steady and a dramatically higher COP. Many actual electrochemical systems adjust rapidly to shifting loads and in fact show more efficient performance at lower current density. There appear to be no technical reasons why a DERC could not perform with a continuously variable cooling power. This would eliminate the cycling and start up losses inherent in single speed vapor compression systems.

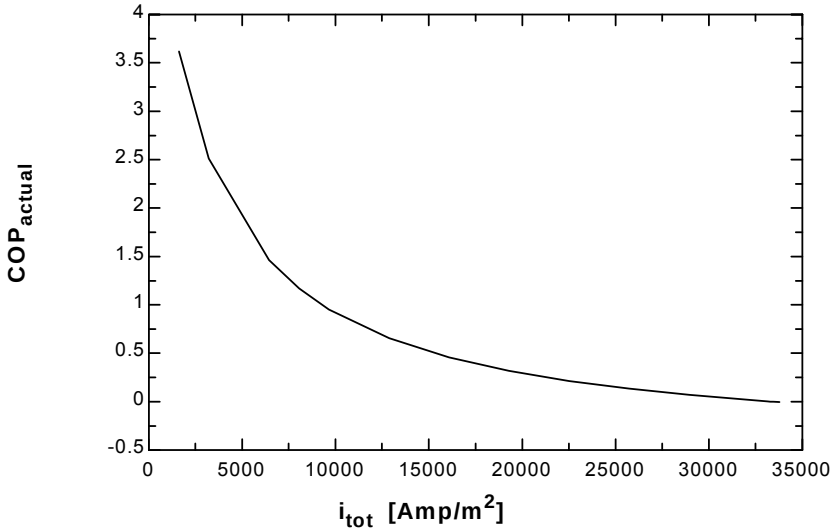

Figure 5.3.4 Computed COP versus current density for a fixed thickness ($28x10^{-6}$ m), electrolyte resistivity (0.25 Ohm*m), and viscosity ($9.9x10^{-6}$ kg/m*s)

The cooling power decreases linearly with electrolyte resistivity (Figure 5.3.5) because the Ohmic loss is linear in resistance. The COP likewise decreases as $1/\rho$, where ρ is resistivity (Figure 5.3.6). The optimal electrode spacing decreases with increasing resistivity (Figure 5.3.7).

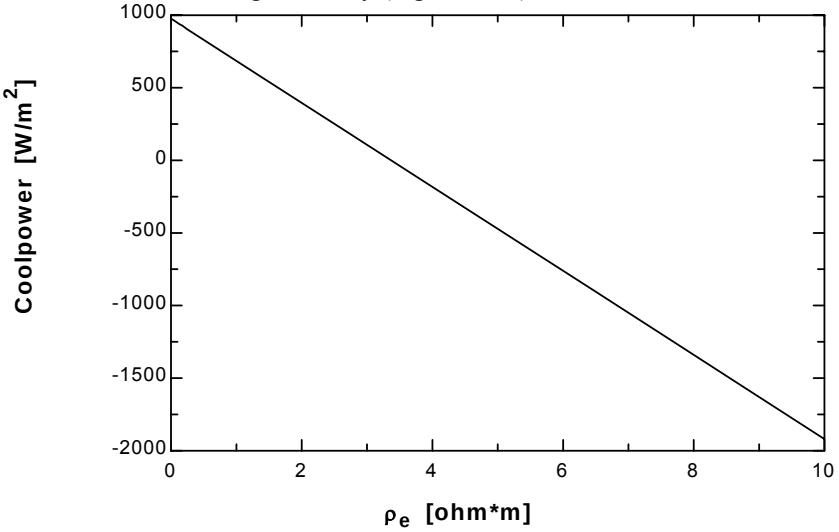

Figure 5.3.5 Computed cooling power decreases linearly with increasing electrolyte resistivity for a fixed thickness (28×10^{-6} m), viscosity (9.9×10^{-6} kg/m*s), and current density (3216 A/m^2).

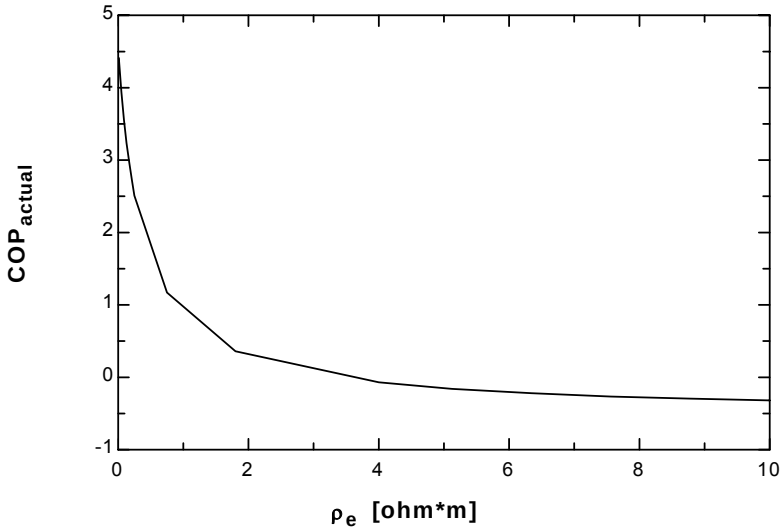

Figure 5.3.6 Computed COP decreases with increasing electrolyte resistivity for a fixed thickness (28×10^{-6} m), viscosity (9.9×10^{-6} kg/m*s), and current density (3216 A/m^2).

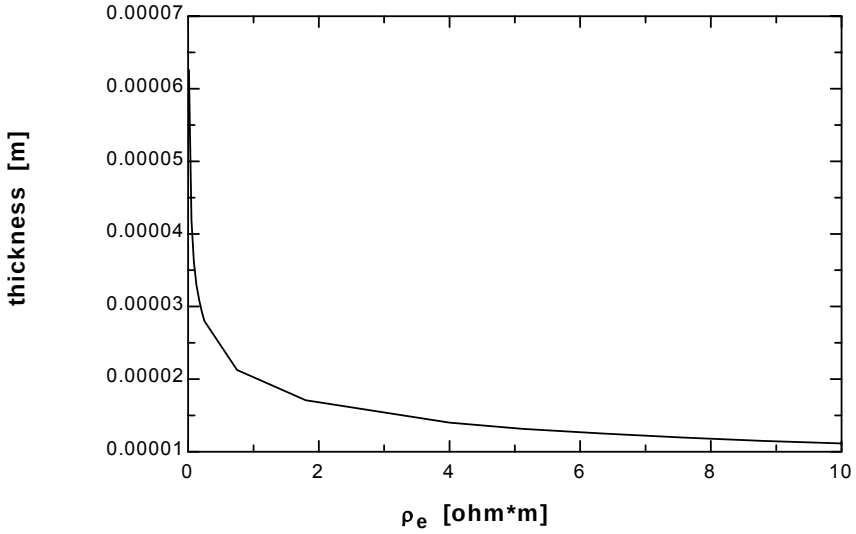

Figure 5.3.7 Optimal thickness for highest COP versus electrolyte resistivity for a fixed thickness ($28x10^{-6}$ m), viscosity ($9.9x10^{-6}$ kg/m*s) and current density (3216 A/m^2).

The effects of increasing electrolyte viscosity on COP and net cooling power mimic that of increasing resistivity (Figures 5.3.8 and 5.3.9). However, an increase in viscosity favors a wider electrode gap (Figure 5.3.10).

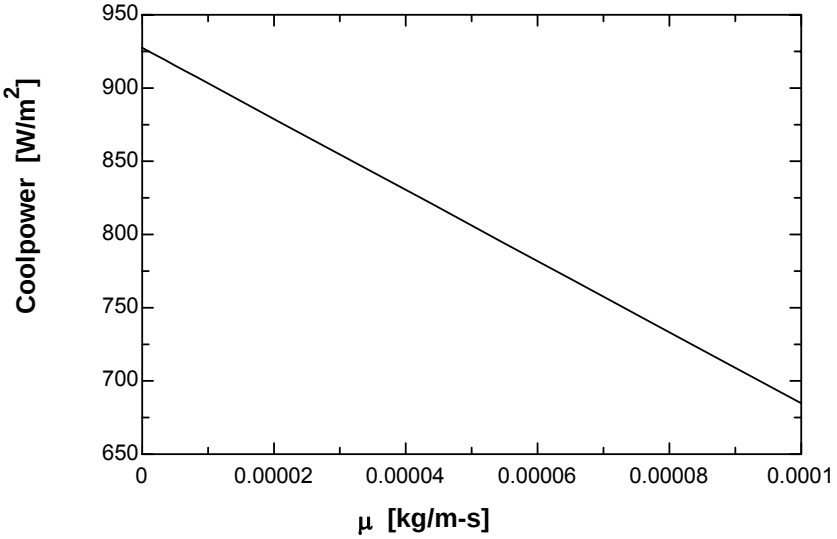

Figure 5.3.8 Computed cooling power decreases linearly with increasing electrolyte viscosity for a fixed thickness ($28x10^{-6}$ m), viscosity ($9.9x10^{-6}$ kg/m*s), and current density (3216 A/m^2).

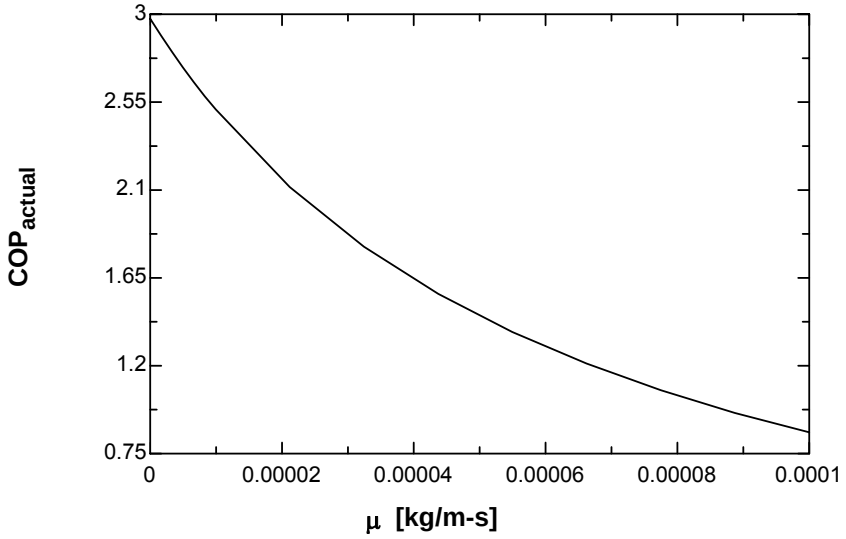

Figure 5.3.9 Computed COP decreases with increasing electrolyte viscosity for a fixed thickness ($28x10^{-6}$ m), electrolyte resistivity (0.25 Ohm*m), and current density (3216 A/m^2).

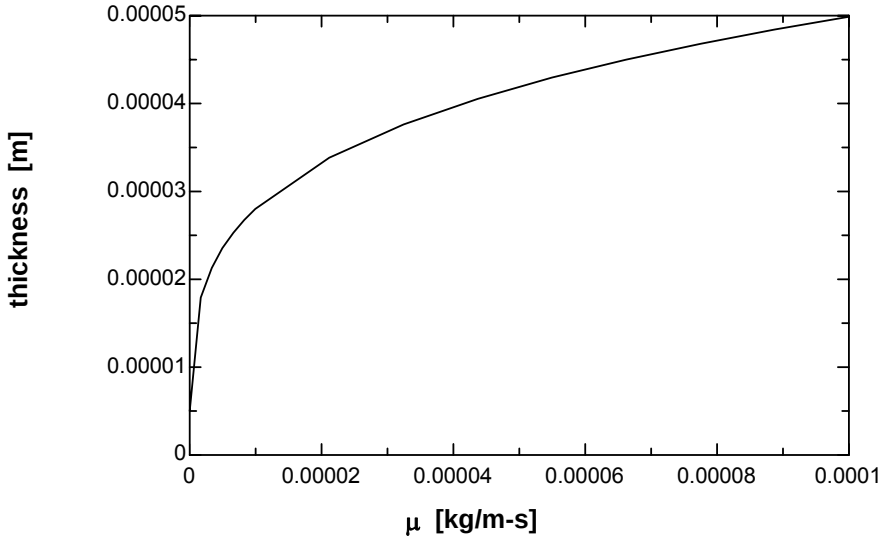

Figure 5.3.10 Optimal thickness for highest COP versus electrolyte viscosity for a fixed thickness ($28x10^{-6}$ m), electrolyte resistivity (0.25 Ohm*m), and current density (3216 A/m^2).

Resistivity changes in realistic range can cause negation of cooling effect. Viscosity changes for an aqueous solution within a reasonable range generally still allow a cooling effect. Therefore attention should be directed more towards improving conductivity than viscosity. A possible avenue towards reducing resistance is the use of room temperature molten salt systems as discussed in Chapter 8.

5.4 Conclusions

With the modeling assumptions presented in this chapter, an optimal channel size on the order of tens of microns can be computed depending on the electrical resistivity and viscosity. The current cooling power curve is a parabola and at some current the resistance and pumping losses dominate over the cooling effect. The maximum cooling flux is on the order of 1000 W/m^2.

However, some of these conclusions are dependent on the assumption of two parallel plate electrodes with flow between them. The conclusions may differ somewhat for other configurations, such as flow through porous electrodes or electrodes attached to a membrane with new solution flowing on the outside of the electrode-membrane assembly.

Chapter 6. Complex Model

6.1 Introduction

A model of the continuous flow direct electrochemical refrigeration system more detailed than those described in the previous chapter has been developed. The model calculates the theoretical equilibrium performance and losses including kinetic, pumping, ohmic resistance, and mass transport losses. This model is more sophisticated than a "back of the envelope" calculation. However, it is not intended to accurately match any specific system. This model is a tool for further exploring the feasibility of electrochemical systems and estimating the relative importance of various effects.

6.2 Reactions Modeled

Published thermodynamic and kinetic data for the aqueous reaction $Fe^{2+} + Mn^{3+} \Leftrightarrow Fe^{3+} + Mn^{2+}$ are used in this model to ensure that the results are reasonable. This reaction is simply an example of a typical reaction that could be used and has values similar to other transition metal redox reactions. In addition, the data for this reaction was readily available. However, the solubility limits of the reactants are ignored in this study. It is by no means proposed that this reaction is optimal or superior to other couples.

6.3 Model Plan

This model was written with EES (Engineering Equation Solver), a Newton-Raphson software package, used with other models in this work (Klein 2003).

To simplify calculations the cells were viewed as parallel plate reactors in fully developed laminar flow as in Chapter 5. The nominal length of the cells in the flow direction was one meter and calculations were conducted on unit meter depth perpendicular to the electrolyte flow and the current. The electrodes were viewed as rough or porous with a surface area approximately 1500 times that of the nominal projected area.

The equations for the hot and cold side are identical for most of the losses and are written using a duplicate command that copies the needed equations without rewriting them. In the following equations this will be noted by the annotation "for j = 1 to 2." The cold side is 1 and the hot side 2.

The current efficiency is assumed to be 100%. All electrons that pass through the circuitry participate in the desired reactions. There are no side reactions. The total current in both cells is the same. For this model the cells are assumed identical in size and therefore the current density is the same in both.

6.4 Thermodynamic State Calculations

The changes in the thermodynamic state of the working fluid are assumed to be wholly determined by the thermodynamic states of the cations. The change in the oxidation state of the cations is assumed to not affect the state of the anions or water. The cations' states are calculated as functions of temperature only. Concentration effects and any solvent or anion effects are ignored. The enthalpies of the cations are calculated by linear least squares fits to data from Barner (1978):

$$h := h_0 + C_p \cdot (T - 298.15) \qquad 6.4.1$$

where h is the molar enthalpy, h_0 is the molar enthalpy at 25°C, C_p is the specific heat, and T is the temperature. The entropy of the cations is calculated by:

$$s := s_0 + C_p \cdot \ln\left[\frac{T}{298.15}\right] \qquad 6.4.2$$

where s_0 is the molar entropy at 25°C taken from Barner (1978). The molar Gibbs free energy is calculated from its definition:

$$g := h_{in} - s_{in} \cdot T_{in} \qquad 6.4.3$$

The g, h, and s are all calculated by functions that take the variables on the right hand side of the above equations as inputs.

6.5 Cell Equilibrium and Nernst Potentials

The equilibrium potentials of the cells are calculated from the Gibbs free energy of reaction. For the kinetic model used it was convenient to separately calculate the potential of each half cell reaction with respect to the standard hydrogen electrode (SHE). The SHE is the accepted primary reference for electrochemical reactions and is defined as the potential of the hydrogen evolution or disassociation reaction, i.e:

$$2H^+ + 2e^- \rightarrow 2H_2 \qquad 6.5.1$$

when the H_2 is at unit activity. The potential of each half cell was calculated as the potential of a hypothetical cell where one half reaction is the reaction in question and the other reaction is the SHE. The hydrogen reactions cancel each other in the calculation of the overall cell potential. The electrode potential at standard state for one electrode is calculated by:

$$E_{0A} := \frac{-(2 \cdot \mathbf{g}(h_{Aox}, s_{Aox}, T) + \mathbf{g}(h_{H2}, s_{H2}, T) - 2 \cdot \mathbf{g}(h_{Ared}, s_{Ared}, T))}{2 \cdot \frac{9.648670E7 \quad [Coulomb/kmole]}{1000}} \qquad 6.5.2$$

where 2 is the number of electrons involved in the reaction, the Faraday constant (96485 coulombs/mole) is divided by 1000 to maintain the proper order of magnitude of the units, and E_0 is the equilibrium voltage of the system. Although the reaction on the hot side is reversed, the same equation was used for the potential. The sign of the potential was handled separately with a variable, $sign_j$.

The effect of concentration on the cell potential was modeled using the Nernst equation (Prentice, 1991). The Nernst equation is typically written with a natural logarithm. However, during computation of the solution, the natural logarithm might be evaluated at a negative input causing an error. Therefore the equation was rearranged as:

$$\mathbf{exp}(f_{s,j} \cdot n \cdot (E_{0A,j} - E_{nernstA,j})) = \frac{Conc_j][2}{Conc_j][1} \qquad \text{for } j = 1 \text{ to } 2 \qquad 6.5.4$$

The subscript A refers to one of the reaction couples. A similar equation was used for the other electrode with a subscript B. The two electrode voltages were summed to get the overall Nernst voltage:

$$E_{nernsttot,j} = E_{nernstA,j} + E_{nernstB,j} \qquad \text{for } j = 1 \text{ to } 2 \qquad 6.5.5$$

6.6 Heat Effect Calculation

The entropy change of reaction in a cell is calculated by:

$$\Delta S := s_{Aox} + s_{Bred} - s_{Ared} - s_{Box} \qquad 6.6.1$$

where the ox and red subscripts refer to the oxidized and reduced forms of the reactants.

The reversible heat effect was calculated as the change of entropy due to the complete cell reaction times the cell temperature:

$$Heateffect := T \cdot \Delta S \qquad 6.6.2$$

The cold side heat effect is the maximum cooling power of the system per mole of reaction. Only the cold side heat effect is needed in the model, as the heat rejection is not important to the refrigeration model. However, this would need to be included for a heat pump model.

6.7 Electrode Kinetics Model

There is a chemical kinetic barrier to the electrode reactions proceeding. The chemical reaction can be driven faster by increasing the overpotential to overcome this barrier. The non-spontaneous electrochemical reactions in the electrolytic cell can be driven faster by increasing the applied cell voltage above the equilibrium voltage. The excess energy needed to drive the reaction is a loss. Conversely, the voltage produced by the spontaneous reaction in the galvanic cell is decreased due to these kinetic losses.

The cell kinetics were modeled using the Butler-Volmer equation, a standard equation for electrochemical kinetics. The reaction rate is a function of the electrode overpotential, the difference between the potential as determined by thermodynamics and the actual potential. The overpotential (ε) for one reaction is:

$$\varepsilon_{A,j} = E_{A,j} - E_{nernstA,j} \qquad \text{for } j = 1 \text{ to } 2 \qquad 6.7.1$$

where E_{Nenrst} is the Nernst potential at the electrode. The other overpotentials are similar.

The Butler-Volmer equation depends on two empirically measured parameters: i_0 and α. i_0 is the exchange current density. This is a measure of how rapidly the reaction proceeds given a certain kinetic overpotential. It is equal to the current density that flows across the electrode-solution interface at equilibrium. Although the net flow is zero at equilibrium, a large number of electrons are flowing back and forth across the interface. The exchange current density is a function of the redox couple, the reactant concentrations, and the electrode surface and can vary by many orders of magnitude. For instance a catalytic electrode surface can be used to increase the reaction rate. Platinum group catalysts are typically used in fuel cells to overcome the sluggish reactions, especially on the oxygen electrode.

The symmetry of the voltage-current curve around equilibrium is a measured by α. An α of 0.5 means that an increase in voltage causes the forward reaction to proceed at the same rate that the same quantity of decrease in voltage will make the reverse reaction proceed. Although the data used in these computations is in the right range for the reactions considered (Vetter, 1967), the actual values are strong functions of the electrode material. If a prototype system is built, i_0 will probably be a fitting parameter. In the present model, α is assumed as 0.5.

The Butler-Volmer equation for an electrode is:

$$i_B = i_{0B} \cdot \left(e^{(-\alpha_B \cdot f_s \cdot \varepsilon_B)} - e^{((1-\alpha_B) \cdot f_s \cdot \varepsilon_B)} \right) \qquad 6.7.2$$

where i is the current density in Amp/m^2. The variable f_s is a grouping that shows up frequently. It is the Faraday constant, divided by the ideal gas constant and temperature.

6.8 Ohmic Resistance Losses

Another major irreversibility is the loss due to ohmic resistance in the cell. This is the electrical resistance to the current flowing through the electrolyte. The resistance consists of the resistance in the electrodes, the electrolyte, and the separator. In this study the electrical resistance of the electrodes, cell interconnections, and external circuitry are ignored, although they may be significant in real systems. The cell resistance is determined by the composition of these components and their geometries. The resistivity of the solution is affected by the concentration and mobility of the ions. Therefore an accurate computation of the resistance of the cell requires a specific design for the cell.

In earlier versions of this model a resistance value in a reasonable range was simply chosen. The resistance of Nafion membrane was used (Prout and Moorhouse, 1990, pg. 307). Nafion is a hydrogen ion conducting polymer used as the membrane in polymer electrolyte (PEM) fuel cells and some chlor-alkali production units. The resistance could be increased by multiplying it by a scaling factor. The cell performance was very sensitive to ohmic resistance.

In this model the conductivity of the solution is computed by a function, kappa2. The absolute value of the ion charge (Z_i), the ionic mobility, and the concentration are multiplied. This value is then summed with the values from all the other ions. This is multiplied by the Faraday constant to get the conductivity. The reciprocal of conductivity is the resistivity. The resistance for one cell is:

$$R_{cell,j} = resistivity_j \cdot \frac{thickness}{nominalarea_{seg}} \quad for\ j = 1\ to\ 2 \qquad 6.8.1$$

The resistance overpotential (E_{resist}) is:

$$E_{resist,j} = I_{tot} \cdot R_{cell,j} \quad for\ j = 1\ to\ 2 \qquad 6.8.2$$

The ionic mobilities are considered to be constants. No supporting electrolyte is used in this model.

6.9 Mass Transport Limitations

Several techniques were attempted to model the losses due to mass transport and the effects of reactant depletion on the cell performance. The unsuccessful methods are detailed in Appendix F. The reactants must be transported to and away from the electrode surfaces where the reactions take place. Diffusion driven by finite concentration gradients causes entropy generation and expends energy.

The final model uses the assumption of a very long parallel plate reactor in laminar flow with a constant surface mass flux. The loss due to transferring mass to the nominal electrode surface area was computed. However, the mass transport into or out of the porous electrodes was not calculated. Under these assumptions, the non-dimensional heat transfer coefficient, Sherwood number (Sh), is a constant. Pickett (1979) states that:

$$Sh = 5.384 \qquad 6.9.1$$

This value is set equal to an equation that relates the mass transport limited current density (i_l), concentration, plate spacing, and diffusion coefficient of the slowest diffusing component (D_1) to the Sherwood number (Prentice, 1991):

$$Sh = i_{l,j} \cdot 2 \cdot \frac{thickness}{n \cdot Far \cdot D_1 \cdot Conc_j][1} \quad for\ j = 1\ to\ 2 \qquad 6.9.2$$

The concentration overvoltage (E_{conc}) is related to the current and limiting current density by:

$$\mathbf{exp}\left[\left[-E_{conc,j} \cdot \frac{n \cdot Far}{R \cdot T_j}\right]\right] = 1 - \frac{I_{tot}}{nominalarea_{seg} \cdot i_{l,j}} \quad for\ j = 1\ to\ 2 \qquad 6.9.3$$

The diffusion coefficients were calculated from published data on the ion size parameters (Freiser, 1963). The ion size parameters are the effective particle diameter of the ions assuming a sphere in Stokes flow. The radius in terms of the temperature (T), viscosity (η) and diffusion coefficient (D) is:

$$r = \frac{1.380622e{-}23\ [J/K] \cdot T}{6 \cdot \pi \cdot \eta \cdot D} \qquad 6.9.4$$

where the numerical value is the Boltzmann constant. There was no value for Mn^{3+} and Fe^{3+} so a value in the middle of the range of other trivalent ions (La^{3+}, Tl^{3+}) was used (Robinson, 1955). This assumption is generally valid for the level of description of this model. The order of magnitude and first significant digit are fairly constant for metal ions of the same charge. In ionic size parameters for adjustment of activities, ions of the same charge also typically have the same size to one significant digit (Freiser, 1963). The trivalent ions are controlling as they are largest and diffuse slowest.

The drop in concentration across the reactor ($Conc_{change,j}$) is calculated by setting input and output concentrations and taking the difference:

$$Conc_{change,j} = Factor_{depletion} \cdot (Conc_{in,j}][2 - Conc_{in,j}][1) \quad \text{for } j = 1 \text{ to } 2 \qquad 6.9.5$$

The variable, $Factor_{depletion}$, was adjusted to help step the model to a different regime where good guess values were not known. The flow rate needed to provide the mass flux required given the total current is calculated by:

$$Conc_{change,j} = sign_j \cdot I_{tot} \cdot \frac{Conv_1}{9.648670E7 \ [Coulomb/kmole] \cdot flowrate_{vol,j}} \quad \text{for } j = 1 \text{ to } 2 \qquad 6.9.6$$

The variable sign controls the direction of the reaction and concentration changes so that the two cells run in reverse of each other.

6.10 Pumping Power

Energy must be expended to pump the solution from one reactor to the other and to push the solution through the reactors. This energy is converted into heat in the flow by viscous dissipation. The pumping losses are very dependent on the geometry of the device. However, the tradeoffs between resistance and pumping losses are analyzed in Chapter 5. The same set of equations was used to calculate the pumping losses. In addition, the pumping power was divided by the total current flow to obtain a psuedo-voltage ($Eequiv_{pump}$). Although this voltage is never applied to the electrochemical system, it is useful in comparing with other overpotentials to determine which losses are the most significant.

The pumping loss may also include energy expended to stir the solution or force the solution into a turbulent flow regime. This energy would be a tradeoff with the decreased mass transport losses. Turbulent flow was not studied in this work.

6.11 Heat Exchanger Effects

The heat transfer in the regenerative heat exchanger causes losses. The transfer of heat across a finite temperature gradient generates entropy. In addition, the mismatch of specific heats in the reactant streams causes the flows with higher specific heats to enter the cold cell warmer than the material flowing out. The energy expended to warm up this stream is a loss.

The regenerative heat exchangers between the streams were modeled with the effectiveness method (Incropera, 1996). Each reaction couple passed through a separate counterflow heat exchanger so that there were two heat exchangers. The smaller specific heat for each couple was calculated and used to determine the heat transfer rate ($q°_1$):

$$q°_1 = \eta \cdot C_{pmin1} \cdot (T_2 - T_1) \cdot flowrate_{vol,1} \qquad 6.11.1$$

where η is the effectiveness or the fraction of the maximum heat transfer that is achieved. The effectiveness was an input variable and was not calculated. Appendix D contains a calculation of the effectiveness of a proposed laboratory heat exchanger. The heat transfer was then applied to the streams to determine the actual temperature change:

$$q°_1 = C_{pAox} \cdot (T_{Aox} - T_1) \cdot flowrate_{vol,1} \qquad 6.11.2$$

where T_{Aox} is the temperature of the A oxidized form flow entering the other cell. Similar calculations are made for the other streams.

The flow entering the cold side is warmer than the cell temperature. Some of the reversible heat effect must be expended to cool the stream. This decreases the cooling power of the system and the COP. The heat transfer needed to cool the fluid streams (qAred and qBox) is calculated as:

$$qAred = C_{pAred} \cdot (T_1 - T_{Ared}) \cdot flowrate_{vol,1}$$

$$qBox = C_{pBox} \cdot (T_1 - T_{Box}) \cdot flowrate_{vol,1} \qquad 6.11.3$$

The loss is calculated as the sum of these energies:

$$HX_{loss} = |qBox| + |qAred| \qquad 6.11.4$$

This loss is subtracted from the cooling power of the system, but does not add directly to the energy input in the same ways as the pumping power or overvoltages.

On the hot side, some energy may be expended to warm the fluid. However, these effects are not modeled here.

The four reactant streams could be passed through a heat exchanger that places all of the streams in thermal contact (see Figure 6.8.1). Each stream could exchange heat with every other stream. This could increase the maximum heat transfer possible depending on the combinations of specific heats and flow directions.

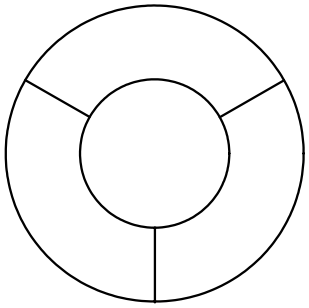

Figure 6.11.1 Cross sectional view of proposed heat exchanger for four flow streams

6.12 Overall Performance Calculations

The overall performance of the two cell system is calculated by summing the overvoltages the Nernst potential. The pumping and heat transfer losses are then added to the system.

The total voltage applied to a cell is the sum of the electrode potentials, resistance overpotential, and the concentration overpotential:

$$E_{tot,j} = E_{B,j} + E_{A,j} + sign_j \cdot E_{resist,j} + sign_j \cdot E_{conc,j} \quad \text{for } j = 1 \text{ to } 2 \qquad 6.12.1$$

Note that the kinetic overpotential and the Nernst potential are already summed in $E_{B,j}$ and $E_{A,j}$. The variable, $sign_j$, ensures that the power producing cell decrease in voltages with losses and the power consuming cell voltage increases with overpotentials. The total lost in each cell are calculated by taking the absolute value of the difference between the applied voltage and the Nernst voltage and multiplying by the total current. The pumping power is simply added to the loss:

$$loss_j = \left| E_{tot,j} - E_{nernsttot,j} \right| \cdot I_{tot} + pump_{power,j} \quad \text{for } j = 1 \text{ to } 2 \qquad 6.12.2$$

The total voltage applied to both cells in series (E_{added}) is the sum of the hot side and cold side potentials:

$$E_{added} = -E_{tot,1} + E_{tot,2} \qquad 6.12.3$$

The overall work consumed by the system (W_{tot}) is the applied voltage times the current flow plus the pumping power:

$$W_{tot} = E_{added} \cdot I_{tot} + pump_{powertot} \qquad 6.12.4$$

The total cooling power is the reversible heat effect minus the cold side losses including the heat exchanger loss:

$$Coolpower_{tot} = Coolpower - loss_1 - HX_{loss} \qquad 6.12.5$$

The COP is the total cooling power divided by the work input:

$$COP = \frac{Coolpower_{tot}}{W_{tot}} \qquad 6.12.6$$

6.13 Modeling Results

The model was solved for a number of parameter conditions. Except where noted, the heat exchanger effectiveness is set to 1. Therefore, the specific heat difference between the fluid streams causes all of the losses from the regenerative heat exchange.

The design space for the DERC is determined by various sets of three factors. Two useful groupings are: 1) size (electrode spacing and total surface area), cooling power, and COP, and 2) volumetric cooling power, COP, and current. One factor is COP and the other two are combinations of the amount of cooling produced and the degree of system utilization, or how fast the reactions are driven. Any two of the variables can be considered independent and their choice determines the value of the third variable.

Due to the complexity of the model, the optimization routine in EES was unable to optimize the thickness for maximum COP. Therefore, the optimal plate spacing was found by varying the thickness and observing the apparent peak COP (Figure 6.13.1). The peak COP was at approximately 43 microns over several orders of magnitude. This value was used for all other calculations where the thickness was not varied. Above a certain current density the losses exceed the reversible heat effect and no cooling is produced (see Figure 6.13.2). When the losses greatly exceed the reversible heat effect, all energy input is expended as heat and a COP of –1 is computed (Figure 6.13.1).

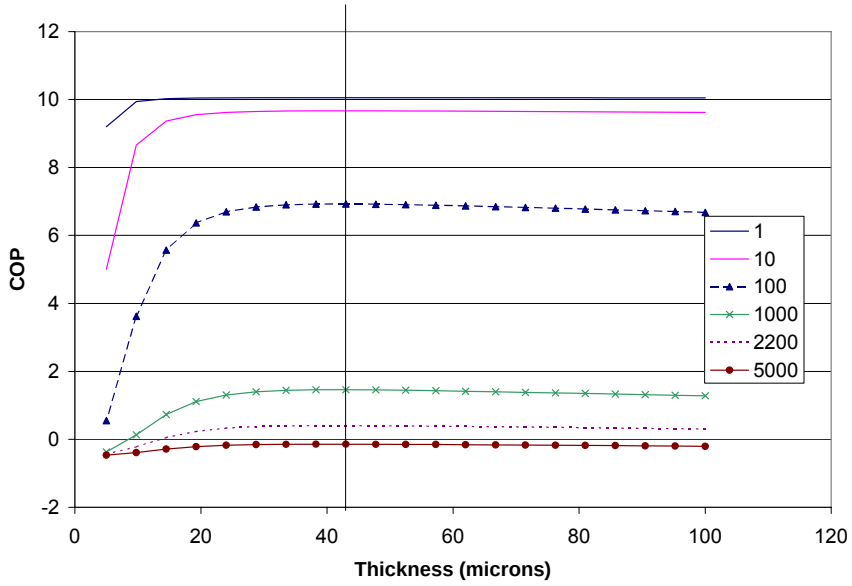

Figure 6.13.1 COP at several current levels (Amp/m^2) as a function of electrode gap thickness. The vertical line is at 43 microns

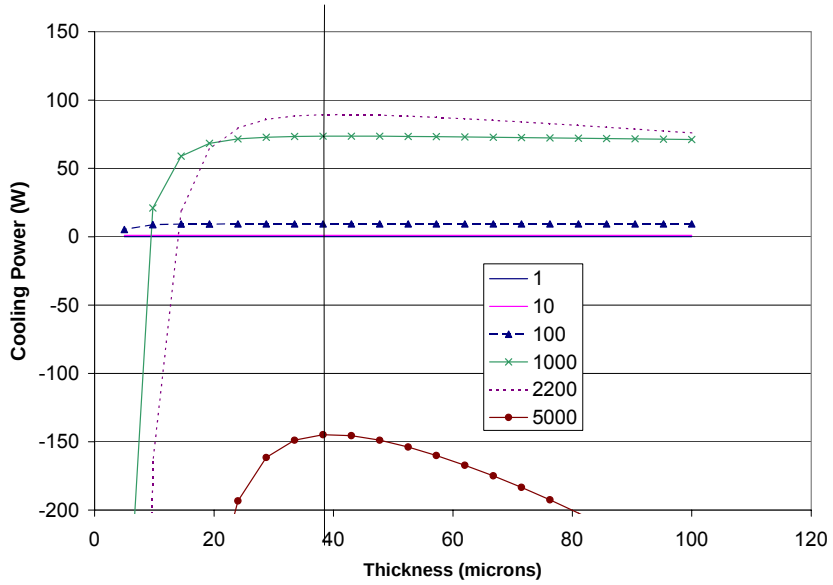

Figure 6.13.2 Total cooling power at several current levels (Amp/m^2) as a function of electrode gap thickness. The vertical line is at 43 microns.

The various overpotentials all increase with current (Figure 6.13.3). In the region near the optimum the kinetic overpotential dominates. As noted elsewhere in this work, the kinetic overpotential could be greatly reduced by choosing different electrode/reactant combinations or varying the reactant concentrations. The kinetic dominance in this model is not a general result, but specific to the kinetic constants used.

The resistance and pumping losses increase linearly with current. Because the model was optimized with respect to the tradeoff between these values, the values are of the same magnitude. The slight offset in the figure is due to any numerical inaccuracies and the fact that the model was manually optimized.

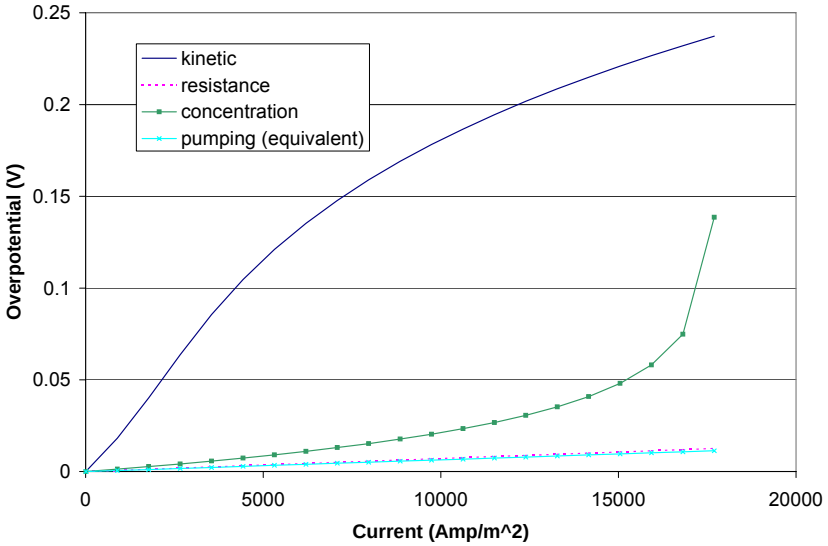

Figure 6.13.3 Variation of overpotentials with current

A significant aspect of Figure 6.13.3 is the dramatic increase in the mass transport losses as the limiting current is approached. Because of the assumption of constant surface flux, the increase in current equals an increase

in velocity. However, the mass transport rate is not increased by the increased flow and the limiting current density is only a function of the electrode spacing (see Figure 6.13.4 and equations 6.9.1-6.9.3). If the mass transport were modeled as a function of velocity, the concentration overpotential would be a stronger function of current. In situations where the mass transport dominates it limits the heat flux achievable on the electrode. The limiting current is 17781 Amps for both cells at the 43 micron plate spacing.

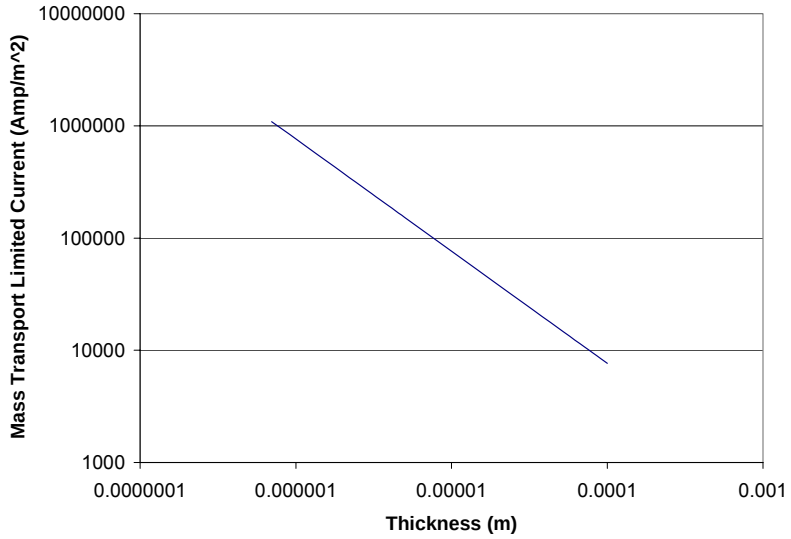

Figure 6.13.4 Variation in limiting current with thickness.

At low current the hot and cold cell voltages have a small offset due to the temperature difference. The voltages of the hot and cold cells diverge as the current increases. As the input current nears the mass transport limiting current, the voltage input required to drive the system increases more rapidly (Figure 6.13.5).

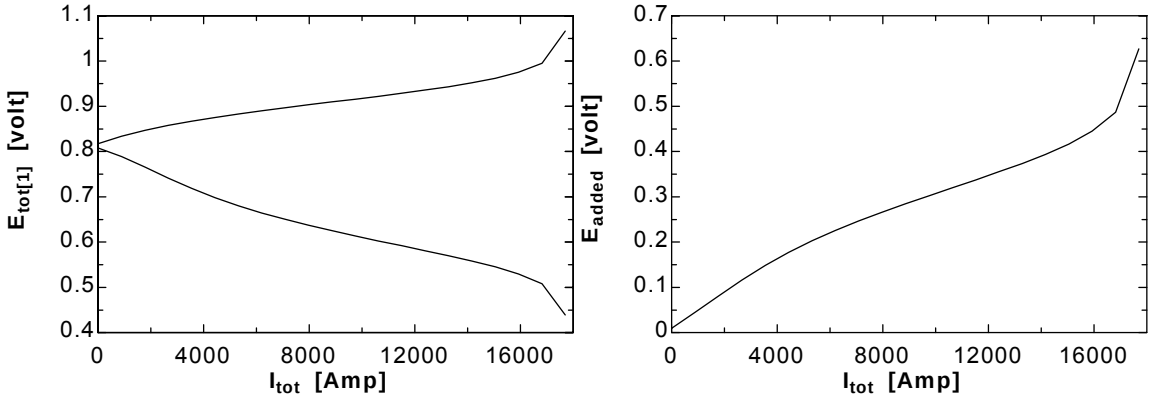

Figure 6.13.5 Left: High temperature cell voltage ($E_{tot[2]}$) and low temperature cell voltage ($E_{tot[1]}$) versus total current ($E_{tot[2]}$ is the dotted line). Right: Voltage added to the system versus total current

The cooling power versus current curve shows the same behavior as described earlier, reaching a maximum and then decreasing with current (Figure 6.13.6). However, the curve is not a symmetrical parabola as before, due to the kinetic and mass transport losses. The kinetic losses cause the maximum in cooling power to occur earlier. If the exchange current densities are increased by an order of magnitude, the peak cooling power occurs later and the

curve is similar to those presented earlier (Figure 6.13.7). However, the exponential increase in the mass transport overpotential causes the cooling power to drop off rapidly near the limiting current.

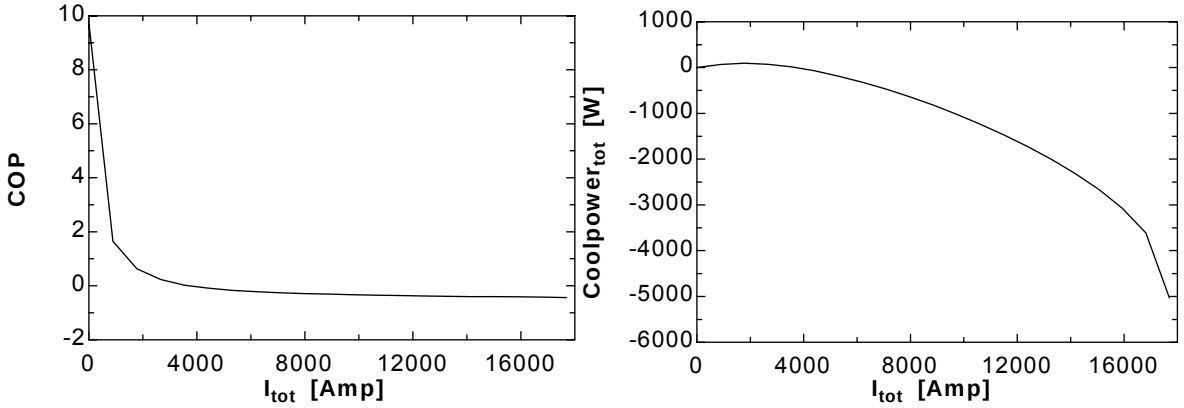

Figure 6.13.6 Left: Cycle COP versus total current Right: Total cooling power versus total current (T_c=25°C, T_h=50°C).

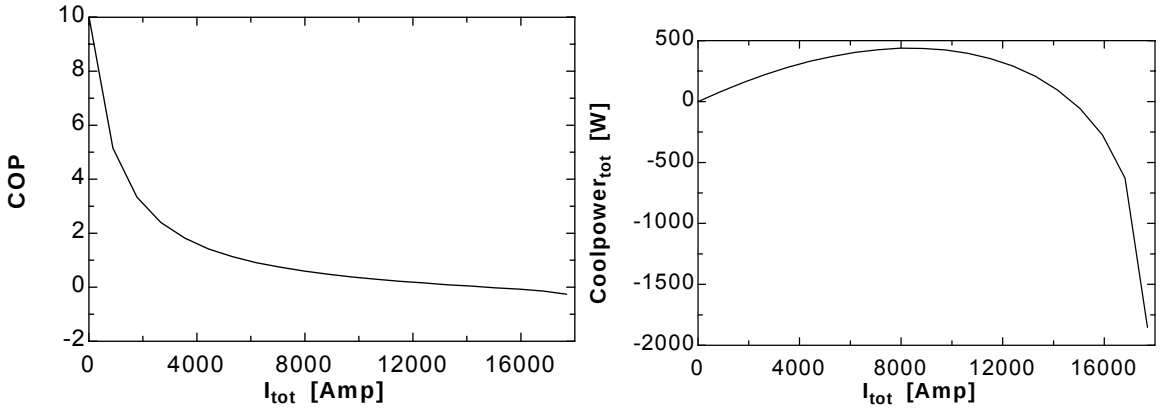

Figure 6.13.7 Effect of lowering kinetic overpotential Left: Cycle COP versus total current Right: Total cooling power versus total current (T_c=25°C, T_h=50°C)

Figure 6.13.8 shows the relationship between the cooling power per volume of electrode gap, the applied current, and COP. The volume used is simply the electrolyte between the electrodes on the cold side. It does not include the volume of the electrodes, containment system, any piping, pumps, or other equipment. The total volume of the system may be many times the listed volume, so the volumetric cooling power of the whole system may be much smaller. Starting at a high COP and a low cooling power, the COP at constant current decreases slowly with increased volumetric cooling power (thinner electrode gap), until it hits a point when the COP drops precipitously. Eventually, the losses are so large that the cooling power decreases along with the COP. The envelope of achievable COPs and cooling powers is sketched into the figure. This line is drawn for illustrative purposes and not calculated.

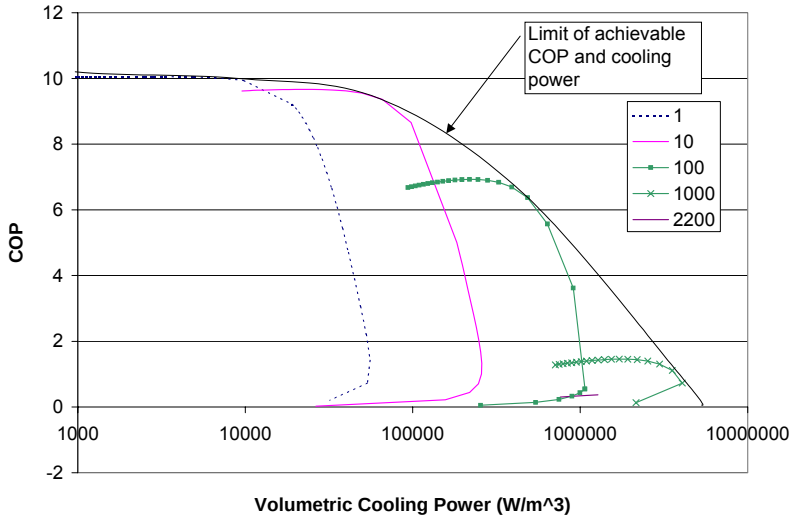

Figure 6.13.8 COP as a function of volumetric cooling power at several currents (43 micron electrode spacing).

The heat exchanger effectiveness affects the cooling power and COP linearly (6.13.9). Even with a perfect heat exchanger (η=1) there is a 16% decrease in cooling capacity due to the specific heat mismatch (Figure 6.13.10).

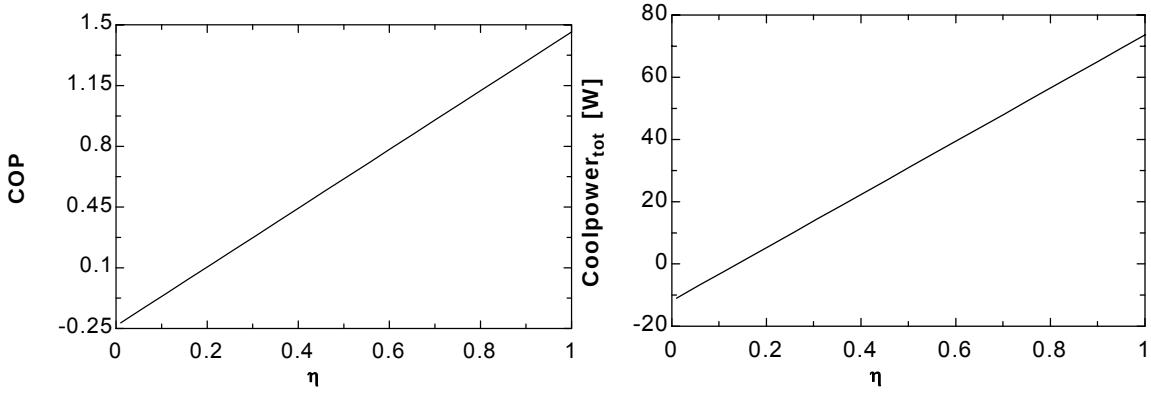

Figure 6.13.9 Left: COP vs. heat exchanger effectiveness. Right: Total cooling power vs. heat exchanger effectiveness (I_{tot}=500 Amps).

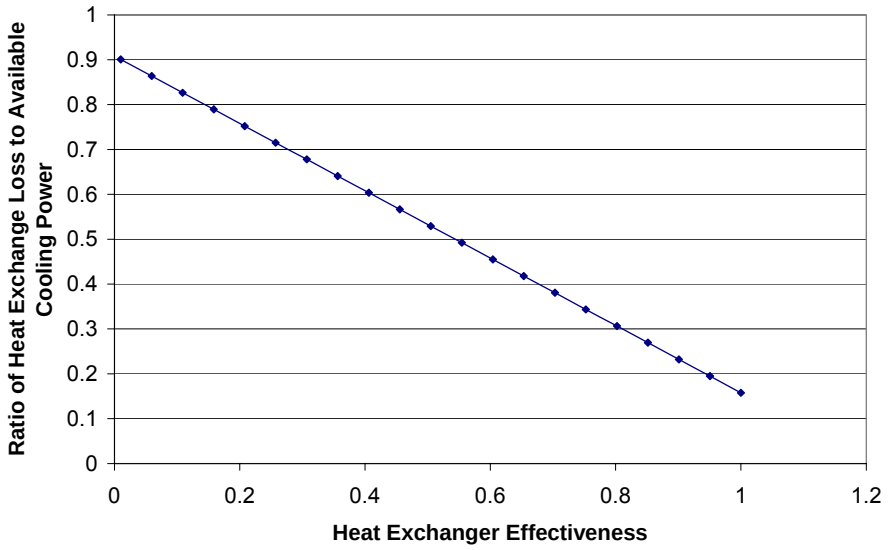

Figure 6.13.10 The fraction of the cooling power before subtraction of losses that is used to cool the fluid entering the cold cell increases with decreasing heat exchanger effectiveness (I_{tot}=500 Amps).

6.14 Conclusions

The design space for the DERC is a tradeoff between size (electrode spacing and total surface area), cooling power, and COP. Kinetic losses may be important depending on the reaction/electrode combinations selected. Mass transport losses decrease the performance of the DERC as the mass transport limiting current is approached. The drop off is much more dramatic than that caused by the ohmic or pumping losses. The maximum volumetric cooling power achievable at a COP of 5 is around 1000 kW/m^3. The mismatch in the specific heats in the heat exchanger decreases system COP and capacity. The effectiveness of the heat exchanger is an important parameter for determining cycle COP and capacity.

Chapter 7. Chlorine-Hydrogen Direct Systems

7.1 Introduction

Systems that produce chlorine and hydrogen by the electrolysis of aqueous chloride solutions show potential as direct electrochemical cooling systems. Testing has demonstrated a cooling effect while operating in a batch mode.

This reaction is very similar to the proposed hydrogen-oxygen electrochemical refrigeration cycle. However, it is unlikely that the H_2-O_2 system could practically produce a cooling effect due to the high kinetic overpotential of the oxygen electrode. The kinetic overpotential of the chlorine generation reaction is much lower. In fact the equilibrium potential of oxygen evolution is lower than that of chlorine evolution, but the kinetic overpotential for the chlorine reaction is so much lower than for the oxygen that chlorine generation overwhelmingly dominates.

This reaction was chosen as a useful laboratory model due to its simplicity and high entropy change. The electrolyte in contact with both electrodes can have the same composition. It is necessary to keep the chlorine and hydrogen separated to prevent them from reacting. The reaction is a loss and could also cause a potentially dangerous explosion. However, a small amount of leakage may be tolerable and reduces the performance requirements for the separator.

The same reaction is used in chlor-alkali production units for producing chlorine and sodium hydroxide from salt water. This is a large scale industrial process that has been extensively researched. Data for the reaction properties and materials designed specifically for this reaction are available.

A number of chlorine-hydrogen generation tests were run in a variety of configurations. All these tests were performed in a batch mode without replenishment of the reactants.

7.2 U-Tube Cell

In order to test the feasibility of a chlor-alkali cell without a separator, a chlorine and hydrogen producing electrochemical cell was made from a 8 mm internal diameter glass U-tube. The tube was encased in foam to insulate it. Small gauge platinum wire coils wrapped around a bit of sponge were used as electrodes. A thermocouple was attached to the outside of the glass U-tube so that temperature changes due to the reaction could be monitored. The tube was filled with a saturated solution of KCl. Foam rubber was secured over the top of the cell to insulate it. When a voltage slightly above the equilibrium value was applied, hydrogen and chlorine were rapidly evolved. However, the temperature of the cell steadily increased. The cell resistance between the electrodes was most likely too high and excessive ohmic heating occurred. Due to the catalytic nature of platinum, it may be assumed that the kinetic overpotential was fairly low in this cell.

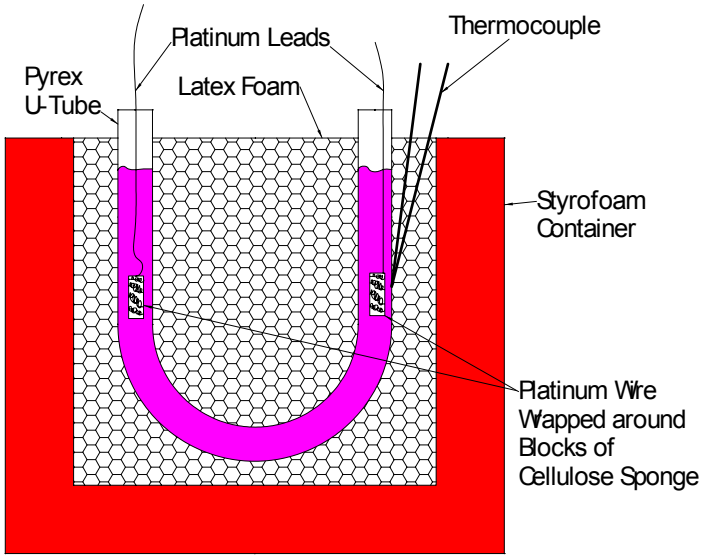

Figure 7.2.1 Chlorine-hydrogen producing electrochemical cell made from a glass U-tube with platinum wire electrodes

7.3 Vacuum Bottle Calorimeter

In order to adiabatically test small electrochemical cells, small vacuum insulated calorimeters were constructed from commercial thermos bottle liners (see Figure 7.3.1). The liners were just the right size for a standard 400ml beaker to slip in with the lip resting on the top edge of the liner. The liners were covered in a latex glove, then placed in a cardboard box where latex foam was blown around them. The box and foam protected the glass liners and made a stable base. A lid was fabricated of extruded polystyrene foam board. A large hole for electrode leads, thermocouple wires, and tubing was located in the middle of the lid. The lid attaches to the base with draw pull latches. Foam rubber is stuffed in the lid hole and between the lid and the base. When the latches are closed, they compress and seal the foam.

Figure 7.3.1 Vacuum bottle calorimeter, left to right: foam lid with hole, open cell foam gasket, and vacuum bottle calorimeter. Top: 400ml beaker.

7.4 Stainless Steel Spiral Cell

A chlorine producing cell fabricated of two spiral wrapped plates of stainless steel (See Figure 7.4.1) was tested in the vacuum bottle calorimeter. Before rolling, the plates were approximately 21 and 26 cm by 5 cm by 1.5 mm thick. The plate separation, which varied due to fabrication error, was approximately 4 mm. A separator of filter paper was inserted between the plates to eliminate electrical conduction directly between the plates. The assembly was immersed in a 400 ml beaker of saturated NaCl and connected to a power supply by the tabs.

The cell produced visible bubbles near the equilibrium voltage for gaseous chlorine and hydrogen production. The largest density of bubbles was produced on the rough sawn ends of the plates. It is unclear if this was due to greater nucleation sites or a thinner oxide coating on the metal in this region. In an attempt to increase the chlorine production, the plate surface was roughened with sandpaper and files. There was not a noticeable difference in the quantities of bubbles produced. When the cell was tested in the vacuum bottle calorimeter described earlier, only temperature increases were measured.

Later tests with hydrochloric acid as the electrolyte showed corrosion of the stainless steel as would be expected.

Figure 7.4.1 Chlorine producing cell with stainless steel electrodes. Left: Electrodes separate, Right: electrodes interleaved.

7.5 Swiss Roll Carbon Cloth Cells

A series of tests were performed with electrodes of graphite cloth rolled with a cellulose (paper towel) separator. The graphite cloth had no catalytic materials on it and was in fact manufactured for use in structural composite materials (6K, 5HS from Fibre Glast Developments Corp.). The electrodes were approximately 70 cm by 600 cm. The rolled cell design was placed in a 400 ml beaker inside the vacuum bottle calorimeter described in section 7.3.

When saturated solutions of NaCl or KCl were electrolyzed the cell temperature either did not change significantly or rose. Even when the cell over voltage was very small and cooling would be expected from the current and difference from equilibrium voltage, cooling was not observed. However, these calculations assume that the cell reaction is in fact the production of chlorine from chloride ions at 100% current efficiency. However, the real system may have a number of side reactions that generate heat or have a different equilibrium potential. At a neutral pH, hypochlorites, chlorites, chlorates, and perchlorates form by combining hydrogen and oxygen from the water with the chloride (Pourbaix 1966). At low pH, only chlorine and Cl^- are thermodynamically stable and side reactions are suppressed. Therefore hydrochloric acid was substituted for the NaCl or KCl.

Another advantage of using HCl is that H^+ is much more mobile in solution than Na+. This ionic mobility leads to a higher conductivity and lower ohmic losses. It also corresponds to more rapid diffusion and lower mass transfer losses.

This cell demonstrated cooling (Figure 7.5.1) when filled with 10M hydrochloric acid. The cell temperature dropped as the ambient temperature stayed fairly constant.

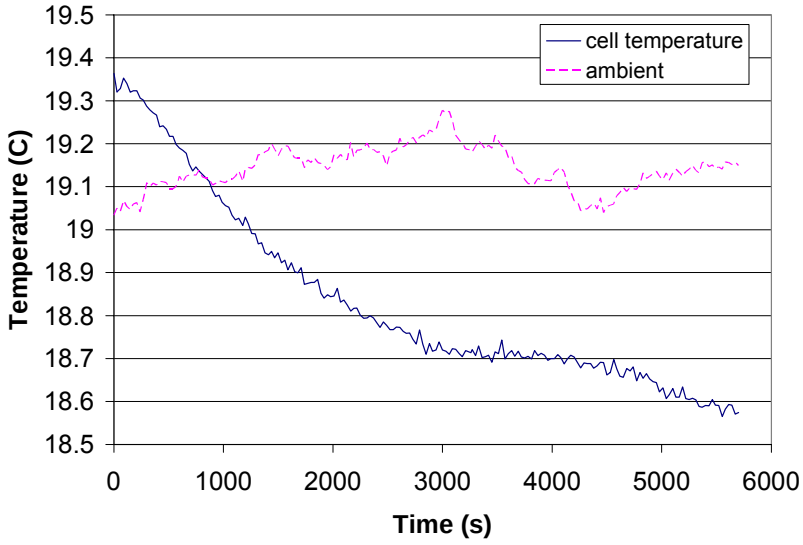

Figure 7.5.1 Chlorine-hydrogen cell temperature decreasing due to electrochemical cooling.

Although in this test there was no means for separating the hydrogen and chlorine gases evolved, in an overall system the separated gases could be sent to a fuel cell to reverse the process. More sophisticated tests with improved materials should yield better results.

7.6 Proposed Gas Separating Cells

Several cell designs that allow separation of the chlorine and hydrogen have been investigated. Considerable effort was directed toward cells made from heat-sealed polyethylene sheet and Tyvek (polyethylene felt) and rolled in a Swiss roll design (see Figure 7.6.1). The heat sealing was performed with a hand held heat sealing iron (Heat Seal, Model S, Cleveland, Ohio) or a modified consumer vacuum sealer for food storage.

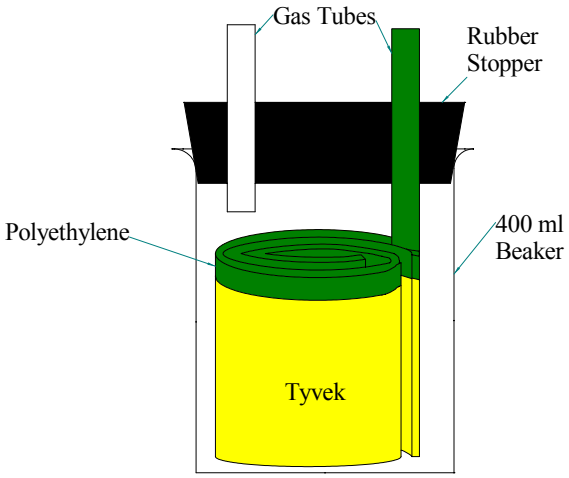

Figure 7.6.1 Heat-sealed plastic rolled cell design with separate exits for chlorine and hydrogen.

The cell design uses Tyvek as the separator and has a polyethylene strip along the top. A rubber grid holds the electrode away from the separator ensuring that there is space for electrolyte and gas flow. The intention was for gas bubbles to form on the electrodes, rise into the polyethylene section, and be directed out of the cell. The bubbles of the other gas would rise into the cell internal area and be directed out. However, this cell would suffer from the bubble clearing problems noted below.

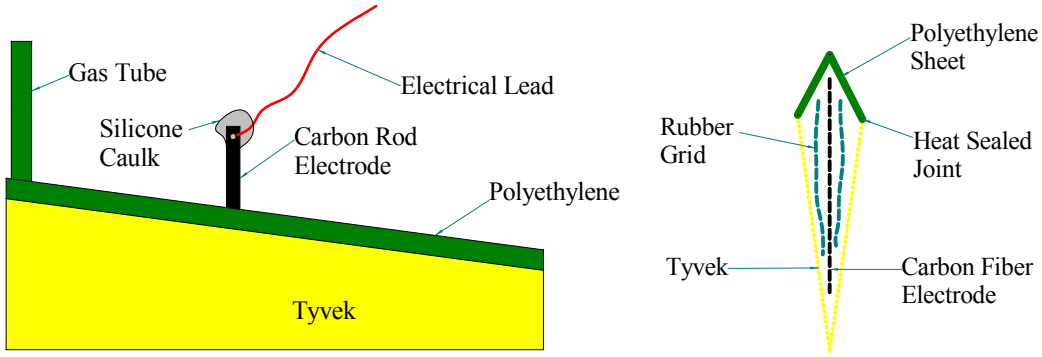

Figure 7.6.2 Left; Cell unrolled. Right: Cross section of cell.

A heat sealed design has several advantages. It may be simple to mass produce in large quantities using existing fabrication technologies. The size scale achievable with plastic films and spacers is similar to the optimal size scale for electrode separation discussed in Chapter 3. In addition, it might present interesting design options such as wrapping the inside of a refrigerator or a room in the flexible material. Because it may be flexible, car seats or cooling blankets could be used directly in contact with people, thus reducing the need for space cooling.

Configurations using stacked plastic plate were also studied. This design is modular and easily modified in size. New electrolyte would be pumped through a series of holes in each plate. The electrolyte enters the space between the plate and separator reacts and flows out of similar holes on the other side. The evolved gas forms bubbles that rise to the surface and exit through holes at the top. The gas holes are arranged on opposite sides of the plates so that the gas streams are kept separate.

The initial design for these plates was a square standing on one corner (see Figure 7.6.3). The electrolyte inlet and outlets are on the opposite corners of the square. The gas exits are at the top and slightly offset from each other. Initial tests were performed with the single cell test setup pictured made from solvent welded PVC. The separator was made from Tyvek with solid polyethylene sheeting around the edges as a gasket. A different separator material could easily be substituted. It was difficult to shut the cell leak tight. This design was tested with iron and copper salts as mentioned in Appendix D but did not produce electricity at levels expected.

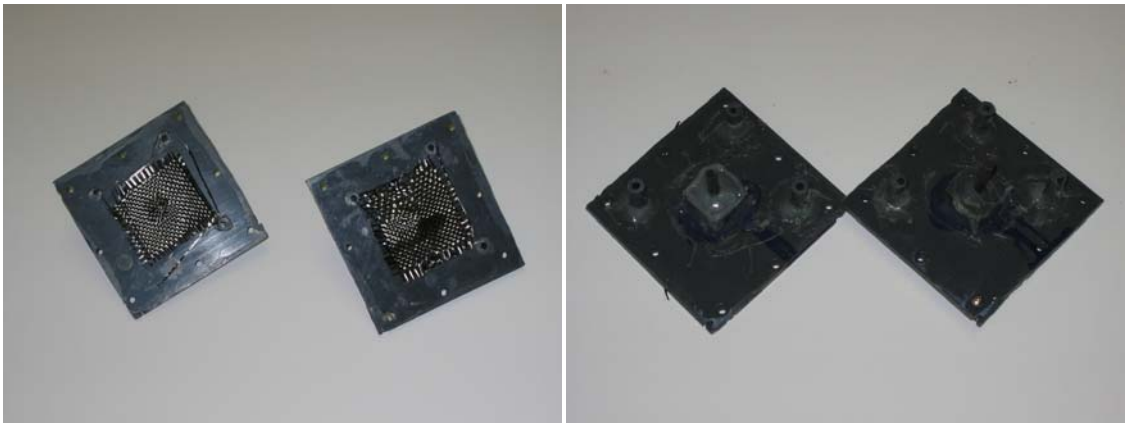

Figure 7.6.3 PVC stacked plate cell design Left: interior Right: exterior

In order to simplify the experimental setup and eliminate the need to position a square on its corner, the design shown in Figure 7.6.4 was produced. The gas would rise to the top of the cell and be directed out the port at the top of the slanting roof. The single cell prototype was milled out of polypropylene plates and used a similar membrane to that used in the PVC cell. The goal was to stack a series of these cells as shown in Figure 7.6.5.

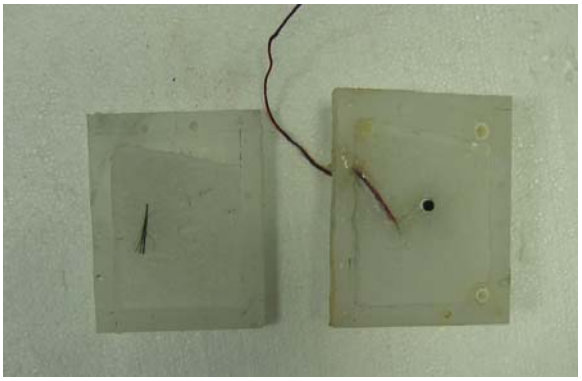

Figure 7.6.4 Improved stack plate design made from polypropylene

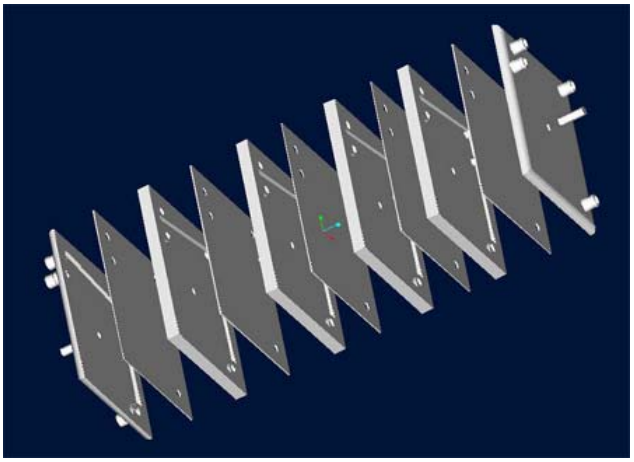

Figure 7.6.5 CAD drawing of improved stack plate design.

All of the designs presented here share the fundamental weakness of relying on buoyancy forces to remove the gas produced from the cells. The gaps between the electrodes and membranes are small as are the spaces

between the electrode fibers. Bubbles produced could stick to the cell components and span the gaps between them. The surface tension would be enough to prevent the bubbles from moving under buoyancy forces. The bubbles would coat the electrodes, reducing surface area for reactions and restricting current flow, thus increasing ohmic resistance.

The cells are composed of materials with low thermal conductivity (plastic and glass) and at this point there is no way to transfer heat with the cells except through conduction from the outside of the cells. It might be possible to leave the cells adiabatic and transfer heat with the exiting reactant stream.

A successful gas separating cell could be connected to a chlorine-hydrogen fuel cell to complete the cycle.

7.7 Chlorine Cell Cooling Power Optimization

Attempts were made to develop a system for optimizing the cooling power of a real Cl_2-H_2 system similar to that discussed in Chapter 2 for NiCd batteries. The voltage-current curve for a real system could be measured and fit to an appropriate function e.g exponential or sigmoidal. The open circuit voltage immediately after the shut off of power could be taken as the equilibrium voltage. The difference between this voltage and the applied voltage times the current is the loss. At 100% current efficiency the ideal cooling power is directly proportional to current and the reversible heat effect can be estimated from published values in dilute solutions. The point where the total cooling power (ideal cooling power minus losses) is maximum can be computed and test performed to verify this value.

7.8 Conclusions

A simple electrochemical cell that produces hydrogen and chlorine has demonstrated cooling. This reaction was chosen as a useful laboratory model due to its simplicity and high entropy change. Several different cell configurations and electrolyte compositions were also investigated. Cells using KCl and NaCl did not show a cooling effect, possibly due to side reactions. A cell that electrolyses 10M hydrochloric acid showed a cooling effect. Further work on this system using gas separating cells is proposed to demonstrate the DERC.

Chapter 8. Ideal Reaction System Characteristics

8.1 Introduction

Various electrochemical reactions have been reviewed for use in a direct electrochemical refrigeration system. An ideal reaction system has not been identified and probably does not exist, as some tradeoffs will inevitably need to be made. However, a number of desirable properties have been identified. A few potential reactions have been identified, but an exhaustive or complete review was not performed.

8.2 General Characteristics

The candidate reaction systems should be relatively non-hazardous, non-corrosive, non-toxic, and inexpensive. As noted in Chapter 4, the reaction should have a high entropy change of reaction with respect to the Gibbs free energy change for a higher ratio of heat pumped to internal energy cycling. Also, the specific heats of the oxidized and reduced forms of the reactants should be similar to decrease the specific heat mismatch in the regenerative heat exchanger.

8.3 Loss Minimizing Characteristics

The reactions should be kinetically facile and allow a low resistance design. By careful selection of the reaction-electrode combination the kinetic overpotential can be made the least significant of the overpotentials. There are many very fast reactions that could be chosen from. For example, Vetter (1967, p. 494) recommends modeling the ferro/ferricyanide reaction with a pure diffusion overvoltage and no kinetic component due to the facility of the reaction.

The ions should have fairly good mobility in solution. For most simple ions there is not a great variation in the ionic mobility. Therefore, the achievable conductance may be largely affected by the solubility limits of the ions. Large ions or coordination compounds may have a much lower mobility. Acidic solutions would contain the highly mobile H^+ ions. Supporting electrolytes could be used to reduce resistance.

8.4 Solubility

For a continuous flow system, the oxidized and reduced forms of the reactants must both be soluble in the solution in concentrations used. If one has a lower solubility, it may deposit on separators or electrodes, causing clogging or increasing resistance.

8.5 Multiple Oxidation State Systems

However, if the two half-cells use different chemicals, they may diffuse through the separator, contaminating the other half cell. Because the reactants and solvent are continuously recycled, this could cause the system to permanently lose efficiency. A substance with three different oxidations states that are stable in the same temperature range and solvent at usable concentrations would be optimal. In this case, diffusion through the separator would be a loss but not a permanent one. The design of the membrane is one of the most difficult technical problems in the design of the DERC. Allowing a small leakage through the separator would lessen the requirements on the membrane. This could reduce electrical resistance and cost. On the microscale the membrane could be eliminated by using two laminar streams that flow parallel (Choban, 2004; Ferrigno, 2002).

8.6 Possible Reaction Systems

Several possibilities for reaction types are:

1. Systems where all the reactants remain as solids, such as some batteries using solid ion conductors as separators.
2. Systems in which the reactant is converted from a solution phase into a solid phase such as plating reactions.

3. Systems in which two or more ions in a liquid electrolyte vary in valence (see information on metal ion reactions in Chapter 1 and Appendix D).
4. Systems in which one or more components may be converted to a gaseous phase.

In systems of type 3 and 4 the reactants can be pumped between cells. This permits a continuous flow design with the advantages mentioned in Chapter 3.

Reactions of transition metal ions have been an area of focus. They have multiple oxidation states and some have very kinetically facile redox reactions. For instance, vanadium exhibits several oxidation states in aqueous solution: V(II), V(III), V(IV), and V(V). These oxidation states have been used in a micro redox fuel cell (Ferrigno, 2002).

Coordination compounds, in which several molecules or ligands surround a metal ion in solution, have a high potential for use. If the charge on the central ion changes, the number or arrangement of surrounding molecules changes. This rearrangement involves a large change in entropy and therefore a large reversible heat effect. Hammond and Risen (1980) used transition metal coordination compounds in their study of electrochemical heat engines. They comment that only a limited entropy change is possible from rearranging the ordering of water molecules around an ion due to a change in charge. However, the change in number of ligands or the swapping of one type of ligand for another can have much larger entropy changes.

Also, the ligands can stabilize the valence state of the ion. This may allow the ion to have three oxidation states as mentioned above. There are a wide variety of these compounds that can be investigated.

Aromatic hydrocarbons such as anthracene undergo facile electrochemical redox reactions (Bard, 2001, Kojima, 1975). Some of these exhibit multiple oxidation states. However, their toxicity and carcinogenicity may preclude their use.

Systems containing halogens also have potential. Chlorine gas generation has been studied as discussed in Chapter 7 and Appendix A. When I^- is reduced it forms I_2. At the appropriate pH I_2 will combine with an iodide ion to form I_3^- in solution. This will remain in solution and allow pumping. This reaction could be coupled with a metal reaction couple, e.g. iron iodide or tin iodide. This would reduce the separator requirements as noted above.

Room temperature molten salts (ionic liquids) have high electrical conductivities and maybe useful systems. High temperature molten salts have been used extensively for thermally regenerative electrochemical systems (Chum 1980 and 1981). There is much current research in ionic liquids and some of the knowledge and techniques could be redirected (Trulove, 1998).

8.7 Conclusions

The reactions should be kinetically facile and allow a low resistance design. Also, candidate reaction systems should be relatively non-hazardous, non-corrosive, non-toxic, and inexpensive. Also, multiple oxidation states, wide solubility limits, and a large entropy change of reaction are beneficial. Coordination compounds, various metallic ions, aromatic organic molecules, iodides, and room temperature molten salts could merit investigation. Clearly there are many other possible reactions that have not been discussed.

Chapter 9. Indirect Methods

9.1 Introduction

Any number of cooling methods could be envisioned that indirectly use electrochemical reactions. A few have been investigated so far. Indirect electrochemical refrigeration methods (IERM) are defined in section 1.4.

Those systems that are described in patents and other open literature are discussed, and a number of new concepts are presented. Limited modeling of these cycles has been performed. One cycle using the chlorine-hydrogen generation system presented in Chapter 7 has been analyzed in greater detail.

9.2 Thermoelectric Effects in Electrochemical Systems

Several researchers have investigated thermoelectric effects in electrochemical systems. An electrochemical cell with its electrodes at different temperatures, a thermogalvanic cell, acts analogously to a Peltier cooling device or thermoelectric power generator. Instead of conduction by electrons or electron "holes," the current is transported by mobile ions in solution.

This effect has been studied for the information it gives about the fundamental thermodynamics of electrochemical systems (e.g. Kamata, 1988). It has also been studied as a power source. For example, Murakami (2003) studied the use of metal hydride reactions in molten salt electrolytes for heat recovery.

Thermogalvanic cells have also been modeled in various ways. Newman (1995) begins with multicomponent transport equations and formulates a detailed model of the thermal effects at the electrode-solution interface. Grimstvedt et al. (1994) also model these effects from a less fundamental standpoint and compare the model to experimental data.

Quickenden and Mua (1995) review published data for electricity production from thermoelectric systems with aqueous electrolyte solutions. They conclude that the efficiency will be in the range of 0.001 to 1.2% of the Carnot efficiency at the same temperature difference. The practical efficiency of Peltier devices is a contest between the heat moved by the device relative to the heat conduction through it. The heat conduction is in the reverse direction and destroys the temperature gradient set up by the device. In a liquid solution, the non-participating solvent molecules do not aid in the movement of heat in the forward direction. However, the solvent decreases the thermal gradient due to convection. Therefore, the potential for using thermoelectric cooling systems constructed with electrolyte solutions is low.

9.3 Evolution of High Pressure Gas

Gases can be efficiently produced at high pressures in electrochemical systems. These gases could be condensed and used in a standard vapor compression system. The gas could also be fed into a Joule-Thomson cooler. The high pressure generated could also pressurize a secondary working fluid.

9.4 Evolution of a High Pressure Condensable Gas

A high pressure gas could be evolved and then used in a standard vapor compression system. The gas would need to be evolved at a pressure where it could be condensed by heat exchange with the environment. It could then be throttled and evaporated to accept heat. The gas would then be electrochemically recovered into the solution to restart the process.

Traditional refrigerants such as ammonia and sulfur dioxide are electrochemically active. In addition, chlorine condenses at pressures and temperatures similar to those of common refrigerants. It may be possible to evolve ammonia and chlorine in the same system using ammonium chloride.

Appendix A discusses an analysis of a system using electrochemically produced chlorine in a vapor compression cycle and hydrogen in Joule-Thompson cycle. For a temperature lift from 0 ºC to 77ºC, the COP is in the range of 1-2. The cycle is more complex than standard vapor compression systems and involves reactive and dangerous chemicals.

9.5 Pump a Secondary Working Fluid

The pressure generated by a gas evolution reaction could be used to compress a working fluid. Newell (2000) proposed a cycle using the evolution and recombination of hydrogen and oxygen to move a membrane. The movement of the membrane alternately compressed or expanded a conventional refrigerant. By appropriately phasing the movement of two membranes, a standard vapor compression cycle could be achieved. This method of electrochemically producing bubbles has been used for actuation in micro electrical mechanical systems, such as Stanczyk (2000) or Neagu (1997). Other microactuators have been developed that rely on a change in the size of a polymer film that undergoes electrochemical oxidation or reduction, e.g. Lewis (1999).

9.6 Evolve High Pressure H_2 for Adsorption into a Hydride System

Hydrogen could be electrochemically produced at a high pressure and then brought in contact with certain metal alloys that adsorb the hydrogen. Large quantities of hydrogen can be adsorbed into the crystal structure of the metals forming a metal hydride. This adsorption releases heat. When the gas pressure is reduced, the hydrogen leaves the system, causing cooling. Working prototypes have been built of metal hydride refrigeration systems using conventional compressor technologies. See Sandrock (2003) and Fischer (1999) for reviews of metal hydride heat pumps and cooling systems.

9.7 Electrochemical Hydrogen Compressors for Joule-Thompson Cryocoolers

U.S. Patents 4,671,080 and 5,024,060 use similar systems to pressurize hydrogen or oxygen for use in a Joule-Thompson cryocooler. U.S. Patent 4,671,080 assigned to Boeing Co. is titled “Closed cryogenic cooling system without moving parts.” An electric field is applied across a membrane of Nafion flouropolymer or various ceramic and oxide materials. The membrane is in contact with gaseous hydrogen and water or ammonia. The hydrogen is oxidized on one side, transported the across the membrane as ions, and then reduced back to H_2. A COP on the order of 0.01 is claimed. This system’s chief advantage is no moving parts for use in space systems.

U.S. Patent 5,024,060 is assigned to United Technologies Corp. and titled “Joule-Thomson refrigeration cycle employing a reversible drive electrochemical compressor.” This design operates in a reversing mode where the working substance is passed through a membrane and expanded. The potential on the membrane is then flipped and the refrigerant flow reversed. The design is symmetrical and includes sorbent beds to remove the water from the gas stream so that it does not interfere with the Joule-Thompson throttling process.

9.8 Solid State Oxygen Ion Compressor for Joule-Thompson Cryocoolers

Ceram Physics Inc. has researched the use of oxygen ion conducting ceramics for use as oxygen compressors for Joule-Thompson cycles (Lawless 1997). Heated air (~600ºC) was passed through certain passages of a honeycomb consisting of niobia doped bismuth sesquioxide ceramic. By an application of voltage to the honeycomb walls pure oxygen was extracted from the air and passed through the walls to other channels at a higher pressure. This oxygen and the waste air were cooled by in the incoming air in a counterflow heat exchanger. The compressed oxygen was to be sent to a fairly conventional Joule-Thompson cryocooler of about 0.12 watts cooling capacity operating in the 54-90 K range.

9.9 Electroosmotic Pumping

Alternatively, water vapor could be pressurized using an electroosmotic membrane where the ions are produced due to surface reactions with the membrane material. Research on electroosmosis for dehumidification has been performed in the Air Conditioning and Refrigeration Center at the University of Illinois at Urbana-Champaign (Mina, 2004). Knowledge gained from this research could be redirected towards cooling applications.

However, it is generally believed that it is ineffective to pump a liquid-vapor mixture with an electroosmotic membrane (Santiago 2004). Vapor bubbles in the pores simply block the flow and cause the flow to route through full flooded pores. In a single pore with a bubble and a wetted wall, the current is forced through the thin wall film. This causes the film to heat up and evaporate, thus breaking the circuit.

9.10 Water or Ammonia Compression with a Fluoropolymer Membrane

Analytic Power Corporation patented an electrochemical compressor using water as the refrigerant (U.S. Patent 4,593,534). This technology is also reviewed by Fischer (1999, pg. 73-6). An electric field across a Nafion or other fluoropolymer membrane in contact with water and gaseous hydrogen oxidizes the hydrogen on one side, transports the hydrogen ions across the membrane, and then reduces them back to H_2. The ion is surrounded by a solvation sheath of water or ammonia. The hydrogen ions drag the water or ammonia with them, thus producing a pressure gradient. The water or ammonia is then used as the refrigerant in a conventional vapor-compression system. The compressed hydrogen may be expanded through a valve or turbine and may be used in a cryogenic Joule-Thompson system. A means of separating the hydrogen and water is discussed.

A COP of 1.21 for a temperature difference of 0ºF to 110ºF is claimed. This is lower than the COP that is achievable with conventional compressors.

The Analytic Power Corp. patent claims that the electrochemical compressor can compress a two-phase mixture of liquid and vapor. However, the optimal design is such that all of the liquid is vaporized by the heat of compression and compressor losses, leaving a saturated vapor. It is not clear if this saturated vapor is on the low or the high side. If it is on the high side, then a constant temperature condensation could be achieved. However, no mention is made in this patent of the difficulties of two phase compression mentioned in the section on electroosmosis. This may be due to a slightly different mode of ionic conduction in Nafion membranes or it may simply be only the liquid phase that is being compressed.

9.11 Osmotic Pumping Gradient

An electric field across a membrane in solution can produce a concentration gradient. A concentration gradient produces an osmotic pressure gradient that can be used as a compressor or pump. Alternatively, a solution can be concentrated this way. When the solution is diluted, it will absorb heat if an appropriate solute-solvent combination is chosen.

9.12 Conclusions

There are many techniques that could be devised to produce a cooling effect with electrochemical reactions, membrane effects, etc. Some of these methods have been reviewed here. Working systems have been developed by various investigators for specific markets. None has made a large impact in marketplace. As there are many conceivable IERMs that have not been explored, there may be potential in this area.

Chapter 10. Conclusions

This study investigated the technical feasibility and design parameters of electrochemical refrigeration systems. It does not address the market niches or specific applications that the system may be used in. As this study is an initial investigation, many open questions and unexplored areas remain. In addition, no particular design or optimal reaction system is espoused here. The modeling has been performed with flat parallel plate cells and the experiments primarily with batteries and gaseous chlorine-hydrogen generating systems. These were chosen due to ease of laboratory use and not as proposed designs.

A number of general performance and design characteristics can be stated for the direct electrochemical refrigeration system. Electrochemical reactions occur on the surface of the electrodes and not in the volume of the electrolyte. Therefore, the total size of the system is determined by how much surface area can be packed in the smallest volume. Inherently, the electrolyte must be a reactive and electrically conductive medium. The reactivity will lead to corrosion and material compatibility issues that must be handled carefully.

The cycle is Carnot limited. However, a mismatch between the specific heats of the flows in the regenerative heat exchange is a major cause of deviation from the ideal.

Electrical power recycled between cells is 10-100 times that of the energy added to the system. This makes the cycle very sensitive to inefficiencies in processing the electricity in either cell. For a single cell a current on the order of 10-100 Amps is needed per watt of cooling. However, the cells could be arranged in electrical series to gain a higher cooling power at lower total current. The molar flow rate needed per watt of cooling is of the same order of magnitude as the molar flow in conventional refrigeration systems. The temperature lift for a single stage without regeneration is limited to about 10 K. The total temperature lift achievable for any electrochemical cooling system is bounded by the freezing and boiling (or decomposition) temperatures of the solvent.

A continuous flow process has several advantages over a batch process. The temperature lift could be higher without periodically reversing the direction of the reaction. The reactors could be separately optimized for the temperature and reactions occurring.

The maximum heat flux is on the order of 1000 W/m^2. However, a secondary refrigerant could be used in situations requiring a higher heat flux. A DERC should have good turndown characteristics and allow variable capacity operation. The COP decreases with increasing current. The cooling capacity increases with current and exhibits a maximum before decreasing.

A parallel plate electrode DERC with electrolyte flowing between the plates should have an optimal separation on the order of tens of microns. The balance between electrical resistance and the viscous dissipation of the flow determine this distance.

The design space for the DERC is a tradeoff between size (electrode spacing and total surface area), cooling power, and COP. Kinetic losses may be important depending on the reaction/electrode combinations selected. The mass transfer losses increase dramatically as the limiting current is approached. The maximum volumetric cooling power achievable at a COP of 5 is around 1000 kW/m^3. The effectiveness of the heat exchanger is an important parameter for determining cycle COP and capacity.

The properties of an ideal reaction system are discussed in Chapter 8 and several possible reaction types are suggested for investigation. A number of indirect methods for refrigeration are reviewed in Chapter 9.

Small scale laboratory tests have demonstrated cooling using a D-sized NiCd battery and a cell generating gaseous chlorine and hydrogen from hydrochloric acid.

Works Cited

Bard, A.J. and L.R. Faulkner. *Electrochemical Methods: Fundamentals and Applications*. New York: Wiley, 2001.

Barner, H.E. and R.V. Scheuerman. Handbook of Thermochemical Data for Compounds and Aqueous Species. New York: Wiley, 1978.

Berndt, D. Maintenance-Free Batteries: Lead-Acid, Nickel/Cadmium, Nickel/Hydride: A Handbook of Battery Technology. New York: Wiley, 1993.

Choban, E.R., L.J. Markoski, A. Wieckowski, and P.J.A. Kenis. "Micro-Fluidic Fuel Cell Based on Laminar Flow." Journal of Power Sources 128 (2004): 54-60.

Chum, H.L. and R.A. Osteryoung. Review of Thermally Regenerative Electrochemical Systems. 2 vols. Golden, CO: Solar Energy Research Institute/U.S. Dept. of Energy, 1980-81.

deBethune, A.J. "Fuel Cell Thermodynamics." Journal of the Electrochemical Society 107 (1960): 937-39.

Dittmar, L., K. Jüttner, and G. Kreysa. "A New Concept of an Electrochemical Heat

Pump System: Theoretical Consideration and Experimental Results." Electrochemical Engineering and Energy: Proceedings of the Third European Symposium on Electrical Engineering 23-25 March 1994, Nancy, France. Ed. F. Lapicque, A. Storck, and A. A. Wragg. New York: Plenum, 1995.

Ferrigno, R., A.D. Stroock, T.D. Clark, M. Mayer, and G.M. Whitesides. "Membraneless Vanadium Redox Fuel Cell Using Laminar Flow." J. Am. Chem. Soc. 124 (2002): 12930–12931.

Fischer, S. and S. Labinov. *Not-In-Kind Technologies for Residential and Commercial Unitary Equipment*. ORNL/CON-477. Oak Ridge National Lab: U.S. Dept. of Energy, 1999.

Gerlach, D. W. and T. A. Newell. "Direct Electrochemical Method for Cooling and Refrigeration." *Proceedings of the 21st IIR International Congress of Refrigeration*, Washington, D.C., August 17-22, 2003.

Gorte, R.J., H. Kim, and J.M. Vohs. "Novel SOFC Anodes for the Direct Electrochemical Oxidation of Hydrocarbon." *Journal of Power Sources* 106 (2002): 10-15.

Grimstvedt, A., S.K. Ratkje, and T. Forland. "Theory of Thermocells: Transported Entropies and Heat of Transfer in Sulfate Mixtures." *J. Electrochem. Soc.* 141.5 (1994): 1236-41.

Hammond, R.H. and W.M. Risen, Jr. "An Electrochemical Heat Engine for Direct Solar Energy Conversion." *Solar Energy* 23 (1980): 443-49.

Hong, J.-S., H. Maleki, S. Al Hallaj, L. Redey, and J. R. Selman. "Electrochemical-Calorimetric Studies of Lithium-Ion Cells." *Journal of the Electrochemical Society* 145 (1998): 1489-1502.

Incropera, F.P. and D.P. Dewitt. *Fundamentals of Heat and Mass Transfer*. New York: Wiley, 1996

Ishihara, A., N. Motohira, K. Ota, and N. Kamiya. "High Temperature Electrochemical Heat Pump Using a Water Gas Shift Reaction: Electrochemical Reduction of CO_2 to CO." *Bulletin of the Chemical Society of Japan* 74 (2001): 1517-23.

Ishihara, A., N. Motohira, K.-I. Ota, and N. Kamiya. "Theory of New Electrochemical Heat Pump and Its Experimental Study." *Proceedings of the Eleventh International Symposium on Molten Salts*. Vol. 98-11. Pennington, N.J.: The Electrochemical Society, 1998. 325-32.

Ishihara, A., T. Fujimori, N. Motohira, K.-I. Ota, and N. Kamiya. "High Temperature Electrochemical Heat Pump using Water Gas Shift Reaction. Part 1: Theoretical considerations." *Journal of Applied Electrochemistry* 29 (1999): 1079-82.

Kamata, M., Y. Ito, and J. Oishi. "Single Peltier Heat of a Hydrogen Electrode in NaOH Solutions at High Concentrations." *Electrochimica Acta* 33.3 (1988): 359-63.

Klein, S.A. *Engineering Equation Solver* (EES). Vers. 6.881. Computer software. F-Chart, 2003.

Kojima, H. and A.J. Bard. "Determination of Rate Constants for the Electroreduction of Aromatic Compounds and Their Correlation with Homogeneous Electron Transfer Rates." *Journal of the American Chemical Society* 97.22 (1975).

Kreysa, G. and G. F. Darbyshire. "Theoretical Consideration of Electrochemical Heat Pump Systems." *Electrochimica Acta* 35.8 (1990): 1283-89.

Kreysa, G., and K. Jüttner. *DECHEMA Monographien* 128 (1993): 21-39.

Lawless, W. N. *Solid State Oxygen Compressors for Joule-Thompson Crycoolers*. NASA Technical Report AD-A323328 DSWA-TR-96-45, March 1997.

Lewis, T. W., L.A.P. Kane-Maguire, A.S. Hutchinson, G.M. Spinks, and G.G. Wallace. "Development of an All-Polymer, Axial Force Electrochemical Actuator." *Synthetic Metals* 102 (1999): 1317-18.

Liebhafsky, H.A. "The Fuel Cell and the Carnot Cycle." *Journal of the Electrochemical Society* 106 (1959): 1068-71.

Mina, E. *Dehumidification Effect by Coupling an Electroosmotic Material with a Desiccant Interface*. Dissertation. Dept. of Mechanical Engineering, U Illinois at Urbana-Champaign, 2004.

Murakami, T., T. Nishikiori, T. Nohira, and Y. Ito. "Thermoelectric Power of M-H Systems in Molten Salts and Application to M-H Thermogalvanic Cell." *Journal of the Electrochemical Society* 150.7 (2003): A928-A932.

Neagu, C. R., J. G. E. Gardeniers, M. Elwenspoek, and J. J. Kelly. "An Electrochemical Active Valve." *Electrochimica Acta* 42 (1997): 3367-3373.

Newman, J. "Thermoelectric Effects in Electrochemical Systems." *Ind. Eng. Chem. Res.* 34 (1995): 3208-16.

Newell, T. "Thermodynamic Analysis of an Electrochemical Refrigeration Cycle." *Intl. J. of Energy Research* 24 (2000): 443-53.

Newell, T.A. Personal Communication. 2000.

Parker, S. ed. *McGraw-Hill Encyclopedia of Chemistry*. 5th ed. New York: McGraw-Hill, 1982.

Pickett, D.J. *Electrochemical Reactor Design.* Amsterdam: Elsevier, 1979.

Pourbaix, M. *Atlas of Electrochemical Equilibria in Aqueous Solutions*. London: Pergamon, 1966.

Prentice, G. *Electrochemical Engineering Principles.* Upper Saddle River, NJ: Prentice Hall, 1991.

Prout, N.M. and J.S. Moorhouse, eds. *Modern Chlor-Alkali Technology*. Vol. 4. New York: Elsevier, 1990. 307.

Quickenden, T.I. and Y. Mua. "A Review of Power Generation in Aqueous Thermogalvanic Cells." *J. Electrochem. Soc.* 142.11 (1995): 3985-93.

Rawat, J.P. and A.A. Ansari. "Redox Exchanger Fuel Cell." *Journal of*

Chemical Education 67.9 (1990): 808-9.

Robinson, R.A. and R.H. Stokes. *Electrolyte Solutions*. New York: Academic Press, 1955.

Sandrock, G. and R.C. Bowman. "Gas-Based Hydride Applications: Recent Progress and Future Needs." *Journal of Alloys and Compounds* 356 (2003): 794-99.

Santiago, J. Personal Communication. 2004.

Shakhashiri, B. *Chemical Demonstrations: A Handbook for Teachers of Chemistry*. Vol. 4. Madison, WI: University of Wisconsin Press, 1992.

Stanczyk, T., B. Illic, P.J. Hesketh, and J.G. Boyd, IV. "A Microfabricated Electrochemical Actuator for Large Displacements." *Journal of Microelectromechanical Systems* 9.3 (2000): 314-20.

Trulove, P.C., H.C. Long, G.R. Stafford, and S. Deki ed.. *Proceedings of the Eleventh International Symposium on Molten Salts*. Vol. 98-11. Pennington, N.J.: The Electrochemical Society, 1998.

U.S. Patent 4,593,534. "Electrochemically driven heat pump."

U.S. Patent 4,671,080. "Closed cryogenic cooling system without moving parts."

U.S. Patent 5,024,060. "Joule-Thomson refrigeration cycle employing a reversible drive electrochemical compressor."

Vetter, K.J. *Electrochemical Kinetics: Theoretical and Experimental Aspects.* New York: Academic Press, 1967.

Appendix A. Analysis of a Novel Refrigeration System Driven by Electrochemical Chlorine Generation

May 7, 2002

Submitted as Term Project Paper in ChE 496-Electrochemical Engineering

A.1 Abstract

Pressure generated by electrochemical reactions can be used to drive refrigeration processes. A refrigeration system is proposed that consists of a high pressure electrolytic cell generating chlorine and hydrogen and a low pressure galvanic cell consuming the products. The chlorine is condensed, throttled, and vaporized to produce a cooling effect. The hydrogen is expanded isenthalpically to produce a cooling effect. A system model and future avenues for research are discussed.

A.2 Introduction

Environmental concerns about the ozone depletion and global warming effects of traditional refrigeration methods have caused the investigation of a variety of new technologies. One area that has not been researched for refrigeration purposes is electrochemical effects. Pressure generated by electrochemical reactions could be used to power refrigeration processes. The open literature contains little information on this concept.

This paper describes a novel refrigeration technique using electrochemically-generated chlorine and hydrogen as working fluids in a refrigeration cycle. Chlorine is easily generated and condenses at temperatures and pressures that are useful for refrigeration.

A.3 Cycle Description

The proposed refrigeration cycle consists of an electrolytic cell linked to its reversible analog, a galvanic cell (see Figure A.3.1). The electrolytic cell is maintained at an elevated pressure and temperature and the galvanic cell at a lower pressure and temperature. Voltage is applied to electrodes immersed in a solution of hydrochloric acid and potassium chloride. The chloride ions in solution are reduced to gaseous chlorine and the H^+ ions are reduced to gaseous hydrogen. The pressure of the gas evolved is chosen so that it is higher than the saturation pressure of chlorine at ambient temperature. The cell is designed so that the gas streams are kept separate. The thermodynamic state of the gases as they exit the cell is defined as state point 1. Both of the gases are cooled to the ambient temperature, by passing through an ideal constant pressure heat exchanger. The chlorine condenses to a saturated liquid state. Throughout the cycle the hydrogen remains a gas at low enough density that it may be considered an ideal gas. The state point on exiting the high temperature heat exchanger is designated as 2.

The chlorine is then throttled isenthalpically to the lower pressure of the galvanic cell. Part of the chlorine may flash to vapor at this point. The hydrogen is passed through an isentropic turbine to the same pressure. The work done by the hydrogen may be utilized elsewhere in the cycle, but this option is not considered here. Both fluid streams decrease in temperature. The chlorine is assumed to be isothermal with the surroundings and in vapor-liquid equilibrium. The hydrogen is at the same pressure as the chlorine, but at a different temperature. This is state point 3.

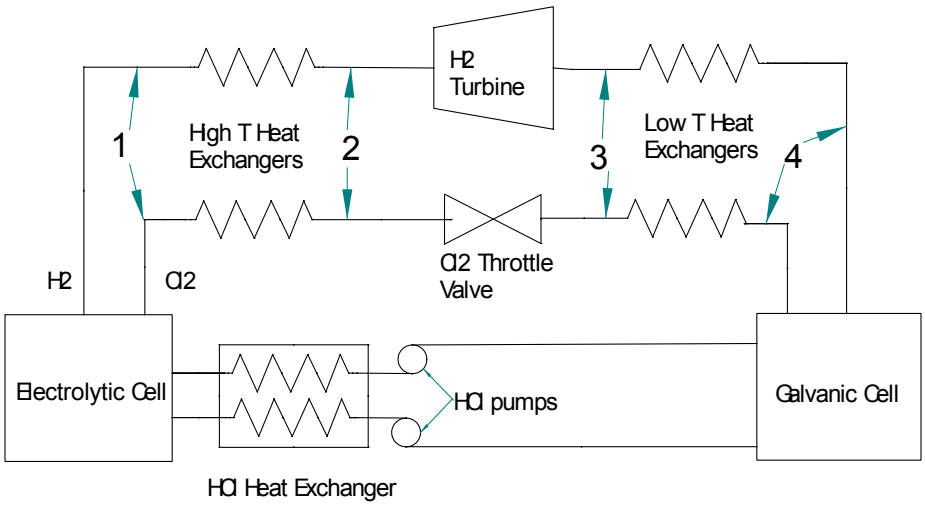

Figure A.3.1 Schematic of refrigeration system using electrochemically-generated chlorine and hydrogen as refrigerants.

The liquid chlorine is then evaporated in a constant pressure/isothermal heat exchanger until it reaches a saturated vapor phase at the temperature of the cold thermal reservoir. No superheating is assumed to occur. The hydrogen is heated in an ideal constant pressure heat exchange to the temperature of the cold thermal reservoir. The heat input to the working fluids in these two processes is the cooling load of the system. The state after the heat exchangers is state point 5.

The gaseous chlorine and hydrogen are then chemically reacted in the galvanic cell to produce hydrogen chloride that dissolves in the aqueous solution in the galvanic cell. This cell is very analogous to the more common hydrogen-oxygen fuel cell. This system also produces electricity that is fed back to the galvanic cell.

The concentration of hydrochloric acid in the galvanic cell is increased by the electrochemical reaction, as the concentration in the electrolytic cell is decreased. The high concentration acid solution is pumped back to the electrolytic cell and low concentration solution returned to the galvanic cell. A heat exchanger regenerates heat from one stream to the other. Due to the concentration difference between the streams, the specific heats of the streams are different. However, this source of irreversibility will be ignored in the present analysis. This is equivalent to assuming that the pumping rate is high enough that the concentration does not vary significantly.

Because the electrolytic and galvanic cells operate at different temperatures and pressures, the electrolytic cell requires more energy than the galvanic cell produces. Therefore, a small voltage must be added to the circuit in order to drive the electrolytic cell. This is the energy input to drive the cycle. It is equal to the difference between the voltages due to the thermodynamic states of the two cells plus any voltage drops due to irreversibilities.

A.4 Model Description

The proposed refrigeration system was modeled using the Engineering Equation Solver (EES) package from F-chart Software (Klein 2003). EES is a Newton-Raphson solver that includes special functions for modeling refrigeration and other mechanical thermodynamic systems.

The complete model is composed of three subprograms for the electrolytic cell, the galvanic cell, and the gas and liquid phase processes of the chlorine and hydrogen. The main program ensures that the output from one part of the cycle equals the input to the next part. The main program also calculates the coefficient of performance (COP) of the cycle. A copy of the EES file accompanies this report.

A.4.1 Gas and Liquid Processes

The part of the cycle operating with molecular hydrogen and chlorine is modeled with standard thermodynamic methods. The electrolytic cell is termed the gas generator in the model. The generator pressure (P_{gen}) and temperature (T_{gen}) are set by the main program. They can be adjusted to optimize performance.

The following equations define the states of the working fluid at point 1:

$T_{1H2} = T_{gen}$ [K]

$P_{1H2} = P_{gen}$ [MPa]

$H_{1H2} = \mathbf{h}('H2', T=T_{1H2})$ [kJ/(kmole]

$S_{1H2} = \mathbf{s}('H2', T=T_{1H2}, P=P_{1H2})$ [kJ/(kmole*K]

$T_{1CL2} = T_{gen}$ [K]

$P_{1CL2} = P_{gen}$ [MPa] A.4.1.1

Call **JANAF**('CL2', T_{1CL2} : CP_{1CL2}, H_{1CL2}, S_{1CL2})

where the subscript H2 refers to hydrogen and CL2 refers to chlorine. The variables H and S are the molar enthalpy and entropy. The functions **h** and **s** are EES functions that calculate the entropy and enthalpy of the substance named at the input conditions. The "Call **JANAF**" function computes the ideal gas specific heat, enthalpy, and entropy of the input substance as a function of temperature. It uses polynomial curve fits from the JANAF tables.

The state of the refrigerants at state 2 is calculated by:

$T_{2H2} = T_{amb}$ [K]

$P_{2H2} = P_{gen}$ [MPa]

$H_{2H2} = \mathbf{h}('H2', T=T_{2H2})$ [kJ/(kmole]

$S_{2H2} = \mathbf{s}('H2', T=T_{2H2}, P=P_{2H2})$ [kJ/(kmole*K]

$T_{2CL2} = T_{amb}$ [K]

$P_{2CL2} = P_{1CL2}$ [MPa]

$H_{2CL2} =$ **Interpolate** ('CL2sat', 'Tsat', 'Hmolsatl', 'Tsat' = T_{amb}) [kJ/kmole] assume no subcooling

$S_{2CL2} =$ **Interpolate** ('CL2sat', 'Tsat', 'Smolsatl', 'Tsat' = T_{2CL2}) [kJ/(kmole*K]

A.4.1.2

where T_{amb} is the ambient temperature. These equations assume that the chlorine leaves the heat exchanger as a saturated liquid. The hydrogen leaves at the ambient temperature. Because EES does not have built in data on the saturation properties of chlorine, the saturation temperature, pressure, and molar enthalpy and entropy as saturated liquid and vapor were entered into a table. The "Interpolate" command uses cubic interpolation to read data from the table.

The state of the chlorine at point 3 was fixed by assuming that it was in liquid-vapor equilibrium at the galvanic cell's pressure and that the throttling process was isenthalpic. The hydrogen state was fixed by assuming an isentropic expansion to the final pressure. The equations are as follows:

$P_{3H2} = P_{3CL2}$ [MPa]

$H_{3H2} = \mathbf{h}('H2', T=T_{3H2})$ [kJ/(kmole]

$S_{3H2} = S_{2H2}$ [kJ/(kmole*K]

$S_{3H2} = \mathbf{s}('H2', T=T_{3H2}, P=P_{3H2})$ [kJ/(kmole*K]

$T_{3CL2} = \mathbf{Interpolate}('CL2sat', 'Psat', 'Tsat', 'Psat' = P_{3CL2})$ [K]

$H_{3CL2l} = \mathbf{Interpolate}('CL2sat', 'Tsat', 'Hmolsatl', 'Tsat' = T_{3CL2})$ [kJ/kmole]

$H_{3CL2v} = \mathbf{Interpolate}('CL2sat', 'Tsat', 'Hmolsatv', 'Tsat' = T_{3CL2})$ [kJ/kmole]

$H_{3CL2} = (1 - x_{3CL2}) \cdot H_{3CL2l} + x_{3CL2} \cdot H_{3CL2v}$ flashes to an unknown quality on exiting throttle valve

$H_{3CL2} = H_{2CL2}$

$S_{3CL2l} = \mathbf{Interpolate}('CL2sat', 'Tsat', 'Smolsatl', 'Tsat' = T_{3CL2})$ [kJ/(kmole*K]

$S_{3CL2v} = \mathbf{Interpolate}('CL2sat', 'Tsat', 'Smolsatv', 'Tsat' = T_{3CL2})$ [kJ/(kmole*K]

$S_{3CL2} = (1 - x_{3CL2}) \cdot S_{3CL2l} + x_{3CL2} \cdot S_{3CL2v}$ [kJ/(kmole*K]

A.4.1.3

where x is the chlorine quality.

The final state (4) of the diatomic chlorine and hydrogen is fixed by assuming that the chlorine is heated to saturated vapor at constant pressure and at cooled region. The hydrogen is also heated to the temperature of the cooled region as follows:

$T_{4H2} = T_{cold}$

$P_{4H2} = P_{3H2}$ [MPa]

$H_{4H2} = \mathbf{h}('H2', T=T_{4H2})$ [kJ/(kmole]

$S_{4H2} = \mathbf{s}('H2', T=T_{4H2}, P=P_{4H2})$ [kJ/(kmole*K]

$T_{4CL2} = T_{cold}$

$P_{4CL2} = P_{3CL2}$ [MPa]

$T_{4CL2} = \mathbf{Interpolate}('CL2sat', 'Psat', 'Tsat', 'Psat' = P_{4CL2})$

$H_{4CL2} = \mathbf{Interpolate}('CL2sat', 'Tsat', 'Hmolsatv', 'Tsat' = T_{4CL2})$ [J/mole] assume no superheat

$S_{4CL2} = \mathbf{Interpolate}('CL2sat', 'Tsat', 'Smolsatv', 'Tsat' = T_{4CL2})$ [kJ/(kmole*K]

A.4.1.4

The heat transfer to and from the heat exchangers are calculated from energy conservation as follows:

$$Q_{12H2} = H_{2H2} - H_{1H2} \quad [J/mole]$$
$$Q_{34H2} = H_{4H2} - H_{3H2} \quad [J/mole]$$
$$Q_{12CL2} = H_{2CL2} - H_{1CL2}$$
$$Q_{34CL2} = H_{4CL2} - H_{3CL2} \qquad \text{A.4.1.5}$$
$$Q_{tothot} = Q_{34H2} + Q_{34CL2} \quad [J/mole]$$
$$Q_{totcold} = Q_{12H2} + Q_{12CL2} \quad [J/mole]$$

where the numbered Q's are the heat transfer in a particular fluid between two states, Q_{tothot} is the heat rejected from the high pressure heat exchanger, and $Q_{totcold}$ is the cold side heat absorption. The reversible amount of work needed to pump the chlorine and hydrogen from state 4 to state 1 was similarly calculated:

$$W_{41H2} = -(H_{1H2} - H_{4H2}) \quad [J/mole] \text{assuming internally reversible}$$
$$W_{41CL2} = -(H_{1CL2} - H_{4CL2}) \quad [J/mole] \text{assuming internally reversible} \qquad \text{A.4.1.6}$$
$$W_{pump} = 0$$
$$W_{tot} = W_{41H2} + W_{41CL2} + W_{pump}$$

This assumes that the pump work (W_{pump}) is negligible.

The theoretical COP of the system can be calculated as follows:

$$COP = \frac{Q_{totcold}}{W_{tot}} \qquad \text{A.4.1.7}$$

A.4.2 Electrolytic Cell

The electrolytic cell was modeled by standard electrochemical methods. It was viewed as a parallel plate geometry with laminar flow through the channel. The anode reaction is the production of chloride gas from the chloride ion in solution:

$$2Cl^- \rightarrow Cl_2 + 2e^- \qquad \text{A.4.2.1}$$

The cathode reaction is the production of gaseous hydrogen from the H^+ ion:

$$2H^+ + 2e^- \rightarrow 2H_2 \qquad \text{A.4.2.2}$$

The electrolyte considered contains 1M HCl and 1M KCl. HCl was used because at low pH alternative reactions are not thermodynamically favorable (Pourbaix, 1966). The KCl was included to increase the electrolyte conductivity and reduce ohmic resistance losses.

The equilibrium potentials (E_0) for the electrodes at standard state were obtained from published sources (Bard, 2001). The effect of temperature on cell potential was modeled by the following equations:

$$E_{Ta} = E_{0a} + \frac{\Delta S_a}{n_a \cdot Far} \cdot (T - T_0)$$

$$E_{Tc} = E_{0c} + \frac{\Delta S_c}{n_c \cdot Far} \cdot (T - T_0) \qquad \text{A.4.2.3}$$

where the subscripts a and c refer to the anode and cathode respectively. "Far" is the Faraday constant (96485.3 Coulomb/mole), n is the number of electrons involved in the reaction (n=2 for both reactions), T_0 is the reference temperature (298.15 K), ΔS is the molar entropy change of the reaction, T is the temperature, and E_T is the electrode potential at T.

The change in electrode potential due to pressure changes was calculated with the Nernst equation. The activity of the dissolved reactants was referenced to a one molar solution. Although the solution used is most likely too concentrated for dilute solution theory, the error should not be significant. The activity of the gas phase products was referenced to a pressure of 1 atm. The activity computations are:

$Far = 9.64853 \cdot 10^4$ [Coulomb/mole]

$c_0 = 1000$ [mole/m^3] solute activity referenced to 1M solution

$P_0 = 1$ [atm] gas activity referenced to 1 atm pressure

$$act_{aox} = \frac{m_{aox}}{c_0}$$

$$act_{cred} = \frac{m_{cred}}{c_0} \qquad \text{A.4.2.4}$$

$$act_{ared} = \frac{P}{P_0}$$

$$act_{cox} = \frac{P}{P_0}$$

where the subscript ox refers to the oxidized species and the subscript red refers to the reduced species and P is the cell pressure. The equations governing the pressure effect are:

$$E_{equiba} = E_{Ta} - \frac{1}{f_a} \cdot \ln\left[\frac{act_{cox}}{act_{cred}}\right] \quad \text{[Volt]}$$

$$E_{equibc} = E_{Tc} - \frac{1}{f_c} \cdot \ln\left[\frac{act_{ared}}{act_{aox}}\right] \quad \text{[Volt]} \qquad \text{A.4.2.5}$$

where E_{equib} is the electrode potential at pressure P and f is Far*n/R*T (R is the ideal gas constant). Adjustments for the depletion of the electrolyte as it passes through the cell were not made.

The non-spontaneous electrochemical reactions in the electrolytic cell can be driven faster by increasing the applied cell voltage above the equilibrium voltage. The excess energy needed to drive the reaction is a loss. Conversely, the voltage produced by the spontaneous reaction in the galvanic cell is decreased due to these kinetic losses.

The cell kinetics were modeled using the Butler-Volmer equation, a standard equation for electrochemical kinetics. The reaction rate is a function of the electrode overpotential, the difference between the potential as determined by thermodynamics. The overpotential (ε) is:

$$\varepsilon_a = E_a - E_{equiba} \quad \text{anodic kinetic overvoltage}$$
$$\varepsilon_c = E_c - E_{equibc} \quad \text{cathodic kinetic overvoltage} \qquad \text{A.4.2.6}$$

where E is the actual potential at the electrode.

The Butler-Volmer equation depends on two empirically measured parameters; i_0 and α. i_0 is the exchange current density. This a measure of how rapidly the reaction proceeds given a certain kinetic overpotential. It is equal to the current density that flows across the electrode-solution interface at equilibrium. α is a measure of the symmetry of the voltage-current curve around equilibrium. An α of 0.5 means that an increase in voltage causes the forward reaction to proceed at the same rate that the same quantity of decrease in voltage will make the reverse reaction proceed. Although the data used in these computations is in the right range for the reactions considered (Vetter, 1967), the actual values are strong functions of the electrode material. If a prototype system is built, i_0 will probably be a fitting parameter. In the present model α is assumed as 0.5.

The Butler-Volmer equations for the electrodes are:

$$i_a = i_{0a} \cdot \left(e^{(-\alpha_a \cdot f_a \cdot \varepsilon_a)} - e^{((1-\alpha_a) \cdot f_a \cdot \varepsilon_a)}\right)$$
$$i_c = i_{0c} \cdot \left(e^{(-\alpha_c \cdot f_c \cdot \varepsilon_c)} - e^{((1-\alpha_c) \cdot f_c \cdot \varepsilon_c)}\right) \qquad \text{A.4.2.7}$$
$$i = i_c$$
$$i_a = -i_c$$

where i is the current density in Amp/m^2. The quantity f is F/RT where R is the ideal gas constant and T is the cell temperature. Adjustments for the depletion of the electrolyte as it passes through the cell were not made.

The maximum current attainable is limited by the rate of diffusion of reactant to the surface. A published correlation for the diffusion limited current in a laminar flow between two flat plat electrodes was used (Prentice, 1991). As the hydrogen ion diffuses extremely rapidly, it is assumed that the chloride ion determines the limiting current. The correlation is:

$$i = \text{translimitcoeff} \cdot i_l$$
$$i_l = 1.23 \cdot n_a \cdot Far \cdot D_a \cdot c_{aox} \cdot \left[\frac{v_{avg}}{d_e \cdot D_a \cdot x}\right]^{(1/3)} \qquad \text{A.4.2.8}$$

where D_a is the diffusion coefficient of the chloride ion, v_{avg} is the average fluid velocity, d_e is the passage hydraulic diameter, and x is the position from the front of the plate. The variable translimitcoeff is the fraction of the limiting current density at which the cell is operating. It is an increasing function of x. It was manually monitored to ensure that the limiting current was not exceeded. The cell total current was calculated by integrating the current density times cell width as a function of x:

$$I_{tot} = \int_{0.0001}^{L} (i \cdot w)\, dx \qquad \text{A.4.2.9}$$

The electrolyte conductivity was calculated by:

$$\kappa = Far \cdot (u_{Clminus} \cdot z_{Clminus} \cdot m_{aox} + u_{Hplus} \cdot z_{Hplus} \cdot m_{cred} + u_{Kplus} \cdot z_{Kplus} \cdot m_{nonreact}) \qquad \text{A.4.2.10}$$

where κ is the conductivity, u is the ionic mobility (an empirically measured quantity), m is the solute molarity, and z is the ion charge. The cell resistance per area, R_ω, and ohmic voltage drop, E_r, are:

$$E_r = i \cdot R_\omega$$
$$R_\omega = \frac{1}{\kappa} \cdot d \qquad \text{A.4.2.11}$$

No adjustment for the added resistance due to bubbles was made.

The total voltage is the sum off the electrode potentials and the ohmic voltage drop:

$$E_{tot} = E_a + E_c + E_r \qquad \text{A.4.2.12}$$

The total power consumed by the electrolytic cell, $Power_{tot}$, is the total voltage times the total current:

$$Power_{tot} = E_{tot} \cdot I_{tot} \qquad \text{A.4.2.13}$$

The power per mole of reaction, power, is:

$$power = Power_{tot} \cdot \frac{Far}{I_{tot}} \qquad \text{A.4.2.14}$$

A.4.3 Galvanic Cell

The Galvanic cell is modeled virtually identically to the electrolytic cell. Of course, the half reactions run the opposite directions of the ones in the electrolytic cell. The differences between the two sub-models are primarily accounted for by reversing the anode and cathode and the reactants and products.

In the interest of simplicity, the Galvanic cell is assumed to operate well below the diffusion limit. This is probably accurate for the hydrogen electrode as gaseous hydrogen also diffuses rapidly. This approximation may not be as good for the chlorine electrode.

A.4.4 Overall COP

The voltage applied to the whole system, E_{in}, is calculated by subtracting the galvanic cell voltage, E_{fc}, from the electrolytic cell voltage, E_{totgen}. The total electrical power consumed by the system is this voltage times the current:

$$E_{in} = E_{totfc} - E_{totgen}$$
$$Power_{electrical} = E_{in} \cdot I_{totfc} \qquad \text{A.4.4.1}$$

The system COP is the heat per mole absorbed from the cold reservoir divided by the electrical power input per mole:

$$COP_{actual} = Q_{totcold} \cdot \frac{I_{totfc}}{Power_{electrical} \cdot Far} \qquad \text{A.4.4.2}$$

A.5 Results and Discussion

The thermodynamic COP of the cycle is in the range of 4 at a T_{amb} of 25C, T_{cold} of 0C, and T_{gen} of 77C. This is competitive with some vapor compression systems. However, the calculated COP including the irreversibilities in the cells is in the range of 1-2. As the applied voltage decreases the COP approaches the ideal COP (see Figure A.5.1). However, the current and cooling rate decrease.

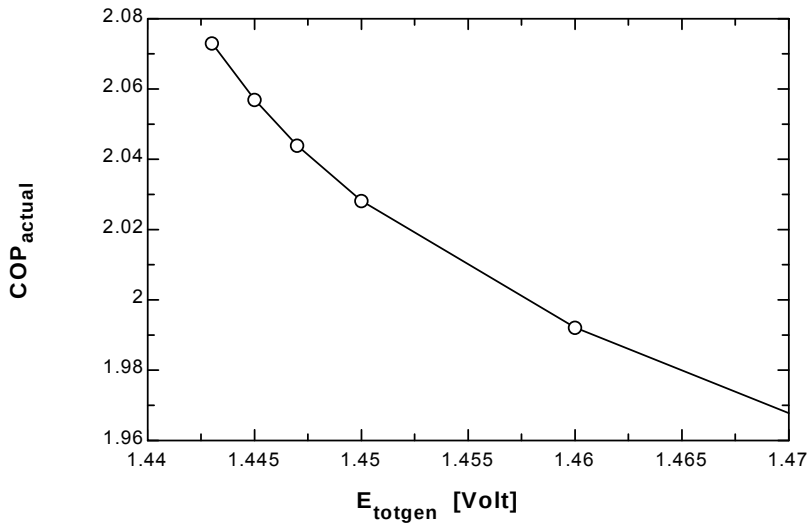

Figure A.5.1 COP of proposed system increases with decrease in applied voltage

A.6 Future Work and Conclusions

The proposed system using electrochemically generated chlorine and hydrogen as refrigerants is thermodynamically feasible. However, it may not be more efficient than current systems in practice.

As the model exhibits the expected and physical behavior, it will be used to analyze the system performance. Alternative pathways for the hydrogen can be explored, such as utilizing the work from the turbine. More detailed analyses of the sources of entropy generation and losses will be performed.

The model described includes the most important effects. However, it could be improved by adding mass transport effects to the galvanic cell. Better kinetic data should be used when an electrode material is identified. Also, the HCl_{aq} heat exchangers and the pumping power should be explicitly modeled. The model could be used to optimize the cell dimensions and the cells' pressures and temperatures could be optimized given a cell design and electrolyte flow rate.

Chlorine forms clathrates with water at low temperatures. This could make the cell design more difficult or impossible if they must operate in a regime where clathrates form. This problem also needs to be researched further.

In addition, chlorine is corrosive and toxic. Handling large quantities of the gas may not be feasible. The proposed system may be most useful on a meso or micro scale for cooling electronics or other small systems. It could be implemented with few or no moving parts. The only moving parts are the pump and the hydrogen turbine. Because the acid solution conducts electricity, the pump could be replaced with a magnetohydrodynamic pump that has no moving parts. A different type of isentropic expansion device other than a turbine could be used.

A different, less hazardous gas with good thermal properties could be generated electrochemically. Both ammonia and sulfur dioxide have been used as refrigerants and are electrochemically active. Alternatively, the hydrogen could be eliminated and a solution phase redox couple substituted. For instance the reaction:

$$Fe^{3+} + e^- \Leftrightarrow Fe^{2+} \qquad \text{A.6.1}$$

could replace the hydrogen evolution. This could simplify the system by eliminating the hydrogen pathway.

If further modeling indicates that this system has promise, prototypes could be built and compared to the model predictions.

Appendix B. Initial Development of a Model for Losses in a Polymer Electrolyte Membrane Electrochemical Refrigeration Cycle

B.1 Introduction

Theoretically, a water electrolyzer will absorb heat and a hydrogen-oxygen fuel cell will release heat[1]. The use of this electrochemical effect to produce a cooling effect has been proposed.[2] As this was the first system proposed, a literature review was conducted of prior models for fuel cells. Because of the temperature range of interest, polymer electrolyte membrane fuel cells were selected as the most relevant for refrigeration.

A fuel cell connected in a cycle with an electrolyzer at a different temperature can act as a direct electrochemical refrigeration cycle (DERC). Because of the second law of thermodynamics, electricity must be put in to the system in order to account for the difference in temperature. Coefficients of performance (COP) of 20-30 have been calculated for temperature regimes of practical interest[2]. However, these calculations assume ideal reversible components. In practice, fuel cells and electrolyzers have large losses due to ohmic losses in the electrolyte and electrodes and energy needed to overcome the chemical activation barriers. The difference between the reversible voltage and the actual voltage is termed overpotential. These losses increase with higher current densities. Much fuel cell and electrolyzer research has been done with the goal of increasing current density in order to decrease the cost and weight of the unit.

It is unclear whether the proposed hydrogen-oxygen electrochemical refrigeration cycle could practically produce a cooling effect. The system must be run at very low current densities so that the heat released by the losses does not overpower the absorption of heat. The current densities may be so low that the resulting system would be excessively large or prohibitively expensive. A more accurate model that takes into account irreversibilities and current density effects is needed.

B.2 Prior Models

Polymer electrolyte membranes (PEM) are the best candidate for the hydrogen-oxygen refrigeration cycle. They are simpler to construct than other systems, are efficient, and operate at temperatures appropriate for use as air-conditioning systems. They have been extensively studied for use in both electrolyzers and fuel cells. PEM fuel cells are in production and use. There are a number of models in the literature for both types of systems.

Fuel cells have been the subject of more modeling effort due to their importance in low emissions vehicles. Some of the simpler models are essentially curve fits to experimental data. Amphlett et al[3,4]. used a mechanistic model to develop the form of equations that should model a fuel cell, then fit data from a production fuel cell to these equations. This model was later generalized so that it could model a wider variety of fuel cells.[5] These empirically based models are restricted to performance prediction and analysis for the particular fuel cell tested or for particular performance regimes.

More theoretically-based models are more suitable for predicting the performance of fuel cells outside of the tested regions. As the electrochemical refrigeration cycle would operate in a lower current density regime than most fuel cells, a more theoretical model is preferred.

In a series of papers, Bernardi and Verbrugge[6,7,8] develop an excellent model incorporating a variety of effects. They assume an isothermal model and solve it in one dimension. However, they include the effect of pressure gradients through the membranes and account for the difference between liquid water and water vapor in the pores of the gas diffusion electrodes. They also explicitly include a catalyst region of finite thickness. Many models assume a very rapid reaction and model the catalyst region as of infinitesimal thickness. The inclusion of the catalyst region is useful in thermal modeling because the reversible heat effect occurs in this region. They also include the variation in potential in the cathode gas diffusion electrode.

The core of this model is four systems of seven coupled differential equations. There is a set for the anode catalyst region, the membrane, the cathode catalyst region, and the cathode gas diffusion electrode. The boundary conditions for these regions are complicated and not completely clear from the paper. The model results match experimental data very well. Because of the fundamental nature of this model and its accuracy, repeated attempts were made to replicate the model. Due to the complexity of the boundary conditions, this model was not completed.

The model proposed by Springer et al. is less complex than the model of Bernardi.[9] It does not account for pressure differences across the cell or liquid and vapor regions in the electrodes. However, it does give special attention to the effect of osmotic drag where the protons (H^+) pull water molecules with them across the membrane. This model also adequately matches the experimental data. Because of its greater simplicity it was also investigated as a possible model for the PEM DERC.

A number of studies have focused on water management in fuel cells. At high current densities water may be produced at the cathode faster than it can be removed. The gas diffusion electrode floods and oxygen is cut off from the catalyst layer, thus decreasing cell voltage. At high current densities the osmotic drag forces exceed the diffusion of water in the opposite direction. Therefore, enough water is removed from the anode that the membrane dries out, increasing the membrane resistance. Bernardi[6], Fuller[10], and Bashuk[11] studied these effects. Since the DERC will function at low current densities these effects can be ignored.

The behavior of the PEM itself has been measured and studied. Choi[12] measured the electro-osmotic drag coefficient of two brands of membranes. Futerko[13] performed a two-dimensional study of the resistance of the membrane and found that the water content and potential inside the membrane vary in the direction perpendicular to the current flow. Eikerling[14] calculated the electrophysical properties of PEMs with respect to membrane water concentration using a random network model of pores. Bultel[15] modeled the catalyst regions in detail using both the thin film and volume models.

Several attempts at modeling PEM electrolyzers have been reported in the literature. Experimental data for PEM electrolyzer designs is given in Dhar[16] and Ledjeff[17]. The performance and stability of catalysts and membranes during electrolysis were studied by Andolfatto et al.[18], Millet[19], and Ahn et al.[20]. The potential distribution inside of the membrane during electrolysis was modeled by Millet[21].

B.3 Features of Model to be Developed

The PEM fuel cell-electrolyzer model was not developed in favor of a more general model that could be used to explore the design space of electrochemical systems. However, some initial model development work was performed. Attempts to use the models of Bernardi[8] were not successful due to the model's complexity, and attempts to use the model of Springer[9] were not completed due to the decision to use a more general model. However, some of the features of a PEM DERC model were determined and show a possible future direction for work on this problem.

In order to investigate the feasibility of the DERC, the one-dimensional approximation is sufficient. The model will be divided into a well-mixed anode gas chamber, an anode gas diffusion electrode, an anode catalyst region, a PEM region, a cathode catalyst region, a cathode gas diffusion electrode, and well-mixed cathode gas chamber. The catalyst regions consist of an area with intermingled electrode and membrane materials and embedded catalyst particles. Since the reversible heat effect occurs in this region it is preferable that it be modeled specifically. The potential and reactant distribution in this region affects the efficiency of catalyst use and thus the overpotential and cell cost.

The model should track the concentration profiles of the main reactant species: H_2, O_2, and H^+. For the purposes of validating the model with respect to published experimental data, the model should include the presence

of N_2 in the cathode chamber. However, the actual DERC will probably have pure O_2 in this region. The model should include the effects of diffusion in the membrane and gas diffusion electrodes and osmotic drag in the membrane. The electrical potential profile should also be modeled. Because the current density is constant through the cross section, the potential profile can be used to determine where losses occur. Modeling of the temperature profile across the cell could provide useful insights. However, as the current density is low the isothermal approximation is almost certainly valid. A lumped capacitance approximation could be used.

The electrochemical kinetics involved in the reaction are of utmost importance as the activation overpotential on the oxygen electrode is the largest loss. Most electrochemical models use the Tafel slope formula

$$E-E_0=a+b\log(I) \qquad \text{B.3.1}$$

where E is the actual cell potential, E_0 is the equilibrium cell potential, and a and b are experimentally-measured constants for a specific reaction[1]. This approximation is only valid at higher current densities. At lower current densities the reverse chemical reaction becomes more important and the potential-current curve becomes more vertical. A different formula should be used in this region.

The gas flowing into the fuel cell will be saturated with water vapor at the input gas temperature. Many fuel cell models have an outflow from the reactant gas chambers. The DERC model may only have water leaving the chamber. This could be modeled by adding a wicking system to the model. Because this would add another level of complexity to the model, the feasibility studies could be performed by assuming that whenever the water vapor concentration in the electrodes reached a certain value such as 110 percent of saturation, the excess water is removed by some as yet unspecified system.

The electrolyzer model would be very similar to that of the fuel cell. The membrane equations would be identical. However, the gas regions would be replaced by water regions containing the dissolved gases produced in the reaction. In addition, the diffusion in the electrodes would be water diffusing to the membrane instead of gases. Of course, the kinetics of the catalyst region would be different as the reactions and catalysts employed are different. Most of these changes are simply variations in the properties and not variations in the fundamental equations used in the model.

The primary difference between the electrolyzer and fuel cell models is the modeling of the bubble formation and detachment on the electrodes. A standard heterogeneous nucleation model could be used for the formation and any bubble that reaches a certain size would be considered to detach. However, bubble formation within the electrodes will affect the flow of water to the catalyst region. This would need to be included.

The models presented in the literature are commonly formulated as systems of coupled differential equations. Attempts made to replicate this structure were not completed. The replication of the model described by Springer[9] may be continued.

An alternate direction is to model the system by discretizing the electrochemical cell and assuming known values for concentrations in one of the reactant chambers. The cell current can be assumed and the voltage guessed. The concentration and potential profiles can then be solved for by marching through the domain. The voltage and concentrations in the other reaction chamber must match the boundary conditions. The guessed voltage value can be adjusted and the solution iterated until the boundary conditions are met.

The two models could be constructed separately and validated against published data. They could then be linked with the output of one connected to the input of the other. If the model shows that the hydrogen-oxygen DERC is feasible, a prototype could be built. The data from testing of the prototype could be used to further validate the model.

B.4 Conclusions

A number of PEM fuel cell models have been reviewed and a possible structure for a model developed. However, this model was not pursued because it was very narrowly related to H2-O2 PEM systems and a more general model of the DERC was desired. In addition, the oxygen electrode is kinetically quite sluggish and would have excessively high losses. Although his model structure could also be converted to a modeling the chlorine-hydrogen fuel cell system discussed in chapter 7, it may be better to modify existing PEM chlor-alkali cell models for the gas evolving cell.

B.5 List of References

[1]Berndt, D. Maintenance-Free Batteries: Lead-Acid, Nickel/Cadmium, Nickel/Hydride. 1993. Research Studies Press Ltd. Taunton, England.

[2]Newell, T.A. "Thermodynamic analysis of an electrochemical refrigeration cycle." International Journal of Energy Research. Vol. 24: 443-453. 2000

[3]Amphlett, J. C., R. M. Baumert, R. F. Mann, B. A. Peppley, and P. R. Roberge. "Performance Modeling of the Ballard Mark IV Solid Polymer Electrolyte Fuel Cell: I. Mechanistic Model Development." J. Electrochemical. Soc. Vol. 142, No. 1, 1-8. Jan. 1995a.

[4]Amphlett, J. C., R. M. Baumert, R. F. Mann, B. A. Peppley, and P. R. Roberge. "Performance Modeling of the Ballard Mark IV Solid Polymer Electrolyte Fuel Cell: II. Empirical Model Development." J. Electrochemical. Soc. Vol. 142, No. 1, 9-15. Jan. 1995b

[5]Mann, R.F., J.C. Amphlett, M.A.I. Hooper, H.M. Jensen, B.A. Peppley, and P.R. Roberge. "Development and application of a generalized steady-state electrochemical model for a PEM fuel cell." Journal of Power Sources. Vol. 86, 173-180. 2000.

[6]Bernardi, D. M. "Water-Balance Calculations for Solid-Polymer-Electrolyte Fuel Cells." J. Electrochemical. Soc. Vol. 137, No. 11,3344-3350. Nov. 1990

[7]Bernardi, D.M. and MW. Verbrugge. "Mathematical Model of a Gas Diffusion Electrode Bonded to a Polymer Electrolyte." AIChE Journal. Vol. 37, No. 8, 1151-1163. August 1991.

[8]Bernardi, D.M. and M.W. Verbrugge. "A Mathematical Model of the Solid-Polymer-Electrolyte Fuel Cell." J. Electrochemical. Soc. Vol. 139, No. 9, 2477-2491. Sept. 1992.

[9]Springer, T. E., T. A. Zawodzinski, and S. Gottedfeld. "Polymer Electrolyte Fuel Cell Model." J. Electrochem. Soc. Vol. 138, No. 8, 2334-2342. Aug. 1991.

[10]Fuller,T.F., and J. Newman. "Water and Thermal Management in Solid- Polymer-Electrolyte Fuel Cells." J. Electrochemical. Soc. Vol. 140, No. 5, 1218-1225. May 1993.

[11]Baschuk, J. J. and Xianguo Li. "Modelling of polymer electrolyte membrane fuel cells with variable degrees of water flooding." Journal of Power Sources. Vol. 86, 181-196. 2000.

[12]Choi, K.-H., D.-H. Peck, C.S. Kim, and D.-R. Shin, and T.-H. Lee. "Water transport in Polymer membranes for PEMFC." Journal of Power Sources. Vol. 86, 197-201. 2000.

[13]Futerko, P. and I.-M. Hsing. "Two-dimensional finite-element method study of the resistance of membranes in polymer electrolyte fuel cells." Electrochimica Acta. Vol. 45, 1741-1751. 2000.

[14]Eikerling, M., A. A. Kornyshev, and U. Stimming. "Eletrophysical Properties of Polymer Electrolyte Membranes: A Random Network Model." J. Phys. Chem. B, 101, 10807-10820. 1997.

[15]Bultel, Y., P. Ozil, and R. Durand. "Modified thin film and agglomerate models for active layers of P.E. fuel cells." Electrochimica Acta Vol. 43, No. 9, 1077-1087. 1998.

[16]Dhar, H.P. "A unitized approach to regenerative solid polymer electrolyte fuel cells." Journal of Applied Electrochemistry. Vol. 23, 32-37. 1993.

[17]Ledjeff, K., A. Heinzel, V. Peinecke, and F. Mahlendorf. "Development of Pressure Electrolyzer and Fuel Cell with Polymer Electrolyte." Int. J. Hydrogen Energy. Vol. 19, No. 5, 453-455. 1994.

[18]Andolfatto, F., R. Durand, A. Michas, P. Millet, and P. Stevens. "Solid Polymer Electrolysis: Electrocatalysis and Long-Term Stability." Int. J. Hydrogen Energy. Vol. 19, No. 5, 421-427. 1994.

[19]Millet, P., T. Alleau, and R. Durand. "Characterization of membrane-electrode assemblies for solid polymer electrolyte water electrolysis." Journal of Applied Electrochemistry. Vol. 23, 322-331. 1993.

[20]Ahn, J., and R. Holze. "Bifunctional electrodes for an integrated water-electrolysis and hydrogen-oxygen fuel cell with a solid polymer electrolyte." Journal of Applied Electrochemistry. Vol. 22, 1167-1174. 1992.

[21]Millet, P. "Water electrolysis Using EME Technology: Electric Potential distribution Inside a Nafion Membrane During Electrolysis." Electrochimica Acta. Vol. 39, 2501-2506. 1994.

Appendix C. Comments on Electrochemical Heat Engines

Although the analyses presented here are focused on refrigeration, they could also be reapplied to heat engines simply by reversing the signs of heat and electricity inputs. The use of electrochemical cells for heat engines has been studied for thermally regenerative electrochemical systems as discussed in Chapter 1.

Lower temperature systems developed for use in cooling could be reapplied to waste heat recover and power production from low quality heat sources such as solar ponds or as a bottoming cycle. Low temperature electrochemical heat engines may have low second law efficiencies at reasonable power density. However, the final objective in power generation is not efficiency, but cost per kilowatt-hour. In heat recovery the cost of energy input is minimal if there is no alternative use for the thermal energy, e.g. space heating or process heat. Therefore capital and maintenance costs would drive the profitability of the system. There is little that can be determined about maintenance costs at the current level of analysis.

If the system used large quantities of cheap electrolytes, the capital cost might be low relative to other heat recovery systems. However, a low temperature TRES will be competing against Stirling or Rankine systems with relatively cheap fluids such as air, helium, butane, or ammonia. Therefore their capital cost advantage would have to be in the cost of piping, reactors, etc. It seems unlikely that an electrochemical system with its material requirements for electrodes and membranes would be cheaper than a traditionally manufactured thermal system.

The technical limiting factor on many such systems, especially the Stirling cycle, is getting heat in and out of engine. As electrochemical systems already require a large surface area and a thin design due to the narrow electrode spacing, it may be simpler to develop a system with a large surface for heat exchange.

The heat input and cooling for systems that pump the working fluid between cells, could be integrated directly into existing waste heat and cooling streams. For instance heat exchangers could be inserted into flue gas and cooling tower flows. This would of course increase complexity and the pressure drop in the systems. However, it would actually decrease the cooling tower load, because some of the heat would be extracted as useful work.

The second law efficiency is expected to increase with higher temperatures. Several of the losses decrease with increasing temperature. The ionic resistivity in general decreases with higher temperature and therefore higher ionic mobility. Also, the kinetics are more rapid and the losses should decrease. These are some of the reasons that most TRES operate at higher temperatures.

Appendix D. Metal Ion Redox Experiments

D.1 Introduction

A number of very simple test setups were tried in order to find a screening method for potential DERC reactions. Also, a test setup was built for crudely measuring separator material resistance. A large test setup was built to run a complete DERC. These test setups were tested with various dissolved metal ions. Most of the designs described in this section suffered from too small of a surface area to pass sufficient current to produce a measurable cooling effect.

D.2 Reactions Studied

The following reactions were chosen for experimentation:

$$Fe^{3+} + e^- \leftrightarrow Fe^{2+}$$

$$Cu^{2+} + e^- \leftrightarrow Cu^- \qquad \text{D.2.1}$$

$$Sn^{4+} + 2e^- \leftrightarrow Sn^{2+}$$

All the reactants remain ions, thus allowing them to be pumped from one reactor to the other. In addition, these ions are not strongly toxic. Because the iron and tin reactions have been used in various chemistry class demonstrations and experiments (Rawat, 1990; and Shakhashiri, 1992) it was anticipated that they would be easy to work with. The copper reaction is possible, but the plating reaction, $Cu^{2+} + 2e^- \leftrightarrow Cu$, is more common.

All the reactions were performed with chlorides. These were chosen due to their solubility and greater safety than nitrates.

D.3 Flowerpot Cell

As many laboratory electrochemical cells use a porous ceramic separator, another cell design was attempted using an easily available small commercial flowerpot as the separator. The flowerpot was composed of the standard tan-red porous ceramic. The pot had no drainage hole in its bottom and was 6 cm diameter and 4.6 cm tall. When soaked in a salt (KCl) solution, the pot conducted electricity. The inside of the pot was packed with loose graphite fibers to act as an electrode (see Figure D.3.1). A carbon rod inserted into the fibers connected them to the external leads. The flower pot was then placed in a beaker. A sheet of graphite cloth lining the beaker formed the other electrode.

The flowerpot was filled with a solution of one of the chemicals listed above and the region surrounding it was filled with one of the other solutions. Care was taken so that the solution levels were lower than the height of the pot separating them. The internal resistance of this cell due to the pot was too high. Although the cell produced the predicted equilibrium voltage at open circuit conditions, it delivered a very low voltage when the circuit was closed through an external load.

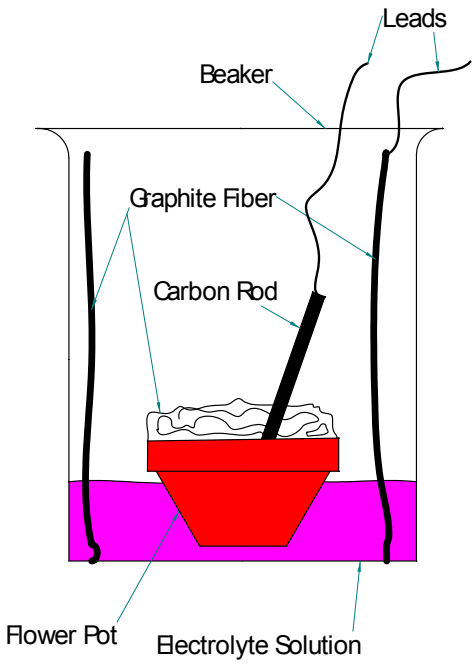

Figure D.3.1 Test cell constructed with a flowerpot as the separator

D.4 Extraction Thimble Cell

A separator made of an extraction thimble was tried. An extraction thimble is shaped like a test tube and made of material similar to filter paper. Rolled up graphite cloth was stuffed in the thimble and the top corked with a rubber stopper (see Figure D.4.1).

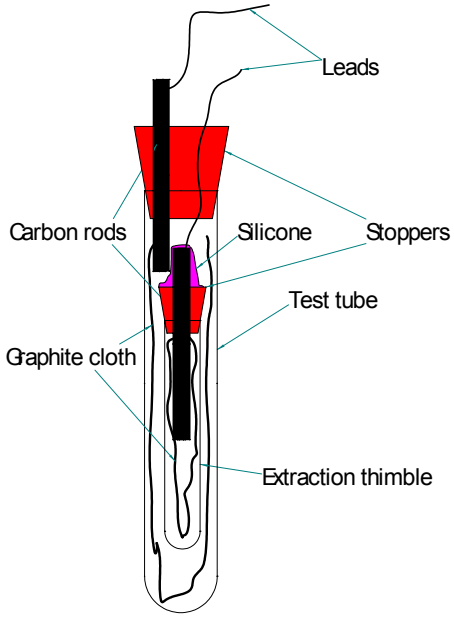

Figure D.4.1 Test cell constructed from a test tube with an extraction thimble as the separator

A graphite rod extended through the stopper and connected to a lead. The rod to lead connection was covered with clear 100% silicone caulking to prevent the cell from short circuiting. The extraction thimble was placed inside a test tube. The other electrode was a layer of graphite cloth located between the test tube and the thimble.

When the thimble was filled with electrolyte, it flowed through the thimble faster than the cell could be assembled. This indicates that the thimble should have a low resistance but the cell would be short lived due to inter-diffusion of the solutions.

D.5 Dialysis Tubing Cell

A separator made of dialysis tubing was tried. Dialysis tubing is a tube of semi-permeable regenerated cellulose membrane (Spectra/Por® molecularporous membrane tubing). This cell was very similar to the prior cell with the tubing substituted for the extraction thimble. Graphite fiber was wrapped around the carbon rod (see Figure D.5.1).

The graphite rod was placed in a piece of knotted dialysis tubing. The tubing was filled with the electrolyte solution and then sealed around the rod with a plastic hose clamp. The rod was then connected to a lead. The dialysis tubing was placed inside a test tube. The other electrode was a layer of graphite cloth located between the test tube and the tubing. The electrolyte appeared to excessively leak through the membrane.

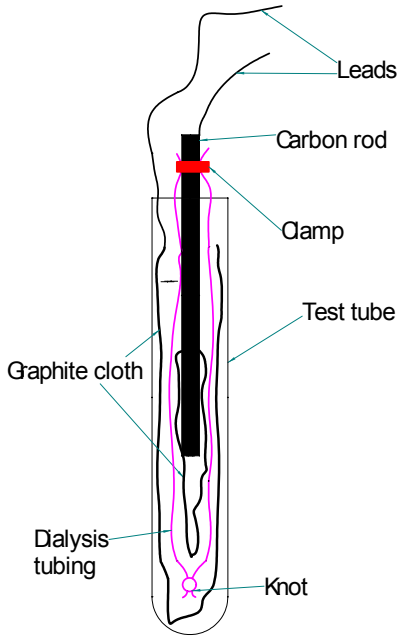

Figure D.5.1 Test cell constructed from a test tube with dialysis tubing as the separator

D.6 Separator Test Setup

A small test setup was built to measure the resistance of various seaparrator materials. The separator specimens could be held firmly by placing them inside a PVC pipe union and screwing it shut (Figure D.6.1). A graphite rod electrode was fixed on each side of the separator. Hose barbs were attached for filling the cell with solution. The pipes extended straight from the coupler in the first setup (left hand cell in Figures D.6.1 and D.6.2). However, it was difficult to ensure that air had been purged from the system. A new set up was built with the pipes bent up. This allowed the air to leave the system as it was filled and ensured that the electrodes were completely immersed in the solution.

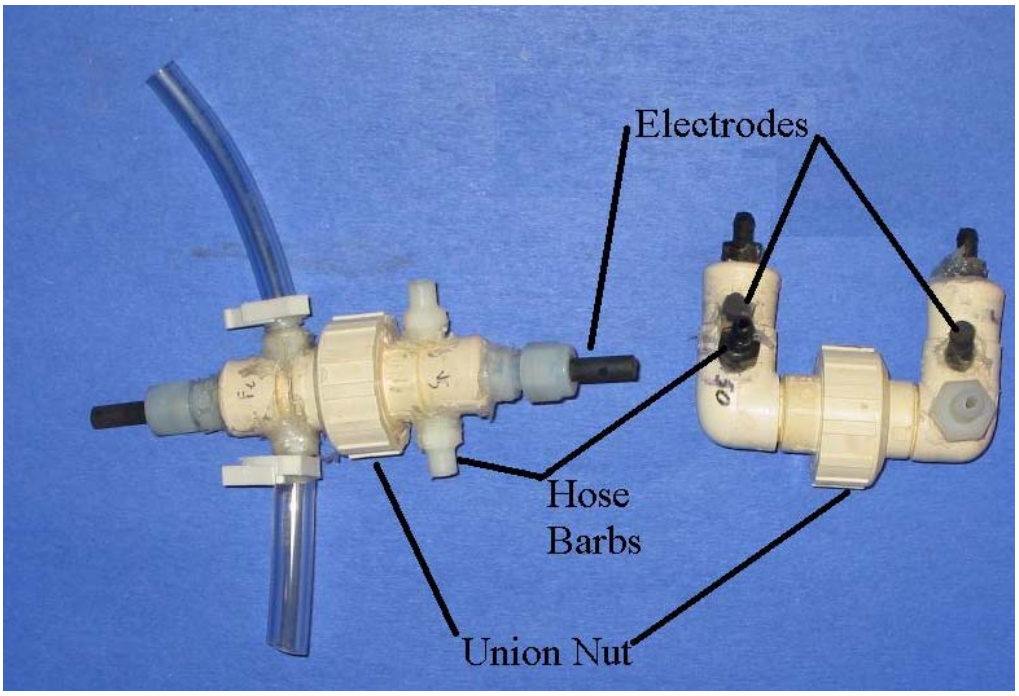

Figure D.6.1 Plumbing unions used for testing separator materials

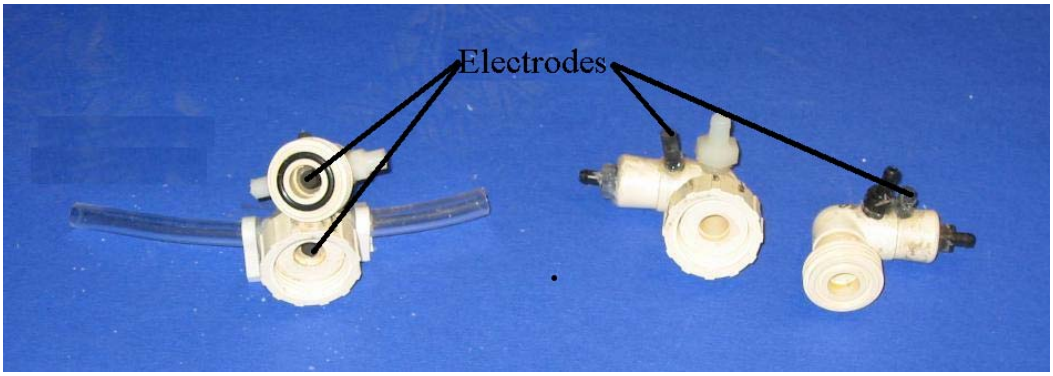

Figure D.6.2 Plumbing union cell interiors

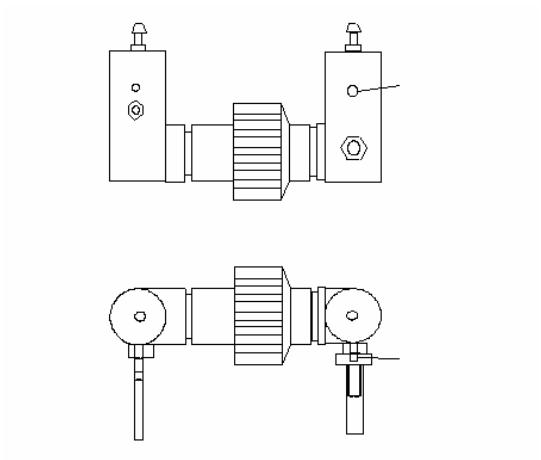

Figure D.6.3 Drawing of plumbing coupler used for testing separator

A separator material was placed in the cell and the cell filled with an electrolyte solution. When the conductivity was measured with a conductivity meter (YSI Scientific model 32), results were inconsistent. This may have been due to the age of the meter.

D.7 Cycle Test Setup on Pegboard

A test setup was built for testing the electrochemical refrigeration cycle with aqueous transition metal salts as the reactants. However, this test setup was never used because a feasible reaction couple was not identified.

The piping and electrochemical reactors were bolted to a piece of pegboard (See Figure D.7.1). The pegboard allowed easy rearrangement of the components. Two-by-four lumber pieces were screwed to the pegboard so it could be stood up in one of two orientations for filling the system with the reactant solutions. When the system was to be operated it was laid flat on soft foam and more soft foam layered on top for insulation. The foam deformed around the components.

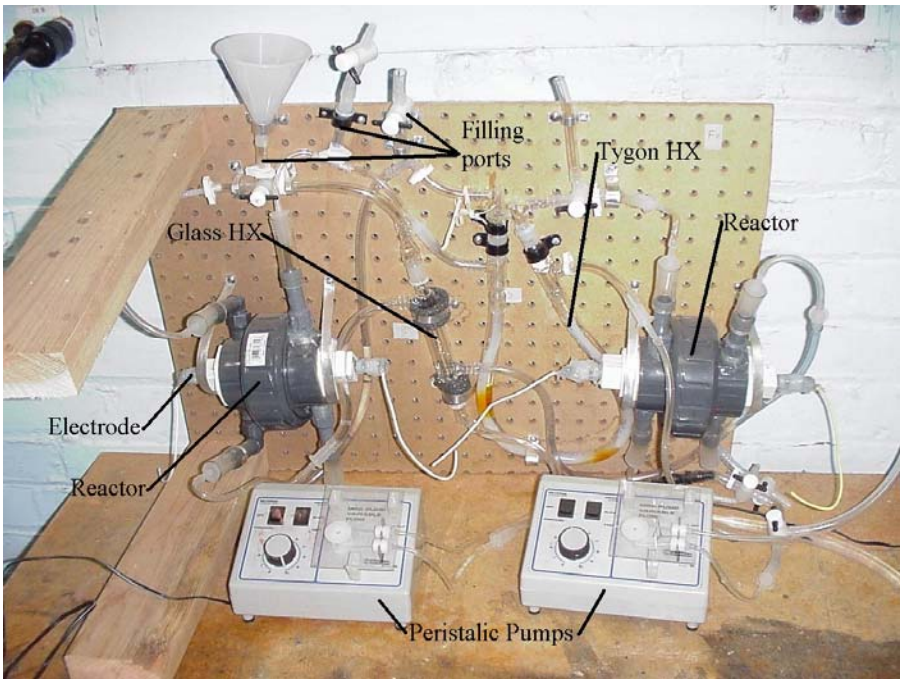

Figure D.7.1 Overall view of two reactor cycle test setup on pegboard

Due to the corrosive nature of the reactant streams all of the components were made of glass or plastic. Peristaltic pumps with a very small flow rate (4.0 to 85.0 ml/min) were used to transfer the solutions between cells.

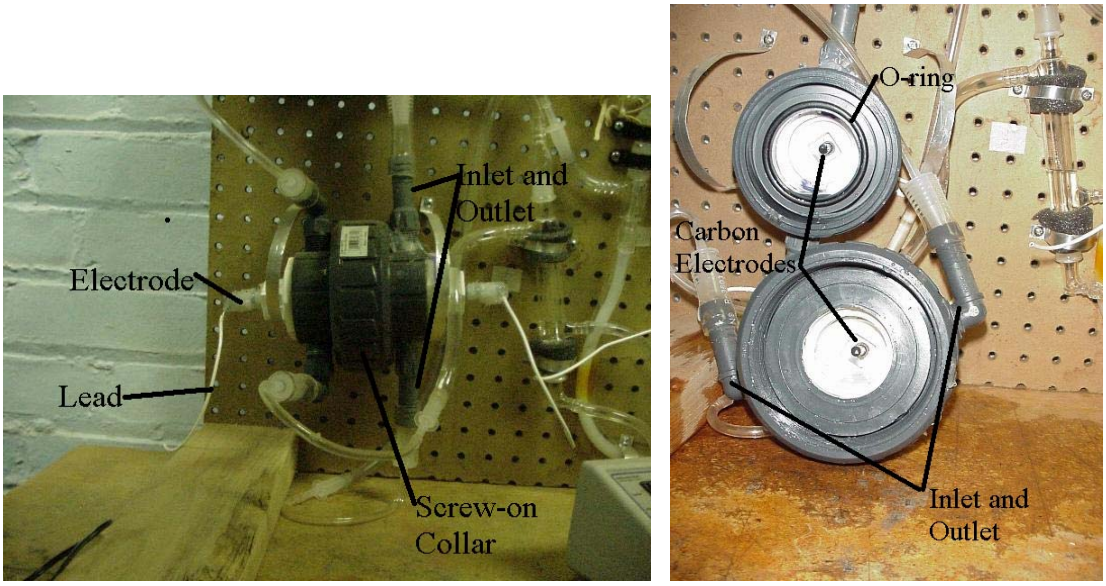

Figure D.7.2 Electrochemical reactors made from PVC pipe couplers

Heat exchangers are needed to transfer heat between the reactant flows. A separate heat exchanger is needed for each reactant flow. In this setup two different types of heat exchangers were used with the intention of investigating their performance in this system. Both heat exchangers are counterflow designs with two concentric tubes. One exchangers is a standard borosilicate glass Liebig condenser used in chemistry for cooling distillation vapors (see Figure D.7.1). The other heat exchanger is composed of Tygon, flexible vinyl tubing (see Figure D.7.3). A glass vacuum adapter was used to connect the tubing at the ends so that the flows in the inner tube and the annulus were kept separate.

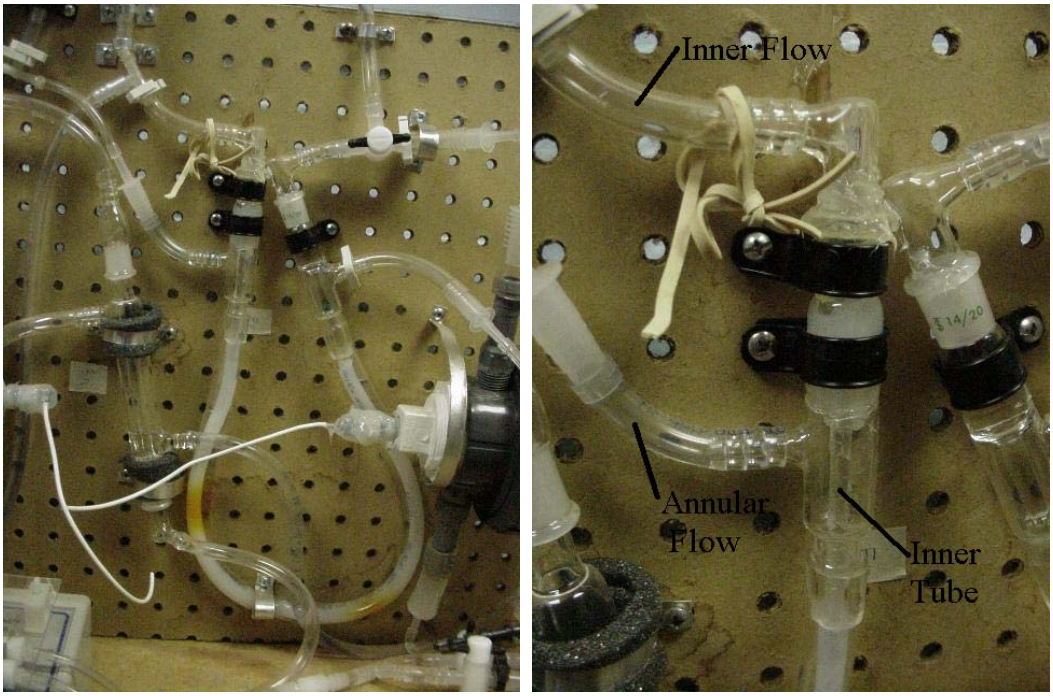

Figure D.7.3 Tygon tubing heat exchanger. Left: Overall view. Right: End connectors.

Because of the low thermal conductivity of glass and polymers, these heat exchangers could potentially be ineffective. The calculated effectiveness for both heat exchangers is about 0.7. However, the flow rate in the system is low enough that with a simple redesign the effectiveness could be fairly high.

D.8 Other Cells Described in Main Thesis

Several designs mentioned in Chapter 7 on chlorine generating experiments were also used with metal ions. A PVC stacked plate cell in section 7.6 was tested and did not produce significant voltage (see Figure D.8.1).

Figure D.8.1 PVC cell with Tyvek membrane stained by Iron chloride.

A cell similar to the rolled Tyvek cell in section 7.6 was tested. The solution stained the Tyvek but the voltage produced was also low.

D.9 Conclusions and Comments

None of the tests performed well enough to pursue construction of a complete thermodynamic cycle. In order to prevent the formation of insoluble hydroxides the reactions discussed should be performed in an acidic solution (Shakhashiri, 1992). Adding hydrochloric acid would be possible. However, none of the tests were run this way and insoluble material settled to the bottom of the containers.

Appendix E. Battery Charging Rate Optimization Tests

E.1 Introduction

As the battery charges or discharges the concentrations of the reactants vary throughout the cell, particularly at the electrode surface. Therefore, the voltage needed for optimal cooling rate varies over the course of the charging. In order to determine the optimal charging voltage-time curve, a series of tests were performed.

E.2 Test Procedure

The goal of these tests was to charge identical batteries at different rates and record the voltage and current information. AA NiCd batteries were placed in a foam block constructed from layers of extruded polystyrene. The battery to be tested had leads soldered to its terminals and a type-T thermocouple taped to its side. The battery was then placed in the hole on top of the foam block and the hole stuffed with open cell foam rubber.

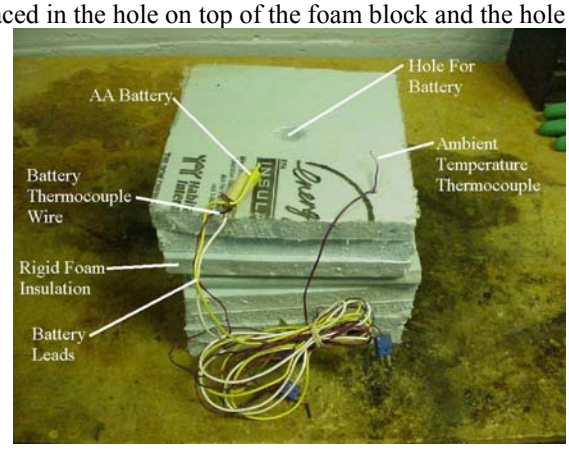

Figure E.2.1 Foam block for testing NiCd AA batteries.

E.3 Proposed Data Analysis Techniques

For any given charge state, there is a voltage that maximizes the cooling power where the effect of the reversible heat effect is largest with respect to the losses. The degree of charging could be determined by integrating the current versus time data. The data from a series of tests could be constructed to create a voltage-current-charge state surface.

Inherent in this analysis is that the battery state is determined by the percentage of full charge. Assuming 100% current efficiency, the total amount of reactants in the cell is determined by the charge state, because the amount reacted is directly proportional to the integral of current. However, the actual spatial distribution of reactants in the battery is determined by the interplay between charging rate and diffusion. Therefore, at any instant the data obtained at a particular fraction of full charge may not be applicable to a battery with a different time history of charging.

The potential cooling due to the reversible heat effect could be approximated by assuming 100% current efficiency and multiplying the reaction rate (as determined by the current) by the temperature and the entropy change from published values for the battery reaction.

The losses are somewhat trickier to calculate. The overpotential times the current equals the loss. While the applied voltage is known, the equilibrium voltage is not. The equilibrium voltage could be estimated by the Nernst equation and assuming that the battery composition as determined from the charge state is uniform. However, these assumptions are presumably poor as noted above. The equilibrium potential could be probed during the test by briefly turning off the applied voltage and measuring the open circuit voltage put off by the cell. The

open circuit voltage quickly changes due to diffusion and other relaxation effects. The instantaneous open circuit voltage could be used as the equilibrium value and considered to be a function of charge state. This assumption is probably poor due to the uncertainty of reactant distribution. The open circuit voltage could also be fit to the charge state and applied current. As the experimental data was incomplete and the open circuit voltage was not measured, none of these data analysis techniques were attempted.

Appendix F. Mass Transport Modeling

F.1 Introduction

Several different techniques were tried to compute the effects of changing concentration without using a two dimensional discretization technique. These attempts were unsuccessful.

F.2 Constant Concentration Assumption

The equilibrium cell potential was assumed to not change significantly due to concentration variations. Adjustments for the depletion of the electrolyte as it passes through the cell were not made.

The transport of the reactants to the surface was assumed to be very efficient. Therefore, there were no mass transport losses or limitations in the model. This assumption is probably highly flawed and mass transport is expected to be a significant loss and limitation on current densities. The model in Chapter 6 confirms this. Most of the laboratory experiments performed so far appear to be diffusion controlled.

F.3 Polynomial Concentration Profile

Attempts were made to compute an approximate concentration profile using a polynomial curve fit. The flow stream was divided into a number of elements along the flow path to account for reactant depletion. The reactant flowing in and consumed by the reaction were used to compute the concentration leaving the segment. The concentration inside of an element was constant.

Three polynomials could be used to fit the profile in a membrane and in compartments on both sides. For the flow channels and membrane, the fluxes and concentrations on each interface would be fitting parameters. In addition, the integral of the polynomial must match the average of the concentration in and out. The membrane did not have to match the in and out concentrations because the solvent was immobilized by the membrane and no concentration was convected in. The derivative of the polynomial was used to calculate the mass transport and resistance losses.

Although, the number of variables in the polynomial matched the number of boundary conditions, this method did not solve readily and the problem may have been ill posed.

F.4 Thin Cell Approximation

Because the model described in Chapter 5 indicated an electrode spacing on the order of tens of microns, the thin cell approximation was tried. In a thin cell diffusion is rapid and the concentration can be assumed as constant across the cell. The concentration was tracked in the same manner as for the polynomial equation.

The method was with a small number of segments covering a one meter electrode length. Decreasing the size of segments and increasing their number did not improve stability. In addition, this method required all of the other cell equations to be solved for each segment. This soon exceeded the capacity of the solver software.

F.5 Conclusion

Because these techniques had not worked, the constant Sherwood number approximation was used in the model as described in Chapter 6.

Appendix G. Component Prices

G.1 Introduction

For those unfamiliar with the materials used in electrochemistry, the prices of a number of components are listed. These prices are collected from a variety of sources and should be viewed as ballpark estimates, possibly accurate to the order of magnitude. Most of the prices are for small quantities of the material or retail sources, rather than industrial bulk pricing.

G.2 Separator

The characteristics of the separator are important to the operation of the cell. The price of this component can vary widely. For instance, Choban (2004) describes a method using laminar flow to keep the electrolytes separate, thus eliminating the membrane. However, this technique uses expensive MEMS manufacturing techniques. In the middle to low end of the price range, polyethylene felt such as Tyvek could be used as a separator. This material costs tens of cents to over a dollar per square meter. At the higher end of the price range is Nafion, a solid polymer acid. It is the standard membrane material for PEM fuel cells. It typically costs in the range of hundreds of dollars per square meter to over a thousand dollars per square meter depending on thickness and other factors. However, some claim the cost will drop below $\$100/m^2$.

G.3 Electrodes

The price of the electrode assembly could vary greatly depending on the material requirements and whether the electrode must be catalytic.

At the high price end electrodes similar to those used in fuel cells could be used. Nafion membranes with carbon electrodes seeded with platinum catalyst are available in the range of thousands of dollars per m^2.

There are many types, forms, and purities of carbon and the price of electrodes made of it will vary accordingly. For instance, graphite plates can cost hundreds of dollars per square meter. Lab grade glassy carbon can be over $\$52{,}000/m^2$. Graphite powder suitable for lubrication can cost under $4.00/kg.

Metal electrode prices also vary widely. Expanded titanium mesh is over $\$500/ m^2$. Lead sheeting is about $\$75$ m^2. Plain carbon steel is less than???(kurland), although its usefulness is limited in corrosive electrolyte solutions.

G.4 Cell Container and Piping

The cell container and piping could be expensive if it is built of corrosion resistant, hard-to-work metals such as stainless steel, titanium, or Inconel. Machined or molded graphite plates could also be use. However, the cells might also be made from conventional plastics such as polyethylene, using cheap blow molding or injection molding techniques. Also, a roll-to-roll heat sealing technology could be used as an inexpensive way to manufacture cells from sheets of polyethylene or other polymers. However, the polymers would have low thermal conductivity.

G.5 Reactants

The amount of reactants needed depends on the total volume of the system including auxiliary piping. The flow rate needed per watt is discussed in Chapter 3 and the volume needed in Chapter 6. The cost of the chemicals varies greatly depending on the particular reactants needed and the purity. The purity required has not been determined, but is driven by the need to prevent side reactions. For example, technical grade anthracene costs $28/kg. At 99.9% purity it costs over $3300/kg. Ferric chloride of 98% purity costs $20/kg. This material is used in large quantities in the circuit board etching industry and may be available at a considerably lower cost in bulk.

G.6 Solvent

The cost of the solvent could vary widely too. Water is of course cheap. Even deionized or otherwise purified water is very inexpensive at cents per liter. Nonaqueous solvents cost considerably more. For instance, acetonitrile and dimethylformamide at 99% purity cost about $23/liter. Anhydrous ammonia is a material produced and consumed in huge quantities and costs a few hundred dollars a ton. Ionic liquids are in the range of dollars to tens of dollars per kilogram.

G.7 Conclusions

At this stage price estimates are virtually impossible as the complete system has not been designed. However, it is unlikely that a DERC will compete on price with conventional vapor compression systems. Most of the materials are fairly expensive per kilowatt of cooling power produced and have stringent performance requirements.